

**DAMAGE VARIATIONS ON TRUNK AND HEAD OF
LOW-CRESTED BREAKWATERS**

by

Rolando Garcia

A thesis submitted to the Faculty of the University of Delaware in partial fulfillment of the requirements for the degree of Master of Civil Engineering

Summer 2014

© Rolando Garcia
All Rights Reserved

UMI Number: 1567806

All rights reserved

INFORMATION TO ALL USERS

The quality of this reproduction is dependent upon the quality of the copy submitted.

In the unlikely event that the author did not send a complete manuscript and there are missing pages, these will be noted. Also, if material had to be removed, a note will indicate the deletion.



UMI 1567806

Published by ProQuest LLC (2014). Copyright in the Dissertation held by the Author.

Microform Edition © ProQuest LLC.

All rights reserved. This work is protected against unauthorized copying under Title 17, United States Code



ProQuest LLC.
789 East Eisenhower Parkway
P.O. Box 1346
Ann Arbor, MI 48106 - 1346

**DAMAGE VARIATIONS ON TRUNK AND HEAD OF
LOW-CRESTED BREAKWATERS**

by

Rolando Garcia

Approved: _____
Nobuhisa Kobayashi, Ph.D.
Professor in charge of thesis on behalf of the Advisory Committee

Approved: _____
Harry W. Shenton III, Ph.D.
Chair of the Department of Civil and Environmental Engineering

Approved: _____
Babatunde A. Ogunnaike, Ph.D.
Dean of the College of Engineering

Approved: _____
James G. Richards, Ph.D.
Vice Provost for Graduate and Professional Education

ACKNOWLEDGMENTS

I would like to thank Nobuhisa Kobayashi for being a great advisor over the past two years. I really enjoyed our discussions and conversations on diverse topics, often beyond the scopes of this study. I would also like to thank César Vidal for providing his report.

I want to thank my wife Macarena for being a wonderful partner in this journey and my daughter Amanda for being a permanent source of happiness and motivation.

The author was supported by Fulbright Chile Program and Conicyt during his two-year Master's study at the University of Delaware.

This study was partially supported by the Artificial Reef Research Center for High Wave Control, Kwandong University in Korea and by the U.S. Army Corps of Engineers under Contract No. W911XK-13-P-0065.

TABLE OF CONTENTS

LIST OF TABLES	vii
LIST OF FIGURES	ix
ABSTRACT	xiii

Chapter

1	INTRODUCTION	1
2	NUMERICAL MODEL	4
2.1	General Description	4
2.1.1	Hydrodynamic Model	5
2.1.2	Stone Movement Model	6
2.2	Computation of Wave Transmission	7
2.3	Computation of Structure Damage	7
3	WAVE TRANSMISSION	9
3.1	Available Data	9
3.1.1	NRC – Wave Transmission Measurements	9
3.1.2	AAU – Wave Transmission Experiments	11
3.1.3	Empirical Formula	13
3.2	Numerical Model Setup	14
3.2.1	Specified Input	14
3.2.2	Calibrated Parameters	15
3.3	Comparison with Data	16
3.3.1	NRC Data	16
3.3.2	AAU Data	18

4	DAMAGE ON TRUNK	22
4.1	Available Data	22
4.1.1	NRC – Structure Stability Tests	22
4.1.2	AAU – Structure Stability Tests	24
4.2	Data Analysis	26
4.2.1	Measured Damage S_v and S_p	26
4.2.2	Trunk Sections Damage Relation	29
4.3	Numerical Model Setup	30
4.3.1	Specified Input	30
4.3.2	Calibrated Parameters	31
4.4	Comparison with Data	34
4.4.1	NRC Data	34
4.4.2	AAU Data	37
5	DAMAGE ON HEAD	41
5.1	Similarity of Trunk and Head Damage	41
5.1.1	Front Head Similarity	42
5.1.2	Back Head Similarity	44
5.2	Comparison with Data	48
5.2.1	NRC Data	48
5.2.2	AAU Data	49
6	EXPERIMENTS	50
6.1	Experimental Setup	50
6.1.1	Flume Layout	51
6.1.2	Sand and Stones	52
6.1.3	Test Conditions	54
6.2	Experimental Procedure	54
6.2.1	Profile Construction	54

6.2.2	Wave Generation	56
6.2.3	Measurements	57
6.2.3.1	Wave Gauges	57
6.2.3.2	Acoustic Doppler Velocimeters.....	58
6.2.3.3	Bottom Profile	58
6.2.3.4	Structure Damage	58
6.2.3.5	Sand Deposition.....	59
6.3	Analyzed Data	59
6.3.1	Free Surface Elevation.....	59
6.3.2	Velocity	63
6.3.3	Bottom Profile	64
6.3.4	Structure Damage	66
6.3.5	Sand Deposition.....	72
6.4	Comparison with Numerical Model	74
6.4.1	Hydrodynamics.....	74
6.4.2	Structure Damage	78
7	CONCLUSIONS	80
	REFERENCES	82
Appendix		
A	AVAILABLE DATA ON LCS	85
B	COMPUTED RESULTS.....	93
C	CHARACTERISTICS OF STONES USED IN THE EXPERIMENT	98
D	LASER LINE SCANNER ERROR OVER THE STONE STRUCTURE	104

LIST OF TABLES

Table 3-1:	NRC experiment conditions	11
Table 3-2:	Experiment conditions in AAU Transmission (rubble structure).....	13
Table 4-1:	Experiment conditions in AAU Stability tests	26
Table 6-1:	Cross-shore location of instruments	52
Table 6-2:	Characteristics of sand used in experiment	52
Table 6-3:	Characteristics of three stones used in experiment.....	54
Table 6-4:	Incident wave conditions and reflection coefficient.....	60
Table 6-5:	Mean free surface elevation $\bar{\eta}$ at wave gauges WG1-WG6	61
Table 6-6:	Standard deviation of the free surface σ_{η} at wave gauges WG1-WG6 ...	62
Table 6-7:	Cross-shore velocity statistics from velocimeters V1 and V2.....	63
Table 6-8:	Measured damage for each stone type used in the experiment	71
Table 6-9:	Deposited sand measurements.....	72
Table A-1:	Test conditions and measured data in NRC experiment	86
Table A-2:	Test conditions and measured data in AAU wave transmission experiment	88
Table A-3:	Test conditions and measured data in AAU structure stability experiment	90
Table B-1:	Computed wave transmission coefficient and damage S_p in NRC experiment	94
Table B-2:	Computed wave transmission coefficient in AAU wave transmission experiment	95
Table B-3:	Computed damage S_p in AAU structure stability experiment.....	96

Table C-1: G stone measurements	99
Table C-2: B stone measurements	101
Table C-3: W stone measurements	102

LIST OF FIGURES

Figure 2-1: Onshore (x), alongshore (y), and vertical (z) coordinates of numerical model	5
Figure 3-1: Wave basin layout in NRC experiments.....	10
Figure 3-2: Wave basin layout in AAU transmission experiments.....	12
Figure 3-3: Comparison of computed K_t for $f_b = 0.02$ and 0.03 in AAU tests	15
Figure 3-4: Comparison of K_t against normalized freeboard in NRC data	16
Figure 3-5: Comparison of K_t against measured values in NRC data	17
Figure 3-6: Measured and computed K_t for oblique waves and $F = -0.05$ cm in AAU data.....	18
Figure 3-7: Measured and computed K_t for oblique waves and $F = 0$ cm in AAU data.....	19
Figure 3-8: Measured and computed K_t for oblique waves and $F = +0.05$ cm in AAU data.....	19
Figure 3-9: Comparison of K_t vs normalized freeboard in AAU data.....	20
Figure 3-10: Comparison of K_t against measured values in AAU data.....	21
Figure 4-1: Trunk and head sections of the LCS in NRC experiments.....	23
Figure 4-2: Wave basin layout in AAU stability experiments	25
Figure 4-3: Trunk and head sections of the LCS in AAU experiments	25
Figure 4-4: Measured damage S_v versus S_p for trunk sections in NRC data	28
Figure 4-5: Trunk sections in NRC experiments.....	29
Figure 4-6: Comparison of measured damage on trunk sections (TS) and (FS+C+BS) in NRC data.....	30

Figure 4-7: Calibration of CSTABN for damage S_p on TS section in NRC data.....	31
Figure 4-8: Calibration of CSTABN for damage S_v on TS section in AAU data	32
Figure 4-9: Calibration of TANPHI for damage S_p on TS section in NRC data.....	33
Figure 4-10: Calibration of TANPHI for damage S_v on TS section in AAU data	33
Figure 4-11: Damage comparison on trunk sections in NRC data with ISEDAV = 2	35
Figure 4-12: Damage comparison on trunk sections in NRC data with ISEDAV = 1	36
Figure 4-13: Trunk sections in AAU experiments	37
Figure 4-14: Damage comparison on trunk sections in AAU data with permeable core	38
Figure 4-15: Damage comparison on trunk sections in AAU data with impermeable core	39
Figure 5-1: Trunk and head sections for front head damage prediction.....	42
Figure 5-2: Similarity of measured head damage FH and measured trunk damage in NRC experiments with S_v damage.....	43
Figure 5-3: Similarity of measured head damage SH and measured trunk damage in AAU experiments with S_v damage	43
Figure 5-4: Definition of trunk section FT for front head damage prediction	44
Figure 5-5: Trunk and head sections for back head damage prediction.....	45
Figure 5-6: Similarity of measured head damage BH and measured trunk damage in NRC experiments with S_v damage.....	46
Figure 5-7: Similarity of measured head damage (MH+LH) and measured trunk damage in AAU experiments with S_v damage.....	46
Figure 5-8: Definition of trunk section BT for back head damage prediction	47
Figure 5-9: Measured and computed damage S_v for head sections FH and BH in NRC experiment.....	48

Figure 5-10: Measured and computed damage S_v for head sections SH and (MH+LH) in AAU experiment.....	49
Figure 6-1: Experimental setup	51
Figure 6-2: Structure dimensions	55
Figure 6-3: Picture of the structure layout.....	56
Figure 6-4: Time series of voltage input for the wavemaker	56
Figure 6-5: Calibration curves of wave gauges WG1-WG6	57
Figure 6-6: Measured bottom profile z_b and eroded depth d_e for N test series.....	65
Figure 6-7: Measured bottom profile z_b and eroded depth d_e for S test series	65
Figure 6-8: Measured structure profiles at the beginning and end of S test.....	66
Figure 6-9: Picture of the structure at the beginning of S test (S 00).....	67
Figure 6-10: Picture of the structure after five runs in S test (S 05)	68
Figure 6-11: Picture of the structure after ten runs in S test (S 10).....	68
Figure 6-12: Fine resolution laser scan of the structure at the beginning of S test (S 00)	69
Figure 6-13: Fine resolution laser scan of the structure after five runs in S test (S 05)	69
Figure 6-14: Fine resolution laser scan of the structure after ten runs in S test (S 10)	70
Figure 6-15: Identification of displaced stones during S test	71
Figure 6-16: Measured profile and deposited sand depth inside the structure after S test	73
Figure 6-17: Initial bottom elevation z_b and measured and computed cross-shore variations of $\bar{\eta}$, H_{m0} , \bar{U} and σ_U for 10 runs in N test.....	76
Figure 6-18: Initial bottom elevation z_b and measured and computed cross-shore variations of $\bar{\eta}$, H_{m0} , \bar{U} and σ_U for 10 runs in S test	77

Figure 6-19: Measured and computed temporal variations of damage S_v in the experiment	78
Figure D-1: Laser scan error over the structure in S 00 test.....	105
Figure D-2: Laser scan error over the structure in S 05 test.....	106
Figure D-3: Laser scan error over the structure in S 10 test.....	107

ABSTRACT

The spatial variation of damage on the different sections of the trunk and head of a low-crested stone structure on a fixed bottom is examined using the cross-shore numerical model CSHORE extended to oblique waves. The computed wave transmission coefficient and damage on the front slope, back slope and total section of the trunk are compared with available data consisting of 188 tests. Similarity of trunk and head damage for a low-crested breakwater is proposed to predict damage on the front head and back head using the cross-shore model. The agreement is mostly within a factor of 2 but the model overpredicts damage on the back head of a submerged structure. An experiment was conducted in a wave flume for a low-crested stone structure located inside the surf zone on a sand beach. The model is shown to reproduce the measured cross-shore wave transformation on the beach without and with the structure as well as the measured small damage on the structure. Sand deposition inside the porous structure will need to be accounted for to predict toe scour and accretion.

Chapter 1

INTRODUCTION

Rubble mound structures with low crests have been constructed on beaches to reduce wave action landward of the structure during storms. Detached low-crested breakwaters have been used for shore protection to reduce the structure cost and allow water circulation. The design of the low-crested stone structure (LCS) against storm waves requires the analysis of armor stability on the entire emerged or submerged structure, because wave impact is not restricted to the seaward slope unlike a high-crested structure with no or little wave overtopping.

Vidal, et al. (1992) and Vidal and Mansard (1995a) conducted a three-dimensional experiment in a wave basin at the laboratories of National Research Council (NRC) in Ottawa, Canada. The experiment was limited to unidirectional random waves normal to the trunk of a LCS in relatively deep water. The measured stone displacement and eroded profile on the different sections of the trunk and round head of the structure indicated the importance of the structure crest elevation relative to the still water level (SWL) in predicting the damage patterns on the trunk and head. Kramer and Burcharth (2003a) conducted a similar experiment using multidirectional random waves in shallow water at the Aalborg University (AAU) in Denmark and proposed an empirical formula for initiation of damage using available data. Burcharth, et al. (2006) reviewed the experimental findings of the hydraulic stability of low-crested stone structures located on fixed bottoms.

The cross-shore numerical model CSHORE was developed to predict irregular breaking wave transmission over a submerged porous structure (Kobayashi, et al., 2007) and was extended to predict damage progression on a conventional stone breakwater with little wave overtopping (Kobayashi, et al., 2010) and deformation of a reef breakwater with wave transmission (Kobayashi, et al., 2013).

In this study, CSHORE is extended to obliquely incident waves and compared with available data on oblique wave transmission over and through a low-crested breakwater. The NRC and AAU damage data are used to assess the capability of CSHORE for predicting the damage on the different trunk sections. The damage on the front and back sections of the round head is predicted assuming similarity of the head and trunk damage for low-crested breakwaters. An experiment was conducted for a low-crested stone structure located inside the surf zone on a sand beach during a storm in order to assess the utility of CSHORE for a typical field application.

In Chapter 2 the numerical model CSHORE extended to oblique waves is described together with computation of wave transmission and structure damage. In Chapter 3 computed transmission coefficients by CSHORE are compared with the data of Vidal and Mansard (1995a) and Kramer and Burcharth (2003b), along with the empirical formula proposed by Goda and Ahrens (2008) and recalibrated by Tomasicchio, et al. (2011). In Chapter 4 available data on trunk damage of LCS by Vidal and Mansard (1995a) and Kramer and Burcharth (2003a) are analyzed and compared with computed results by CSHORE. Head damage prediction is devised in Chapter 5. Chapter 6 explains the setup, procedure and results of the experiment conducted to analyze a LCS located inside the surf zone on a sand beach. Conclusions of the study are presented in Chapter 7. Additional information is provided in

Appendices A to D. A concise summary of this study is presented by Garcia and Kobayashi (2014).

Chapter 2

NUMERICAL MODEL

This chapter explains the cross-shore numerical model CSHORE extended to oblique waves and its application to compute wave transmission and structure damage on a low-crested breakwater (LCS). The first section of this chapter gives a general description of the model. Computation of wave transmission coefficient and structure damage are described in the subsequent sections. The numerical model is described in detail in the report of Kobayashi (2013).

2.1 General Description

Figure 2-1 depicts an emerged LCS with a trunk and a round head. For a submerged structure, its crest is situated below the SWL. The structure is assumed to be parallel to the shoreline. The cross-shore coordinate x is positive onshore with $x = 0$ at the seaward location of the incident irregular wave measurement. The irregular waves are represented by the spectral significant wave height H_{m0} and spectral peak period T_p . The alongshore coordinate y is parallel to the straight trunk. The incident waves are assumed to be unidirectional with $\theta =$ wave angle relative to the shore normal. The vertical coordinate z is positive upward with $z = 0$ at the SWL. The upper and lower boundaries of the stone structure are located at $z = z_b(x)$ and $z_p(x)$, respectively, where the lower boundary is assumed to be impermeable and fixed. Stone movement results in the deformation of $z_b(x)$ but $z_b(x) = z_p(x)$ seaward and landward of the structure. The horizontal SWL and $z_b(x)$ intersect at $x = x_{SWL}$.

and x_s in Figure 2-1 where no intersection exist for a submerged breakwater. The cross-shore model CSHORE assumes alongshore uniformity and is not applicable in the vicinity of the breakwater head.

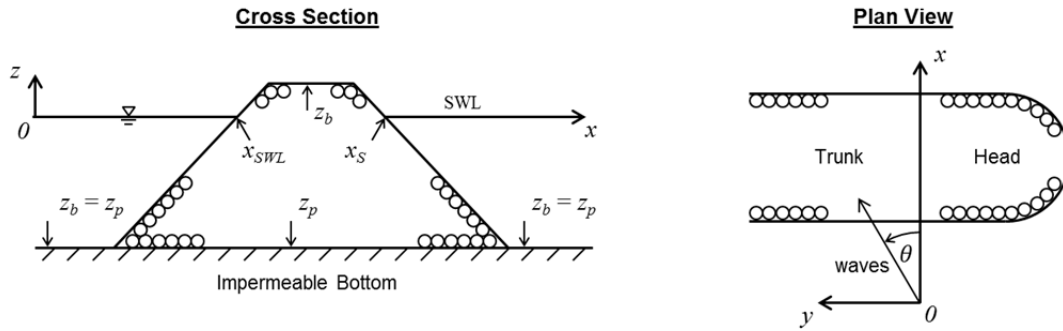


Figure 2-1: Onshore (x), alongshore (y), and vertical (z) coordinates of numerical model

2.1.1 Hydrodynamic Model

For the seaward wet zone of $x < x_{SWL}$ in Figure 2-1 and the entire zone above the submerged structure, the time-averaged continuity, cross-shore momentum, longshore momentum and energy equations along with Snell's law are used to compute the cross-shore variations of the wave angle θ and the mean and standard deviation of the free surface elevation η above the SWL and the depth-averaged cross-shore velocity U and longshore velocity V above the permeable bottom. The time-averaged cross-shore water flux and wave energy dissipation inside the porous structure are included by extending the approximate porous flow model for $\theta = 0$ (Kobayashi, et al., 2007) to oblique waves as presented in the report of Kobayashi (2013). The longshore water flux inside the porous structure is neglected assuming the negligible longshore momentum flux into and out of the porous structure.

For the swash zone of $x_{SWL} < x < x_s$, which is intermittently wet and dry, the wave angle θ is assumed to remain the same as the computed angle θ at $x = x_{SWL}$. The cross-shore variations of the mean and standard deviation of η , U and V are computed using the probabilistic model of Kobayashi, et al. (2010) coupled with the time-averaged nonlinear shallow-water wave equations with the assumption of $(\sin\theta_{SWL})^2$ being much smaller than unity (Farhadzadeh, et al., 2012). The vertical water and cross-shore momentum fluxes into the porous structure are included in the time-averaged continuity and cross-shore momentum equations. In the landward wet zone of $x > x_s$, the simple linear wave model including the water flux inside the porous structure (Kobayashi, 2013) is used to compute the cross-shore variations of the mean and standard deviation of η and U . The mean and standard deviation of V are assumed to be negligible.

2.1.2 Stone Movement Model

After the computation of the hydrodynamic variables above the known bottom elevation $z_b(x)$ for the specified values of H_{m0} , T_p and θ at $x = 0$, the time-averaged cross-shore and longshore stone transport rates are computed using the bed load formula of Kobayashi, et al. (2009) with the criterion for initiation of stone movement proposed by Kobayashi, et al. (2010). The temporal change of $z_b(x)$ is computed using the conservation equation of stone volume per unit alongshore width. The longshore stone transport rate does not contribute to the profile change because of the assumption of alongshore uniformity but the computed cross-shore and longshore transport rates are comparable for oblique waves. This computation procedure is repeated starting from the initial bottom profile until the end of a damage test. The computation time is of the order of 10^{-3} of the test duration.

2.2 Computation of Wave Transmission

Wave transmission coefficient for a breakwater trunk on a flat bottom is defined as:

$$K_t = \frac{H_t}{H_i} \quad (2-1)$$

Where

H_t : transmitted significant wave height measured sufficiently landward of the structure.

H_i : incident significant wave height measured at the seaward toe of the structure.

2.3 Computation of Structure Damage

CSHORE computes the cross-shore bottom elevation $z_b(x, t)$ where x = cross shore coordinate and t = profile evolution time. The erosion depth is then calculated as:

$$d_e(x, t) = [z_b(x, 0) - z_b(x, t)] > 0 \quad (2-2)$$

CSHORE can be set in two ways to compute the bottom elevation $z_b(x, t)$, depending on the specified value for the input parameter ISEDAV.

When ISEDAV=1, erosion and deposition is allowed along the entire structure profile, corresponding to the standard case of armor stone movement. By integrating the erosion depth d_e along a specific section of the trunk, the eroded area A_e is obtained for each section.

If ISEDAV=2, erosion is allowed only on specified sections of the permeable stone structure, while deposition is allowed everywhere. This option is created to mimic the effect of a wire mesh over the structure, which is assumed to prevent erosion under it. The eroded area A_e is obtained by integrating the erosion depth in the same way as ISEDAV=1.

The damage based on the eroded area along the specified trunk section is then computed as:

$$S_p = A_e / (D_{n50})^2 \quad (2-3)$$

Where

S_p : damage based on measured profile

A_e : eroded area on the cross-shore section.

D_{n50} : nominal stone diameter = $(M_{50}/\rho_s)^{1/3}$

M_{50} : medium mass of the stone

ρ_s : density of the stone

Chapter 3

WAVE TRANSMISSION

The numerical model CSHORE described in Chapter 2 is used to calculate wave transmission of normally and obliquely incident waves over low-crested breakwaters (LCS). The computed wave transmission coefficients are compared against available data of two wave basin experiments together with the empirical formula of Tomasicchio, et al. (2011). Available data and the empirical formula are described in the first section of this chapter. In the second section, numerical model input and calibration are described. Finally, compared results are shown.

3.1 Available Data

Use is made of two datasets on wave transmission over LCS by Vidal and Mansard (1995a) at the laboratories of National Research Council of Canada (NRC) and by Kramer and Burcharth (2003b) at Aalborg University, Denmark (AAU). Detailed information on test conditions and measured wave transmission coefficients are included in Appendix A.

3.1.1 NRC – Wave Transmission Measurements

Even though the primary goal of this experiment was to analyze stability of low-crested breakwaters, as described in the report of Vidal and Mansard (1995a), wave transmission was also measured. The experiment was conducted in two stages using two different wave basins. In both facilities a detached breakwater was built, with its longitudinal axis parallel to the wavemaker, as shown in Figure 3-1.

Unidirectional irregular waves were generated. Eight wave gauges were used to measure the water surface elevation across the center of the wave basin and three additional wave gauges were installed in the side channel to characterize the incident wave conditions. Waves in front of the breakwater were measured by a set of three wave gauges at about 3 m from the longitudinal axis of the structure, which was 5.5 m long. Waves in the sheltered area were measured by four wave gauges located at distances of 2.5 m to 5.3 m from the longitudinal axis of the structure, as shown in Figure 3-1. Test conditions and structure main characteristics are summarized in Table 3-1. Detailed data are shown in Table A-1.

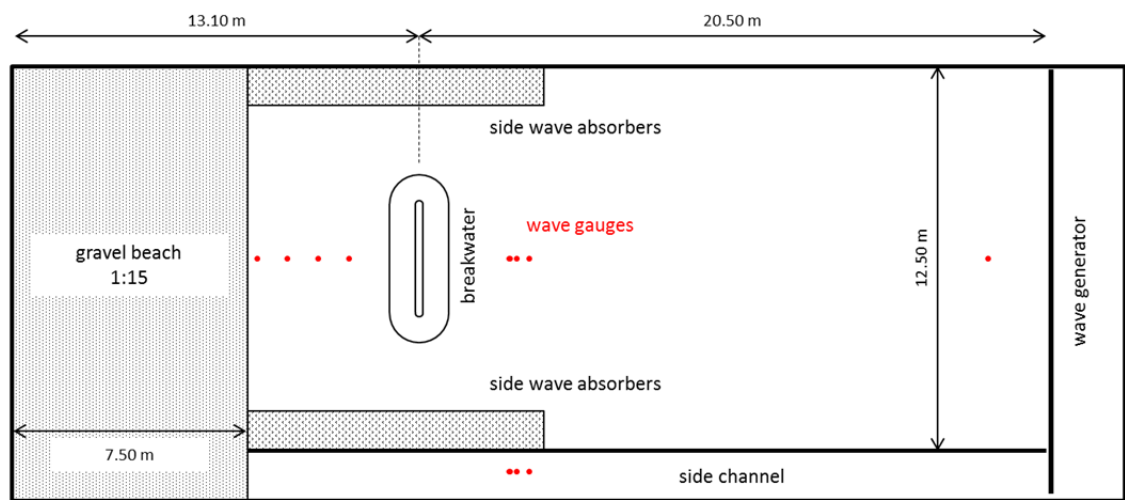


Figure 3-1: Wave basin layout in NRC experiments

Waves behind the detached breakwater were composed of transmitted (over and through the structure) and diffracted (around the structure). The diffracted waves increase with the distance behind the breakwater. The transmission coefficient is taken as the ratio between the wave height closest to the structure (probe1) and the incident wave height.

Table 3-1: NRC experiment conditions

Parameter	Value
Number of tests	35
Structure height (cm)	40, 60
Crest width B_c (cm)	15
Seaward slope	1/1.5
Landward slope	1/1.5
Freeboard F (cm)	-5 to 6
Armor stone size D_{n50} (cm)	2.5
Core stone size D_{n50} (cm)	1.9
Wave angle θ (deg)	0
Wave height H_{m0} (cm)	5 to 15
Wave period T_p (s)	1.4 to 1.8
Test duration (min)	60

3.1.2 AAU – Wave Transmission Experiments

These experiments considered oblique wave transmission over and through low-crested rubble mound and smooth structures. Only rubble mound structure data are used in this study. Multidirectional random waves were generated and three different layouts were built in the wave basin using semidetached structures with different orientations to analyze a wide range of wave incidence angle θ , as shown in Figure 3-2. Two sets of five wave gauges were used to measure incident and transmitted waves seaward and landward of the breakwater. In each layout, transmitted waves were measured in an enclosed area to exclude diffracted waves. Test conditions and structure characteristics are summarized in Table 3-2. Detailed data are shown in Table A-2.

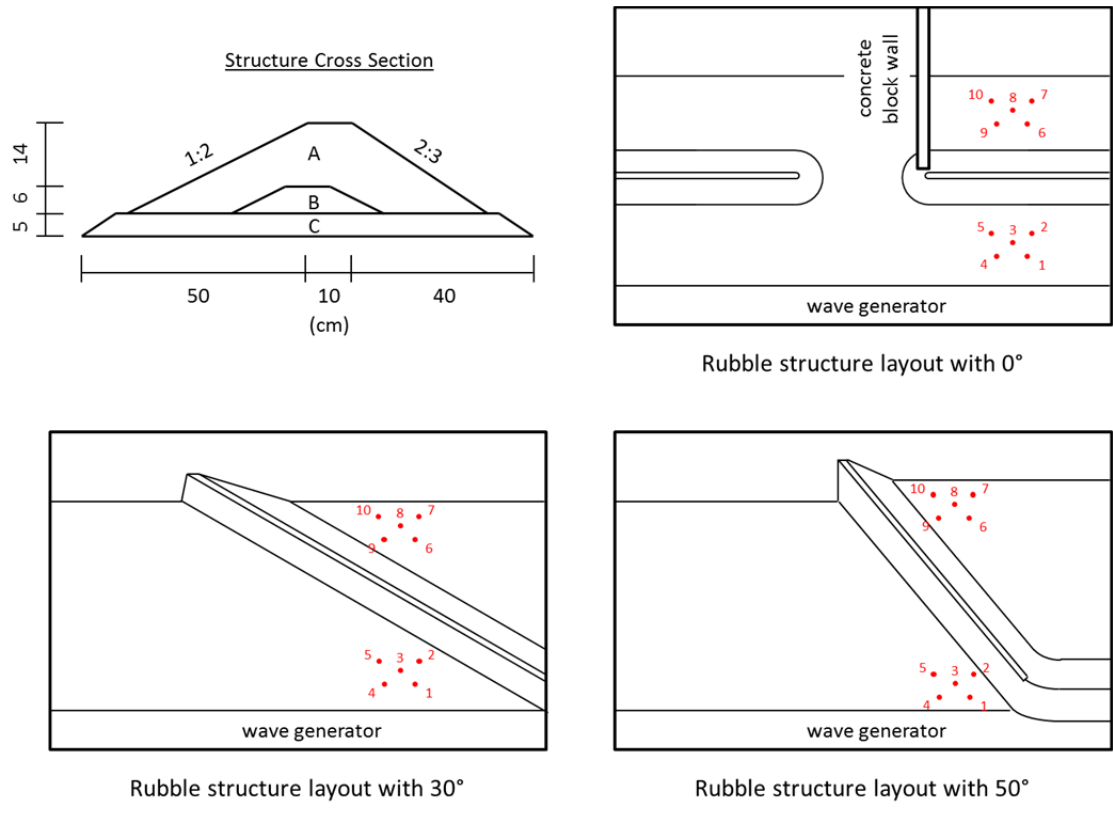


Figure 3-2: Wave basin layout in AAU transmission experiments

Table 3-2: Experiment conditions in AAU Transmission (rubble structure)

Parameter	Value
Number of tests	84
Structure height (cm)	25
Crest width B_c (cm)	10
Seaward slope	1/2
Landward slope	1/1.5
Freeboard F (cm)	-5 to 5
Armor stone size D_{n50} (cm)	4.7
Core stone size D_{n50} (cm)	3.1
Wave angle θ (deg)	-14 to 67
Wave height H_{m0} (cm)	6 to 17
Wave period T_p (s)	1.0 to 2.3
Test duration (min)	15

3.1.3 Empirical Formula

The empirical formula proposed by Goda and Ahrens (2008) for the wave transmission coefficients over and through LCS was recalibrated by Tomasicchio, et al. (2011) using 3,327 points in 33 data sets. The recalibrated formulation is given by the following equations.

$$(K_t)_{all} = \min \left\{ 1.0, \sqrt{(K_t)_{over}^2 + K_h^2 (K_t)_{thru}^2} \right\} \quad (3-1)$$

$$K_h = \min \{ 0.8, h_c / (h + H_i) \} \quad (3-2)$$

$$(K_t)_{over} = \max \{ 0, 1 - \exp [a (R_c / H_i - R_{c,0})] \} \quad (3-3)$$

$$a = 0.248 \exp [-0.384 \ln (B_{eff} / L_0)] \quad (3-4)$$

$$R_{c,0} = \begin{cases} 1.0 & : D_{eff} = 0 \\ \max\{0.6, \min(0.8, H_i/D_{eff})\} & : D_{eff} > 0 \end{cases} \quad (3-5)$$

$$(K_t)_{thru} = 1/[1 + C (H_i/L)^{0.5}]^2 \quad (3-6)$$

$$C = 3.450 (B_{eff}/D_{eff})^{0.65} \quad (3-7)$$

Where

- H_i : incident wave height H_{m0} at the toe of the structure
 H_t : transmitted wave height H_{m0} leeward of the structure
 L : local wavelength
 L_0 : deep water wavelength
 h : water depth
 h_c : structure height
 R_c : structure freeboard $R_c = h_c - h$
 B_{eff} : effective width of the structure
 D_{eff} : effective diameter of the armor unit (D_{n50} for stones)

3.2 Numerical Model Setup

Specified input and calibrated parameters for computation of wave transmission are described in the following sections.

3.2.1 Specified Input

Based on experiment conditions, the following data were specified as input for the numerical model CSHORE.

- Homogeneous mound characteristics based on armor layer stone:

D_{n50} : nominal stone diameter

$s = \rho_s/\rho_w$: specific gravity, where ρ_w = water density

w_f : fall velocity, calculated as $w_f = 1.8\sqrt{g(s-1)D_{n50}}$

- Structure cross section geometry specified for each experiment.
- Measured wave conditions near the toe of the structure characterized by H_{m0} , T_p and θ were specified for each test.

3.2.2 Calibrated Parameters

The effect of the bottom friction factor f_b on the computed wave transmission coefficient K_t was examined for the AAU wave transmission experiments. Figure 3-3 compares computed K_t for $f_b = 0.02$ and 0.03 .

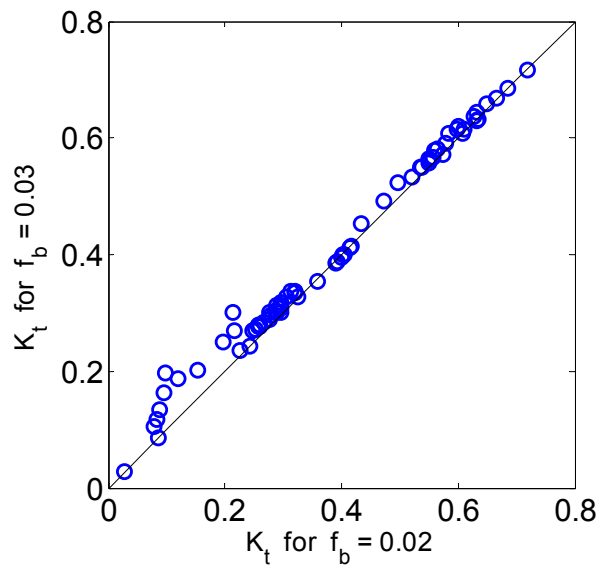


Figure 3-3: Comparison of computed K_t for $f_b = 0.02$ and 0.03 in AAU tests

The computed K_t is insensitive to the value of f_b on the stone surface within a range of $0.02 - 0.03$, because the interaction between the wave motion above the stone surface and the porous flow inside the structure is included in the model. The calibration of f_b on the stone surface was necessary to overcome the numerical

difficulty associated with the small water depth on the emerged crest of the structure for which the computed K_t was less than 0.3 in Figure 3-3. Finally, the bottom friction factor f_b in the numerical model was set as:

- $f_b = 0.01$ on the impermeable bottom
- $f_b = 0.02$ on the permeable stone surface

3.3 Comparison with Data

Comparison of computed wave transmission coefficient against data is presented in the following sections. Computed wave transmission coefficients for each test are shown in Appendix B.

3.3.1 NRC Data

The wave transmission coefficients K_t measured in NRC experiments, computed by CSHORE and predicted by the empirical formula of Tomasicchio, et al. (2011) are shown against the normalized freeboard (F/H_i) in Figure 3-4.

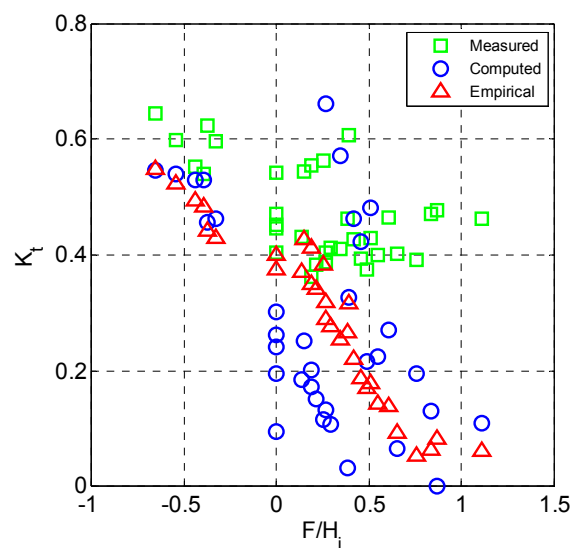


Figure 3-4: Comparison of K_t against normalized freeboard in NRC data

The effect of the freeboard on wave transmission can be observed. The computed and empirical values show similar trends, although the former shows more scatter. The agreement is better for $F < 0$ corresponding to submerged structures. The measured K_t is larger than the computed and empirical values for emerged structures ($F > 0$), for which diffracted waves around the breakwater becomes as important as the transmitted waves over and through the structure.

Figure 3-5 shows the computed and empirical K_t plotted against the measured value. The presence of diffracted waves results in the narrow range of about 0.4 to 0.6 in the measured K_t .

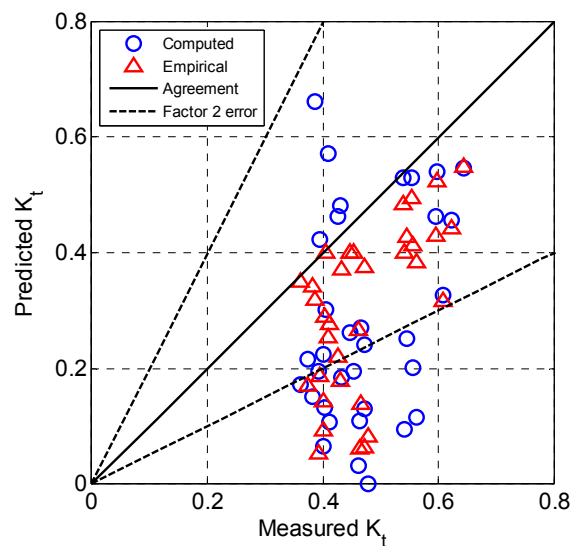


Figure 3-5: Comparison of K_t against measured values in NRC data

3.3.2 AAU Data

The wave transmission coefficient varies with the incident wave angle.

Figure 3-6, Figure 3-7 and Figure 3-8 show the comparison for freeboard values of $F = -0.05$ cm (submerged structure) $F = 0$ cm (structure with crest at SWL) and $F = 0.05$ cm (emerged structure).

Agreement is good for the negative freeboard in the wide range of incident wave direction, where the absolute value of the angle θ is plotted because the values of K_t for $+\theta$ and $-\theta$ should be the same for the case of alongshore uniformity. For the structure crest at the SWL, agreement is good for near normal incident conditions, but K_t is underpredicted for incident wave angles $|\theta| > 30^\circ$. For the positive freeboard, agreement is found reasonable but the computed values of K_t scatter about the measured values of 0.2 – 0.3.

The measured and computed transmission coefficients decrease somewhat with the increase of wave angle, regardless of the freeboard value.

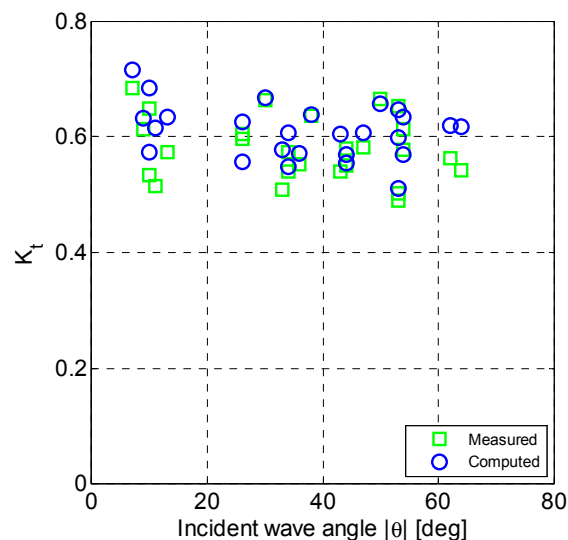


Figure 3-6: Measured and computed K_t for oblique waves and $F = -0.05$ cm in AAU data

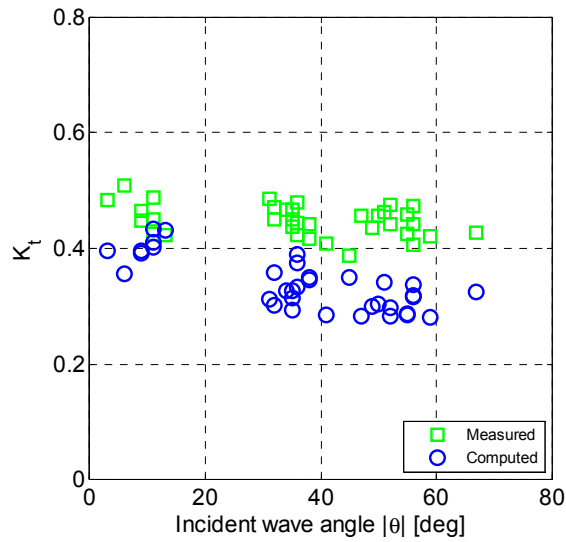


Figure 3-7: Measured and computed K_t for oblique waves and $F = 0$ cm in AAU data

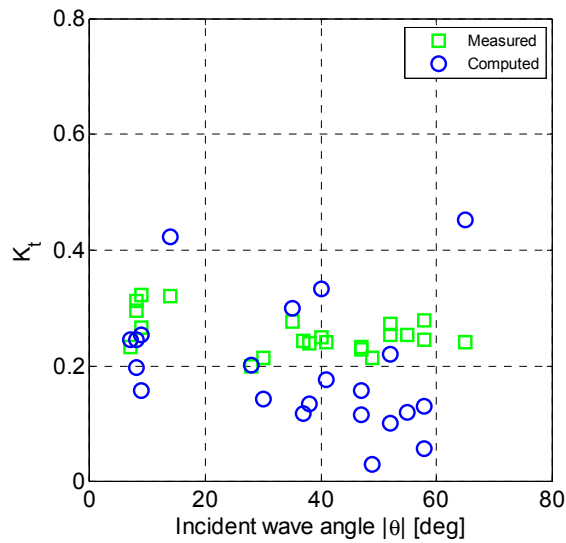


Figure 3-8: Measured and computed K_t for oblique waves and $F = +0.05$ cm in AAU data

Figure 3-9 shows the wave transmission coefficients measured in AAU experiments, computed by CSHORE and predicted by the empirical formula of

Tomasicchio, et al. (2011) against the normalized freeboard (F/H_i) which is regarded as the most important parameter for wave transmission. The empirical formula has been developed for normal incident waves ($\theta = 0$) but is included in Figure 3-9 because transmission coefficients over low-crested breakwaters do not depend significantly on the incident wave angle within the tested conditions ($0 < |\theta| < 67^\circ$ and $F = -0.05$ cm to 0.05 cm).

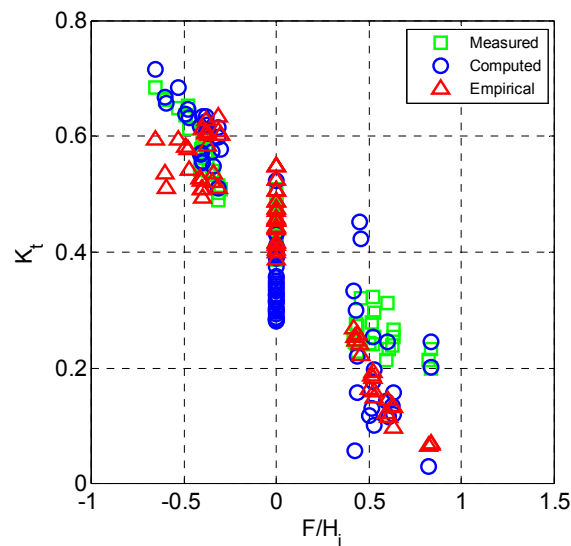


Figure 3-9: Comparison of K_t vs normalized freeboard in AAU data

The transmission coefficients computed by CSHORE and predicted by the empirical formula are plotted against the corresponding measured value in Figure 3-10. Agreement is mostly within 50% errors for transmission coefficients $K_t > 0.3$ and mostly within a factor of 2.0 for $K_t < 0.3$.

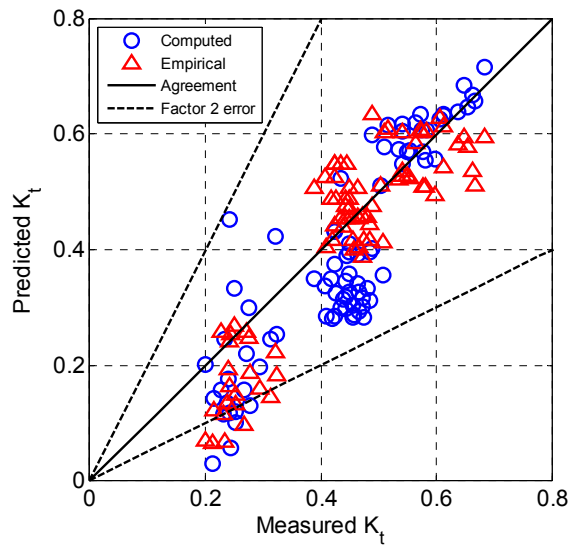


Figure 3-10: Comparison of K_t against measured values in AAU data

Chapter 4

DAMAGE ON TRUNK

Damage variations on the trunk for low-crested breakwaters (LCS) were analyzed. Computed damage by CSHORE was compared with two wave basin damage data on LCS.

The first section of this chapter describes the experimental setup for each data set. Then, analysis of experimental data is presented. In the third section, numerical model input and calibrated parameters are described. Finally, computed and measured values are compared.

4.1 Available Data

Use is made of two data sets on stability of LCS by Vidal and Mansard (1995a) at the laboratories of National Research Council of Canada (NRC) and by Kramer and Burcharth (2003a) at Aalborg University, Denmark (AAU). Detailed information on test conditions and measured damage are included in Appendix A.

4.1.1 NRC – Structure Stability Tests

The general objective of the NRC study was to analyze LCS stability and provide design guidelines. The experiment was conducted by Vidal and Mansard (1995a) in two stages using two different wave basins. In both facilities a detached breakwater was built and subjected to unidirectional irregular waves, as already described in section 3.1.1. Influence on structure stability of crest freeboard, wave height and steepness was studied.

In order to analyze damage on different sections and to avoid rebuilding the entire breakwater after each test, a steel frame and a wire mesh were used to partially cover the breakwater, exposing the specific sections to be analyzed. The trunk was divided into four sections: total section (TS), front slope (FS), crest (C) and back slope (BS). The head was divided into two sections: front head (FH) and back head (BH) with arc angles of 60° and 120° , respectively, as shown in Figure 4-1.

After each test, structure damage was measured in two ways: by counting the number of displaced stones (damage S_v) and by calculating the eroded cross-sectional area from profile measurements (damage S_p), the latter being done only for trunk sections. Damaged sections were rebuilt after each test. Test conditions and structure characteristics are summarized in Table 3-1. Detailed data are shown in Table A-1.

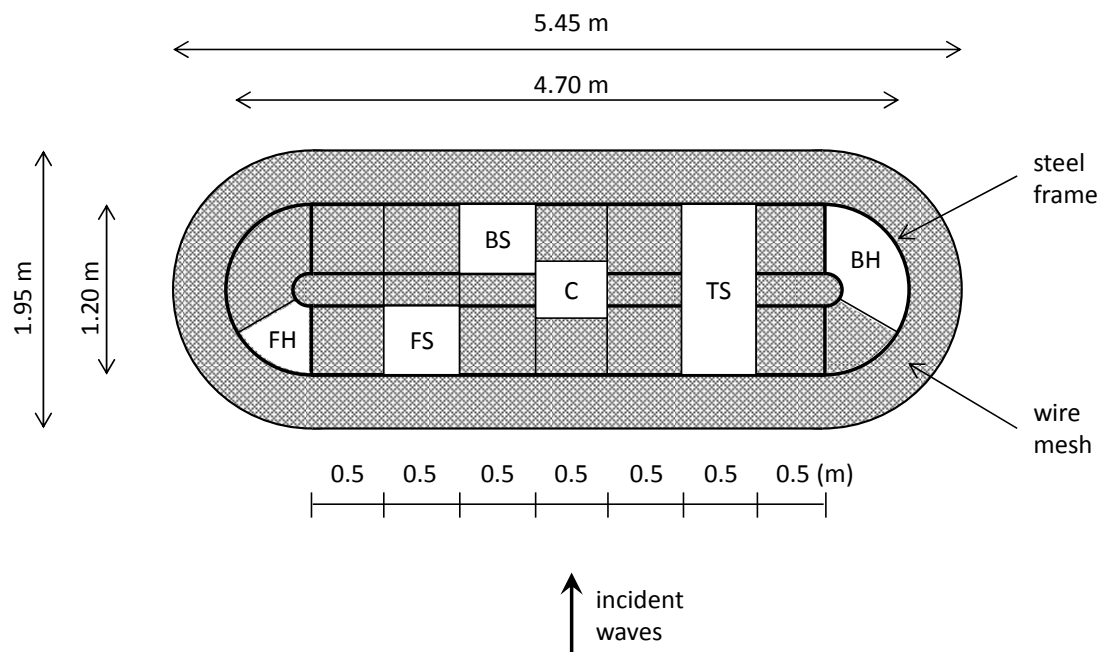


Figure 4-1: Trunk and head sections of the LCS in NRC experiments

4.1.2 AAU – Structure Stability Tests

The stability tests were carried out using multidirectional waves in the wave basin at Aalborg University, Denmark. The objective of this experiment was to supplement existing stability tests on LCS and to identify the influence of: wave angle and directionality, wave height and steepness, crest width, freeboard and structure slope.

A semidetached breakwater was built as shown in Figure 4-2. Colored stones were used to identify sections on the trunk and round head. The trunk was divided into three sections: seaward slope (SS) crest (C) and leeward slope (LS). The head was separated into: seaward head (SH), middle head (MH) and leeward head (LH), each covering an arc angle of 60° as shown in Figure 4-3.

Tests blocks were defined by fixed water level, predominant wave direction and steepness. In each test block, incident wave height was increased until severe damage was observed on the LCS. Three to five tests per block were executed. Damage was measured after each test by counting the number of displaced stones. The breakwater was rebuilt after each test block. Tests conditions and structure characteristics are summarized in Table 4-1. Detailed data are shown in Table A-3.

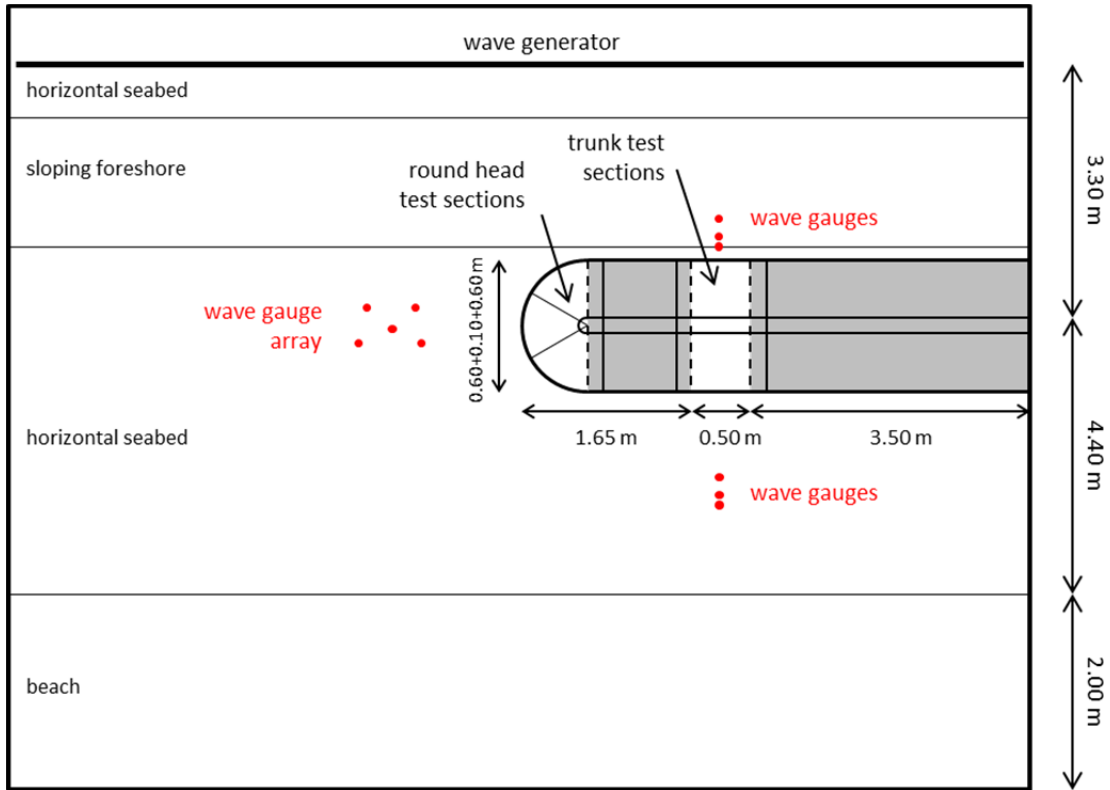


Figure 4-2: Wave basin layout in AAU stability experiments

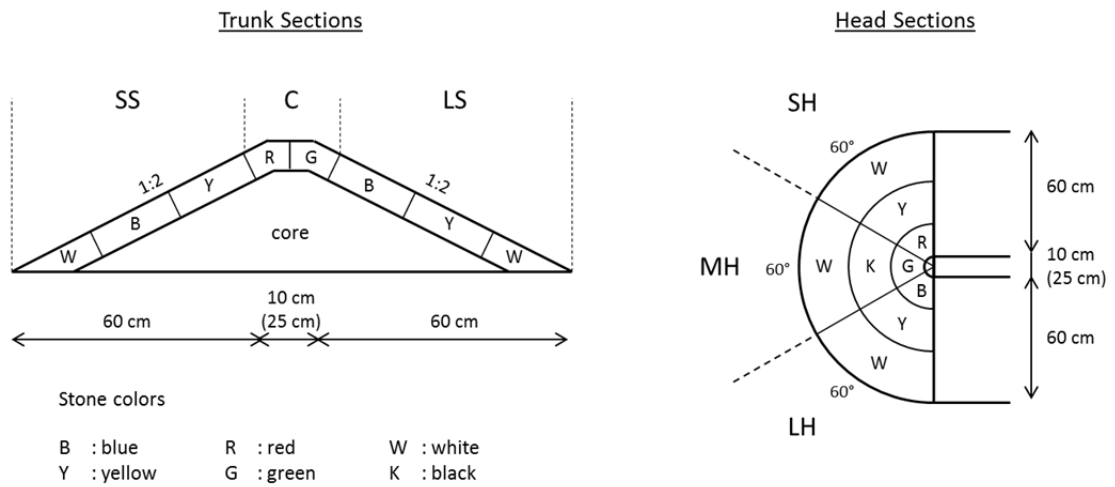


Figure 4-3: Trunk and head sections of the LCS in AAU experiments

Table 4-1: Experiment conditions in AAU Stability tests

Parameter	Value
Number of tests	69
Structure height (cm)	30
Crest width B_c (cm)	10, 25
Seaward slope	1/2
Landward slope	1/2
Freeboard F (cm)	-10 to 5
Armor stone size D_{n50} (cm)	3.3
Core stone size D_{n50} (cm)	1.4
Wave angle θ (deg)	-21 to 26
Wave height H_{m0} (cm)	4 to 25
Wave period T_p (s)	0.9 to 2.5
Test duration (min)	14 to 136*

* Significant wave height was increased in test blocks until severe damage was observed.

4.2 Data Analysis

In NRC experiments, damage on trunk sections was measured in two ways, which are described in the following.

4.2.1 Measured Damage S_v and S_p

Damage S_v is calculated by counting the number of stones displaced at least one nominal diameter D_{n50} and using the following formula:

$$S_v = \frac{N_y D_{n50}}{(1-n_p) l_y} \quad (4-1)$$

Where

- S_v : damage based on number of displaced stones
 D_{n50} : nominal stone diameter
 N_y : number of displaced stones over the alongshore length l_y
 n_p : porosity of the armor layer
 l_y : alongshore length of armor layer

Damage S_p is calculated using the eroded cross-sectional area from profile measurements which is normalized by the nominal stone diameter.

$$S_p = \frac{A_e}{D_{n50}^2} \quad (4-2)$$

Where

- S_p : damage based on measured profile
 A_e : eroded area of the cross-shore profile relative to the initial profile.

If the volume of the displaced stones is equal to the eroded stone volume, as indicated below, then damage S_v and S_p are equal.

$$S_v = S_p; \text{ if } \rightarrow N_y D_{n50}^3 = (1 - n_p) A_e l_y \quad (4-3)$$

Dislodged stones can fall into the void left by other displaced stones. Hence, S_v is expected to be larger than S_p .

Relation between damage S_v and S_p was examined using trunk damage measurements of NRC tests, where 6 tests exceeded destruction damage criterion

(removal of core stone) given by Vidal, et al. (1992). These 6 tests were excluded in the following. Figure 4-4 shows S_v vs S_p for trunk sections TS, FS and BS.

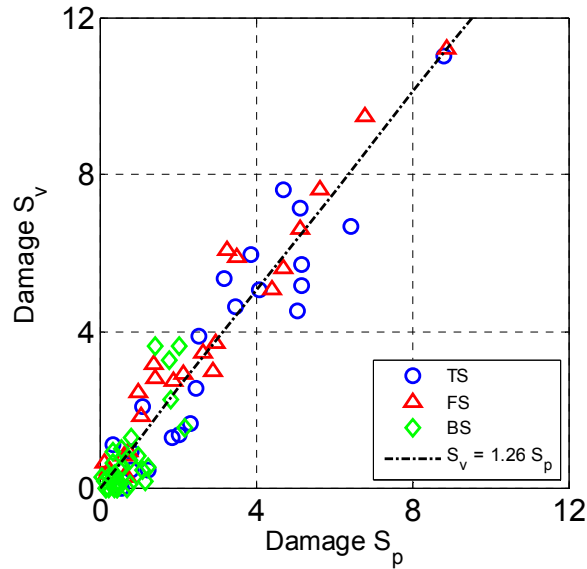


Figure 4-4: Measured damage S_v versus S_p for trunk sections in NRC data

Damage S_v turns out to be larger than S_p and a linear regression analysis yields:

$$S_v = 1.26 S_p \quad (4-4)$$

Relation between damage S_v and S_p for all the trunk sections including the crest (C) in NRC data was also examined, obtaining essentially the same linear relation ($S_v = 1.24 S_p$). In the subsequent comparisons of the measured and computed S_v , the computed damage S_p is converted to S_v using Equation (4-4) for the NRC structure with 1/1.5 slope, because the numerical model cannot predict the number of

displaced stones, as described in section 2.3. However, the accuracy of Equation (4-4) is uncertain for the AAU structure with 1/2 slope.

4.2.2 Trunk Sections Damage Relation

Measured damage on the trunk sections of NRC data was examined within destruction damage level given by Vidal, et al. (1992).

Measured damage on TS section is compared to the sum of the trunk sections (FS+C+BS), as depicted schematically in Figure 4-5. The summed section (FS+C+BS) includes two overlapping zones near the crest. Comparisons of measured damage on the two sections are presented in Figure 4-6, for both damage definitions S_p and S_v .

Damage including the overlapping zones on section (FS+C+BS) was not larger. Agreement for these two similar sections is found to be mostly within a factor of two, indicating the degree of uncertainty of the measured damage using the experimental setup in Figure 4-1.

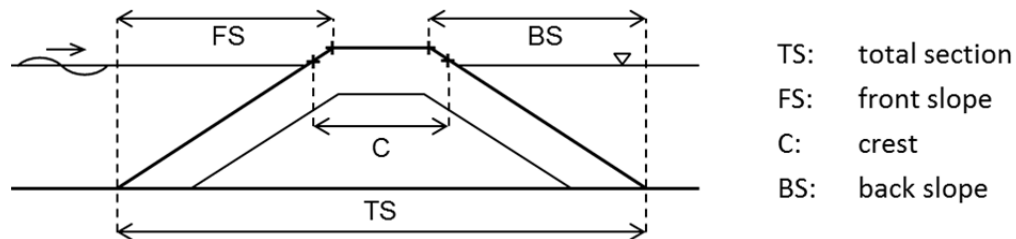


Figure 4-5: Trunk sections in NRC experiments

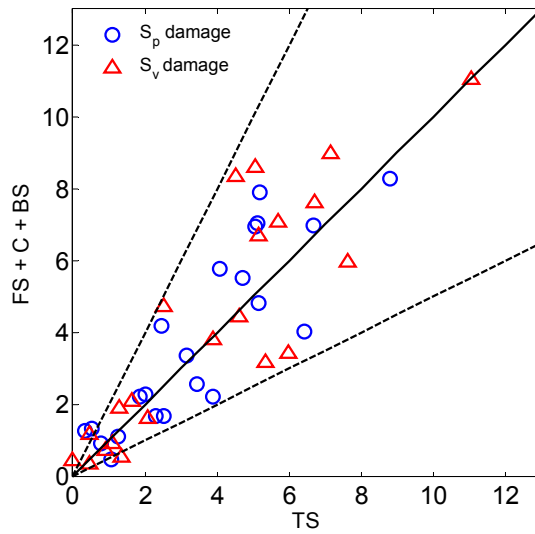


Figure 4-6: Comparison of measured damage on trunk sections (TS) and (FS+C+BS) in NRC data

4.3 Numerical Model Setup

Specified input and calibrated parameters for computation of structure damage are described on the following sections.

4.3.1 Specified Input

The same input as described in section 3.2.1 for wave transmission computation is used for the damage computation. In addition, test sequence is considered for AAU tests. The temporal variations of the measured wave height and period are specified as input to the numerical model to reproduce the measured cumulative damage in each test block as explained in section 4.1.2.

4.3.2 Calibrated Parameters

Two parameters CSTABN and TANPHI in the numerical model affect computed damage. The damage sensitivities to these parameters are examined in the following.

a) CSTABN

This parameter is related to the critical stability number for initiation of stone movement. It determines the critical instantaneous velocity for stone movement, as described in the report of Kobayashi (2013). The decrease of CSTABN increases the probability of stone movement.

Damage on TS section for CSTABN = 0.6, 0.5 and 0.4 was computed for NRC and AAU experiments. Results are shown in Figure 4-7 and Figure 4-8, respectively. For this analysis TANPHI parameter was 0.63.

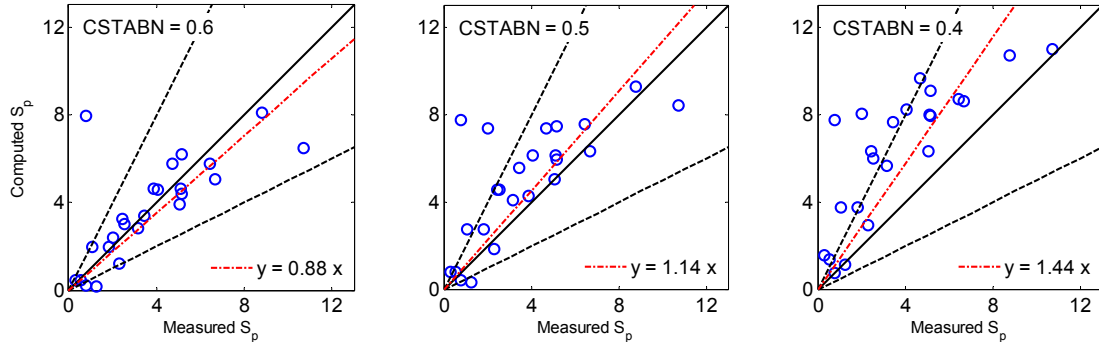


Figure 4-7: Calibration of CSTABN for damage S_p on TS section in NRC data

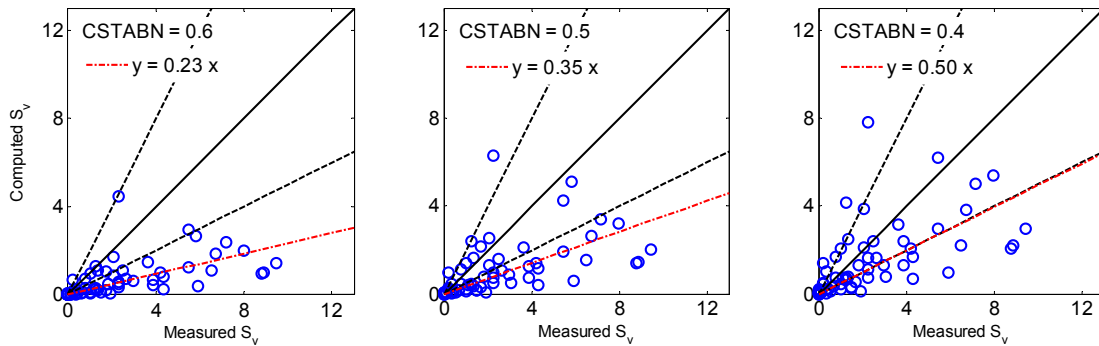


Figure 4-8: Calibration of CSTABN for damage S_v on TS section in AAU data

Computed damage on TS section indicates $CSTABN = 0.5$ or 0.6 for NRC data but $CSTABN$ alone cannot reproduce AAU data. Computed damage can be increased by decreasing $TANPHI$ parameter. In the following, $CSTABN=0.6$ which is the value calibrated by Kobayashi et al. (2010).

b) TANPHI

This parameter is associated with the bottom slope effect on the rate of stone transport on a steep upward or downward slope. The value of $TANPHI = 0.63$ is close to the slope of 0.67 for NRC data. Computed damage for AAU data with the slope of 0.5 increases by reducing $TANPHI$ from 0.63 .

Damage over TS section is computed for $TANPHI = 0.63$ and 0.54 in Figure 4-9 and Figure 4-10. The left panels of these figures correspond to those in Figure 4-7 and Figure 4-8, so as to show the effects of $CSTABN$ and $TANPHI$ separately.

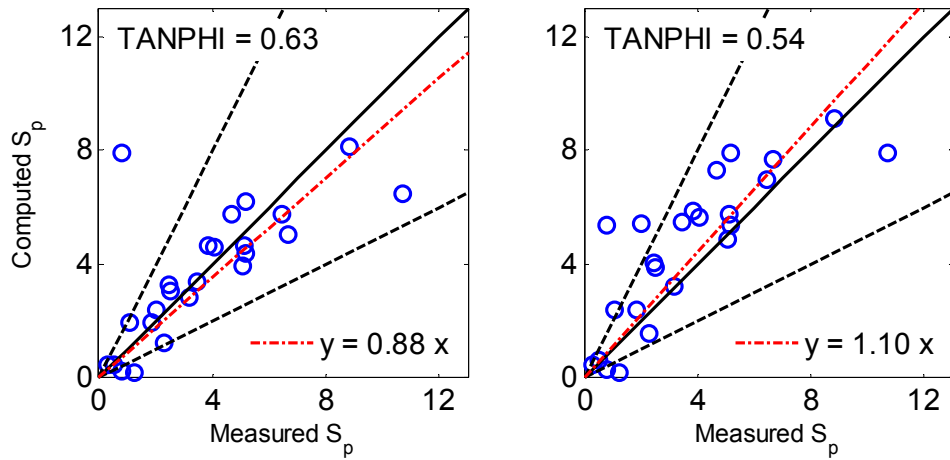


Figure 4-9: Calibration of TANPHI for damage S_p on TS section in NRC data

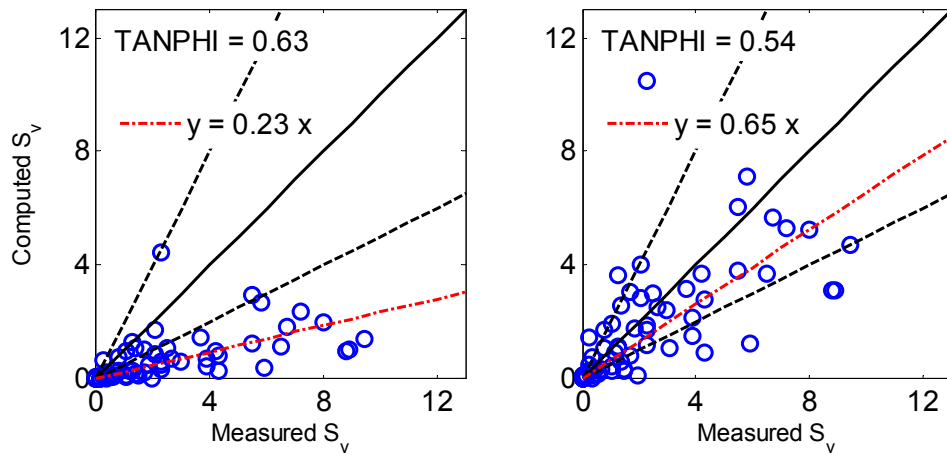


Figure 4-10: Calibration of TANPHI for damage S_v on TS section in AAU data

Agreement is reasonable for the combination of TANPHI = 0.54 and CSTABN = 0.6. Damage on TS section is slightly overpredicted for NRC data and somewhat underpredicted for AAU data. Most of the compared values are within errors of a factor of two for both data sets. These calibrated values are adopted in the

following computations but the above calibrations indicate the empirical nature of the stone transport model in CSHORE.

4.4 Comparison with Data

Comparisons for damage on different trunk sections are presented for NRC and AAU data separately.

4.4.1 NRC Data

Damage for NRC data was computed in two different ways, as described in section 2.3. The first one (ISED AV = 2) allows erosion only in sections of no wire mesh. The second one (ISED AV = 1) neglects the effect of the wire mesh, and damage was obtained from the eroded profile computed for the case of no wire mesh over the entire trunk.

The comparison for each trunk section depicted in Figure 4-5 is shown in Figure 4-11 (ISED AV = 2) and Figure 4-12 (ISED AV = 1). The numerical model does not account for the smaller size of the core stone with $D_{n50} = 1.9$ cm underneath the armor stone with $D_{n50} = 2.5$ cm of two-layer thickness and underpredicts the damage S_p for 6 tests involving the core stone removal. These 6 tests are excluded from these figures.

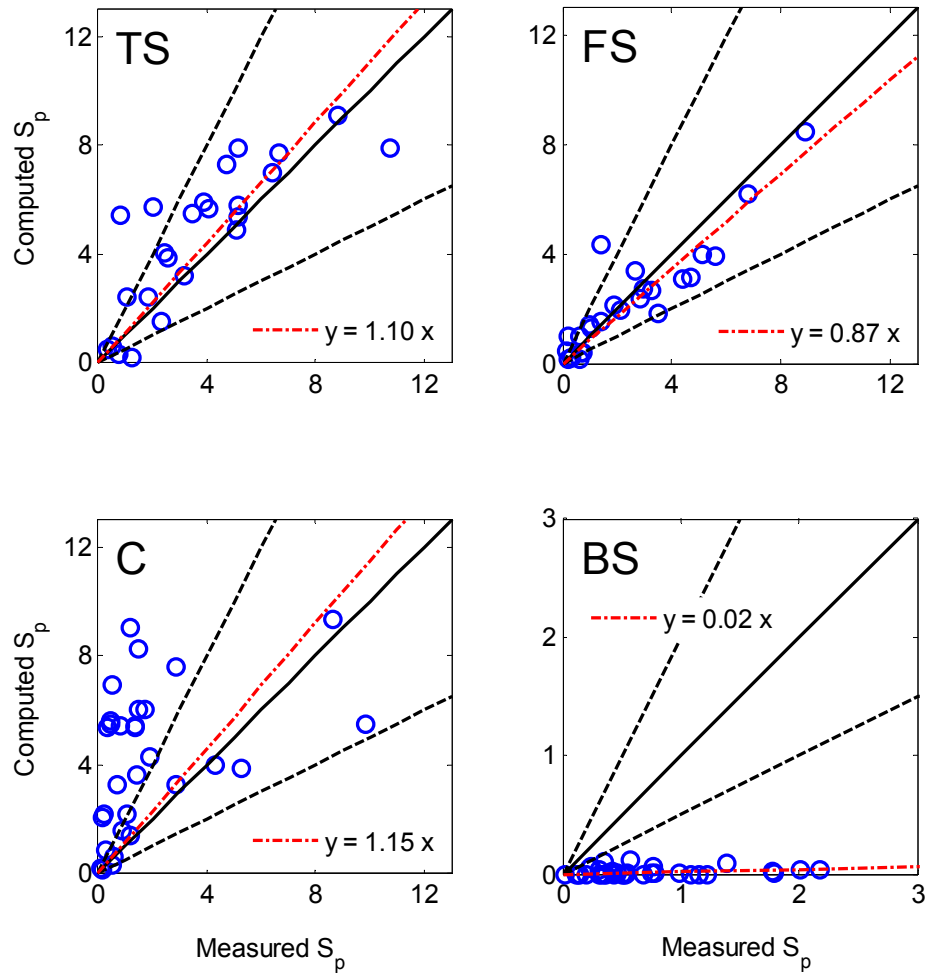


Figure 4-11: Damage comparison on trunk sections in NRC data with ISEDAV = 2

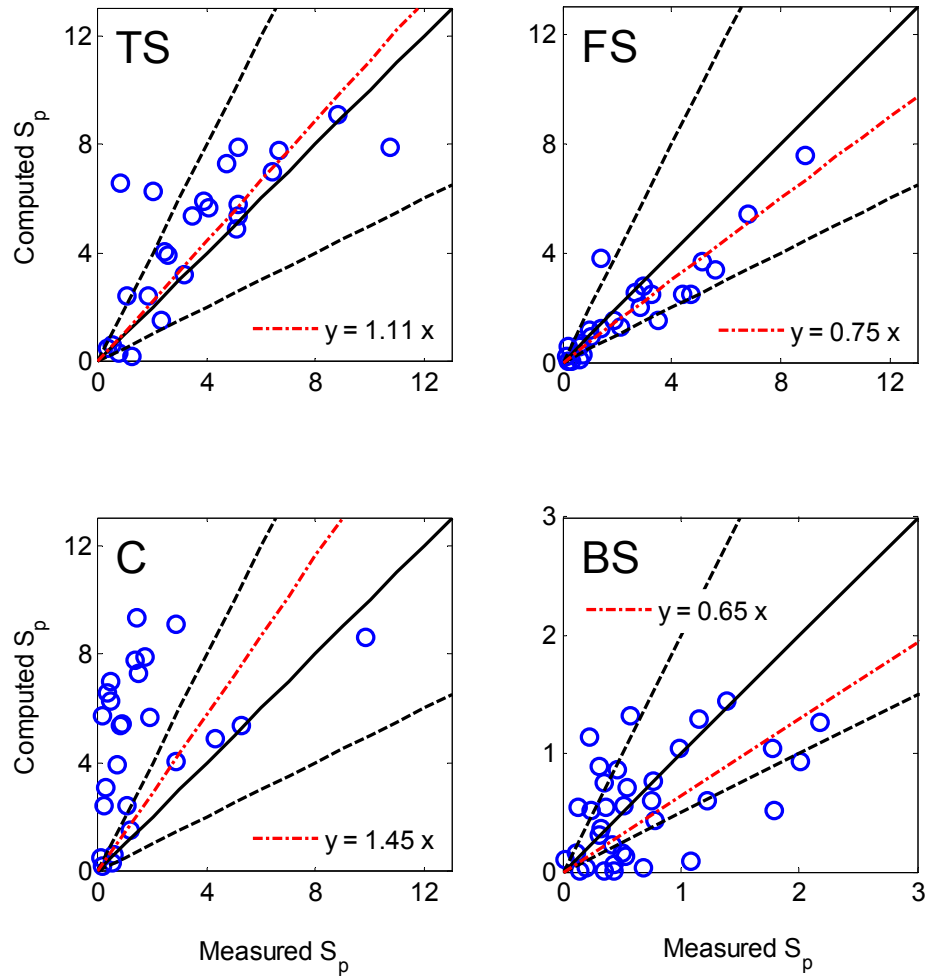


Figure 4-12: Damage comparison on trunk sections in NRC data with ISEDAV = 1

Regardless of the choice of ISEDAV, agreement for TS and FS sections is reasonable and damage is predicted within a factor of two for almost all tests. Damage on C section is overpredicted for both ISEDAV = 1 and 2, which might be related to the peculiarity of the crest (C) section in NRC experiment as discussed in section 4.2.2. On the other hand, agreement for BS section is significantly improved with the choice of ISEDAV = 1. This implies that the back slope damage may be influenced by

the stone movement under the mesh seaward of the back slope. In the following, $ISEDAV = 1$ is adopted for NRC data and no wire mesh was used for AAU data.

4.4.2 AAU Data

Damage in AAU experiments was based on the measured number of displaced stones (S_v damage). The numerical model assumes a homogeneous stone structure. The ratio between the core and armor layer stone sizes in AAU experiments was $D_{n50\ core}/D_{n50\ armor} = 0.42$, while this ratio was 0.66 in NRC experiments. To evaluate the effect of the different stones sizes, the computed damage on the assumed homogeneous structure based on the armor layer stone in the previous computations is compared with that for the armor layer with impermeable core. The impermeable bottom $z_p(x)$ in Figure 2-1 is chosen to be located at the upper boundary of the core for the impermeable core computation.

Computed damage on each trunk section, depicted schematically in Figure 4-13, is shown for the homogeneous structure with permeable core in Figure 4-14 and for the structure with impermeable core in Figure 4-15. In both figures, data are separated for normal and oblique incident waves.

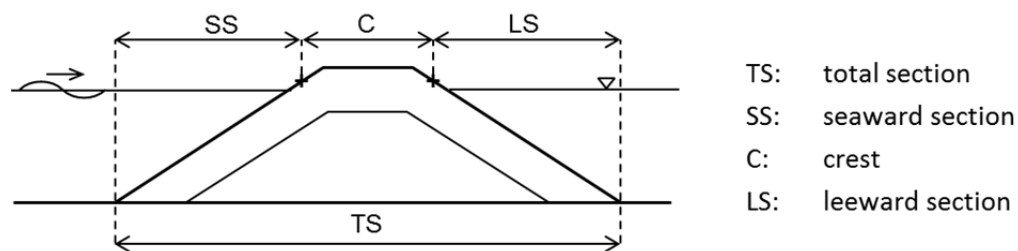


Figure 4-13: Trunk sections in AAU experiments

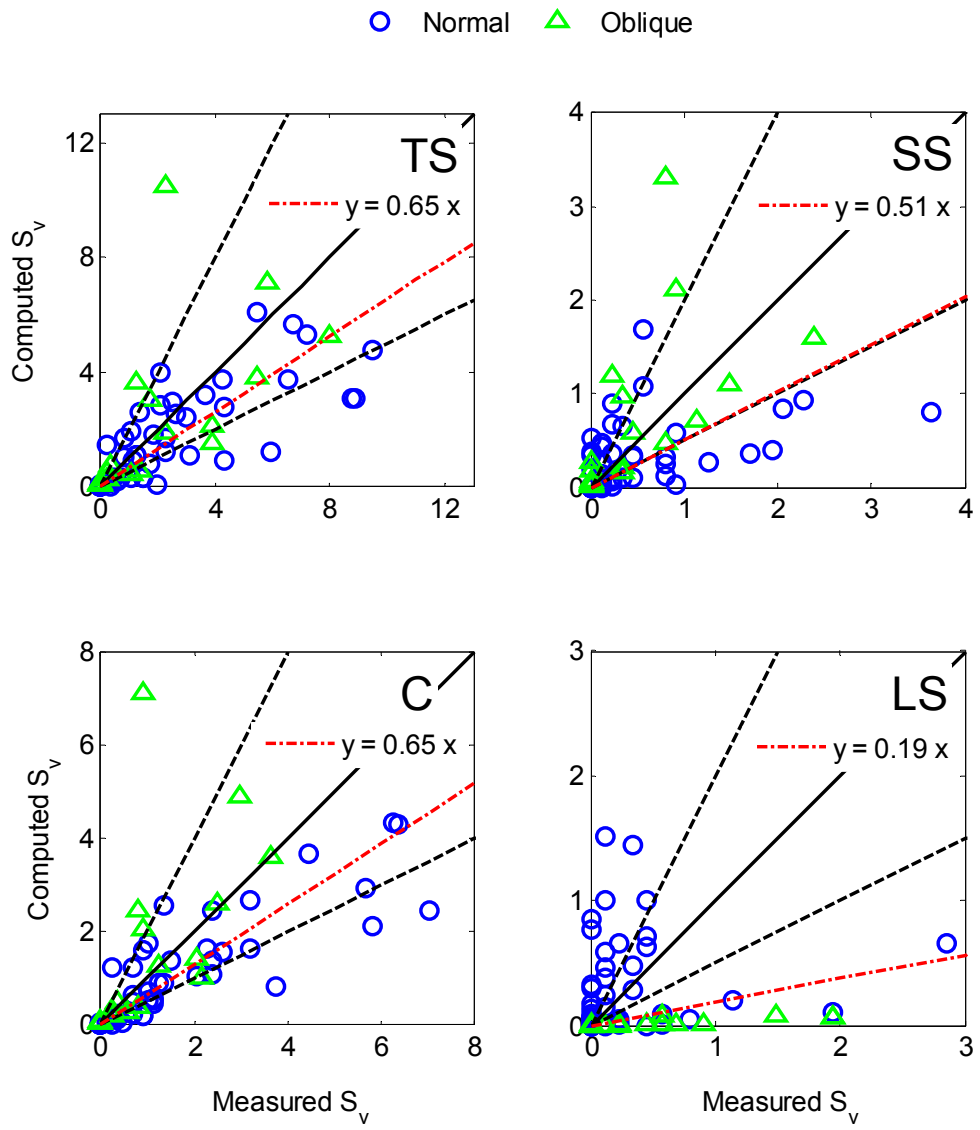


Figure 4-14: Damage comparison on trunk sections in AAU data with permeable core

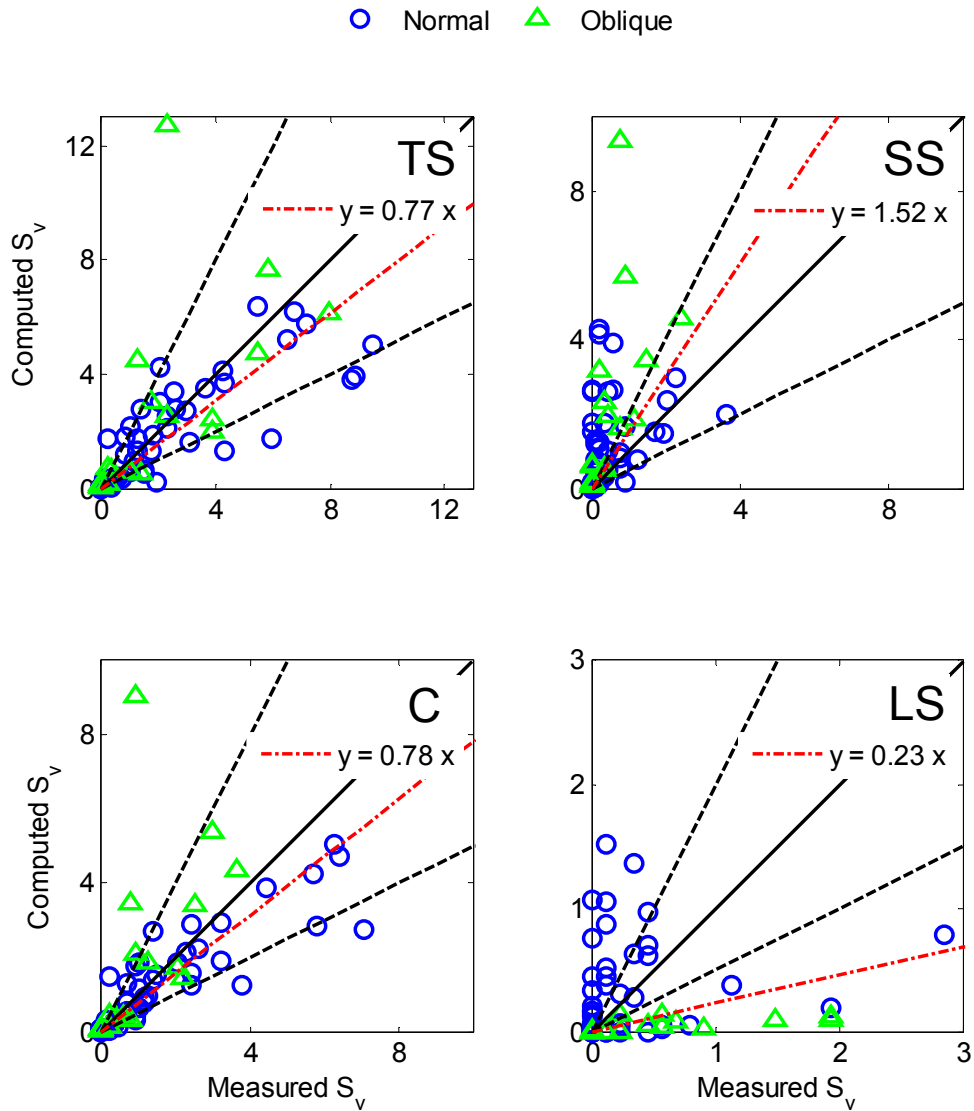


Figure 4-15: Damage comparison on trunk sections in AAU data with impermeable core

Damage on TS section is predicted mostly within a factor of two under both assumptions: homogeneous permeable structure and impermeable core structure. The actual structure was somewhere between these two limiting cases. The computed damage is larger for the impermeable core as expected.

Damage on SS section turns out to be sensitive to the core permeability because of the noticeable difference in Figure 4-14 and Figure 4-15. The reason is not clear but may be related to the relatively small damage measured on SS section. Damage prediction in C section is similar to that on TS section, as C section accounts for the majority of damage in most of the tests. Finally, small damage on LS section is hard to predict accurately and the agreement is the worst of all trunk sections. The computed damage difference is minor in comparison with the prediction accuracy.

Chapter 5

DAMAGE ON HEAD

Similarity of trunk and head damage for low-crested breakwaters (LCS) was examined for head damage prediction with CSHORE. Comparison is made of computed and measured damage at different sections of round head LCS with base diameter equal to the trunk base width. Use is made of head damage in the NRC and AAU wave basin experiments where the measured trunk damage has been used in Chapter 4.

First, similarity of trunk and head damage based on measured values in each experiment is examined. Second, comparison between computed and measured head damage is presented.

5.1 Similarity of Trunk and Head Damage

In NRC experiments, head damage was measured on two sections of the round head: front head (FH), with the front arc angle of 60° ; and back head (BH), with the remaining arc angle of 120° , as depicted in Figure 4-1. In AAU experiments, the round head was divided into three sections with arc angles of 60° : seaward head (SH), middle head (MH) and leeward head (LH), as depicted in Figure 4-3.

Similarity of head and trunk damage was analyzed by examining damage relations between front head sections FH and SH and back head sections BH and (MH+LH) with several different trunk sections in each experiment as explained in the following.

5.1.1 Front Head Similarity

Measured damage on the front head (FH) section of NRC experiments was compared with measured damage on the trunk front slope (FS) section and the trunk front slope plus the trunk crest (C_{TS}) sections, as depicted schematically in Figure 5-1, where damage on the trunk crest (C_{TS}) was not measured specifically and it was estimated as the difference between damage on the total trunk section (TS) and damage on the front and back trunk slopes (FS+BS). The comparisons are shown in Figure 5-2. Damage on FH section was similar to damage on FS section, mostly within a factor of 2. Damage on FH section was smaller than damage on (FS+ C_{TS}) section.

Measured damage on the seaward head (SH) of AAU experiments was compared with measured damage on the trunk seaward slope (SS) and the trunk seaward slope plus trunk crest (C), as depicted schematically in Figure 5-1. The comparisons are shown in Figure 5-3. Damage on SH and SS sections were well correlated, although damage on SH tended to be larger than damage on SS section. Damage on SH section was smaller than damage on (SS+C) section.

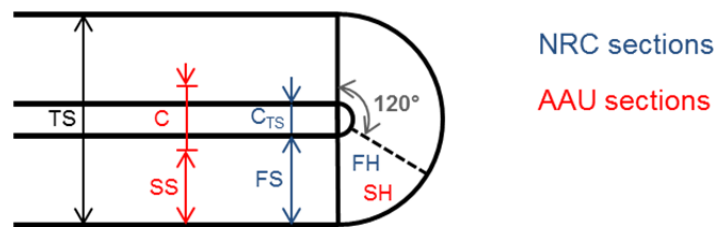


Figure 5-1: Trunk and head sections for front head damage prediction

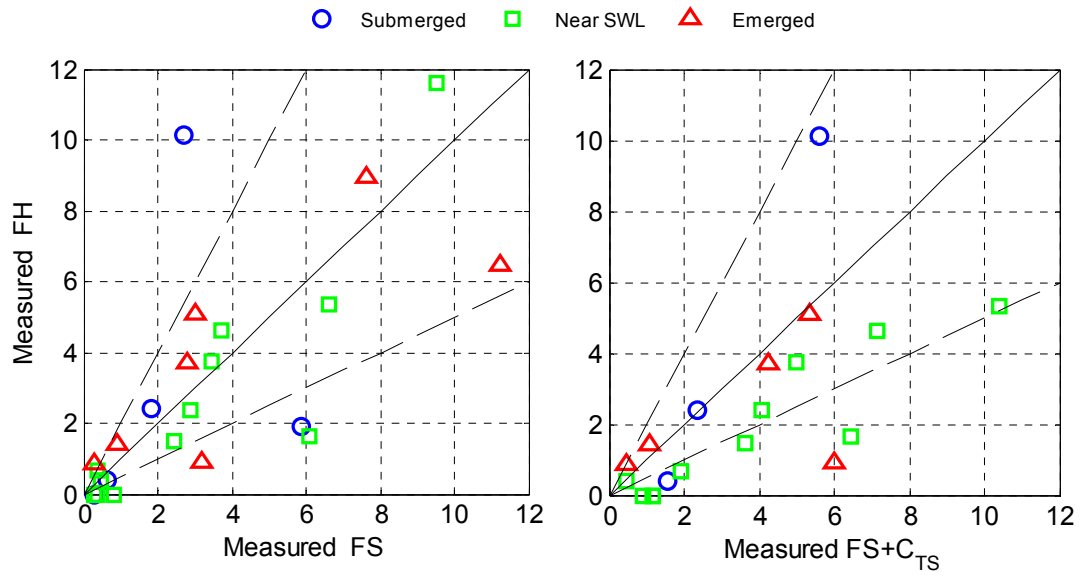


Figure 5-2: Similarity of measured head damage FH and measured trunk damage in NRC experiments with S_v damage

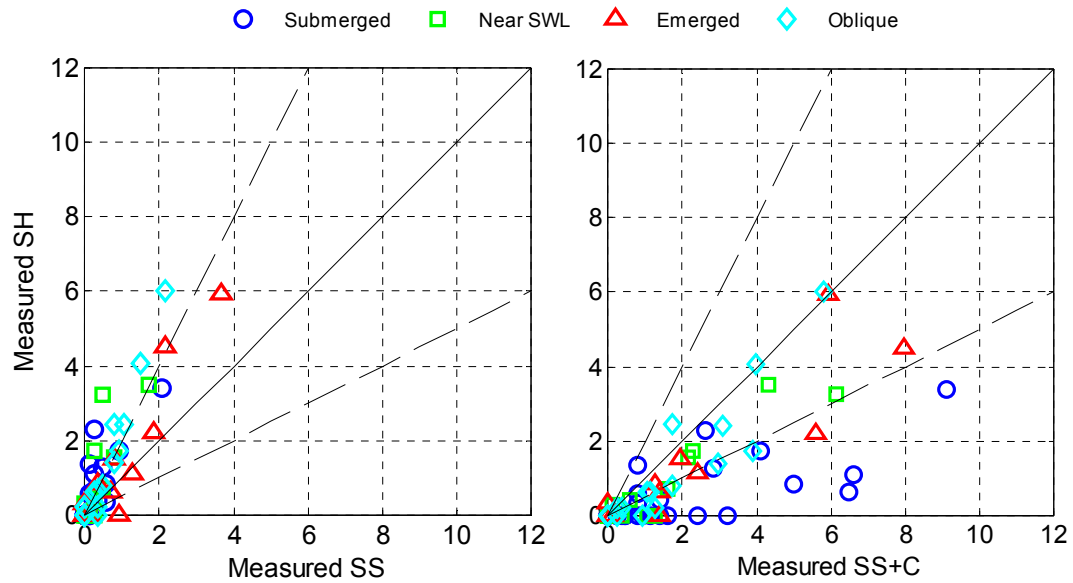


Figure 5-3: Similarity of measured head damage SH and measured trunk damage in AAU experiments with S_v damage

Figure 5-4 summarizes the computed results for damage prediction on front head sections FH and SH. Red thick lines represent trunk sections analyzed for damage similarity. The front trunk (FT) section, which is the same as FS section is chosen for front head damage prediction.

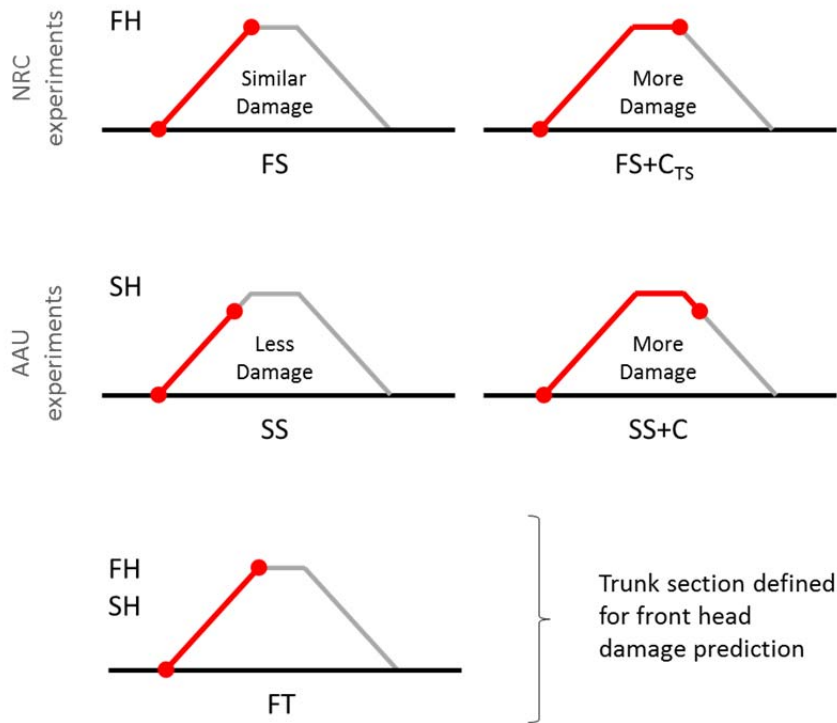


Figure 5-4: Definition of trunk section FT for front head damage prediction

5.1.2 Back Head Similarity

Measured damage on the back head (BH) section of NRC experiments was compared with measured damage on the trunk total section (TS) and the trunk crest (C_{TS}) plus the trunk back slope (BS) sections, as depicted schematically in Figure 5-5. The comparisons are shown in Figure 5-6. Damage on BH section was smaller than

damage on TS section, particularly for submerged structures, but somewhat larger than damage on (C_{TS}+BS) section.

Measured damage on the back head (MH+LH) section of AAU experiments was compared with measured damage on the trunk total section (TS) and the trunk crest (C) plus the trunk leeward slope (LS) sections, as depicted schematically in Figure 5-5. The comparisons are shown in Figure 5-7. Damage on (MH+LH) section was smaller than damage on TS section and similar to damage on (C+LS) section, with exception of submerged structures, for which head damage (MH+LH) was smaller than damage on trunk TS and (C+LS) sections.

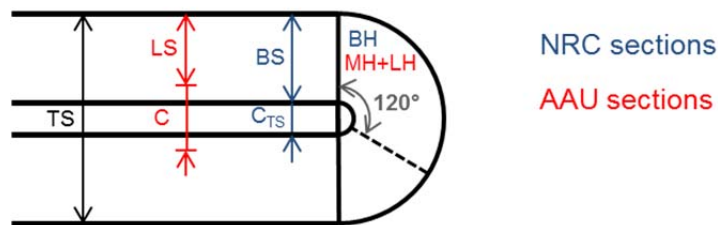


Figure 5-5: Trunk and head sections for back head damage prediction

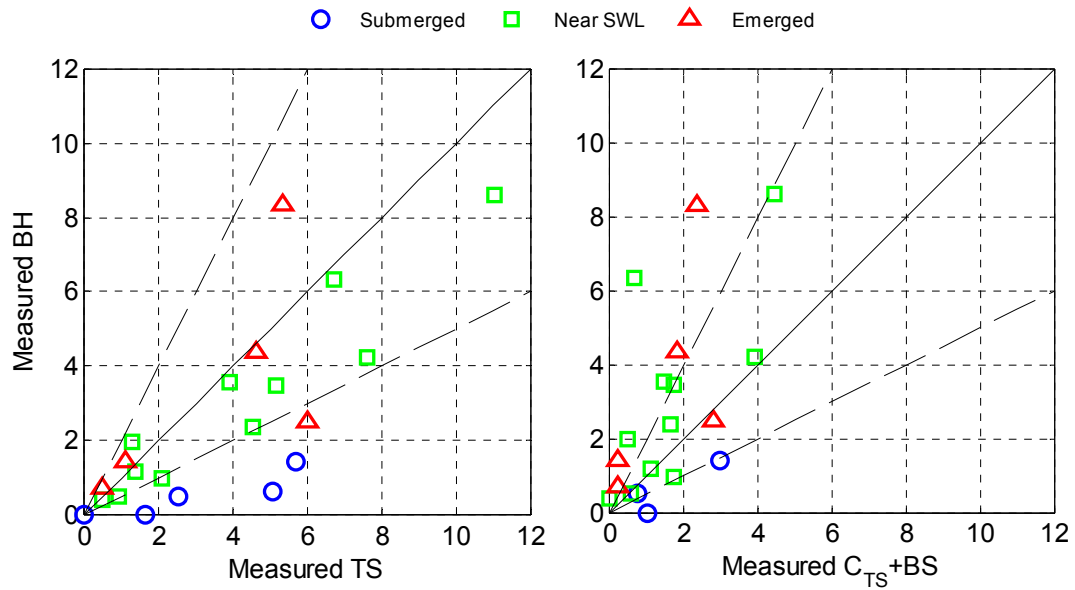


Figure 5-6: Similarity of measured head damage BH and measured trunk damage in NRC experiments with S_v damage

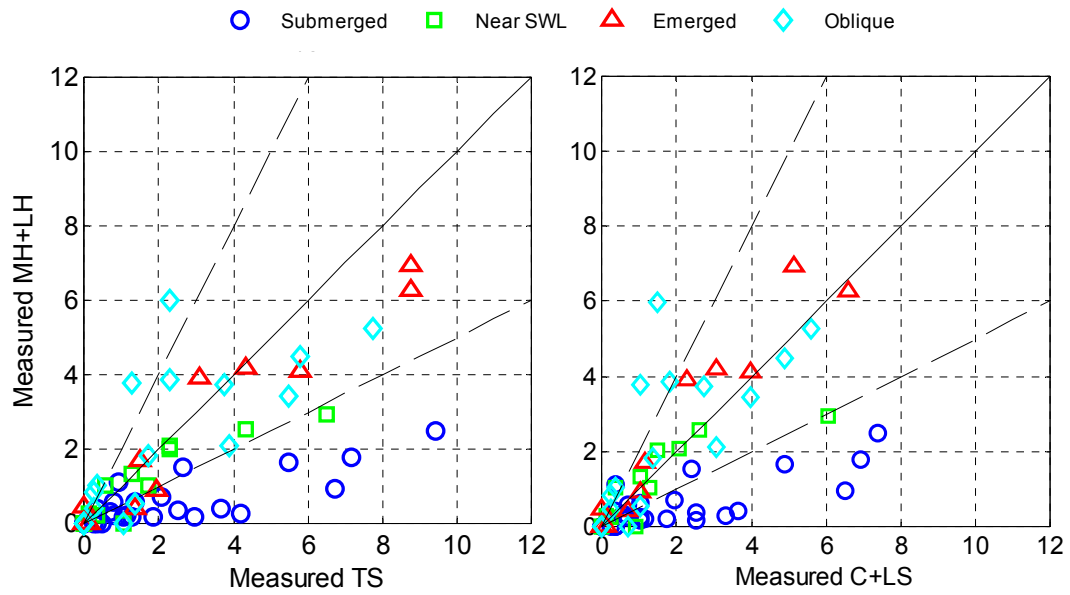


Figure 5-7: Similarity of measured head damage (MH+LH) and measured trunk damage in AAU experiments with S_v damage

Figure 5-8 summarizes the computed results for damage prediction of back head BH and (MH+LH) sections. Red thick lines represent trunk sections analyzed for damage similarity. The back trunk (BT) section is chosen for back head damage prediction, where damage on BH and (MH+LH) sections of submerged structures is expected to be overpredicted by use of this similarity assumption. It is noted that the damage similarity between BH and BT sections cannot be directly assessed using the NRC and AAU data, because damage on BT section was not measured specifically.

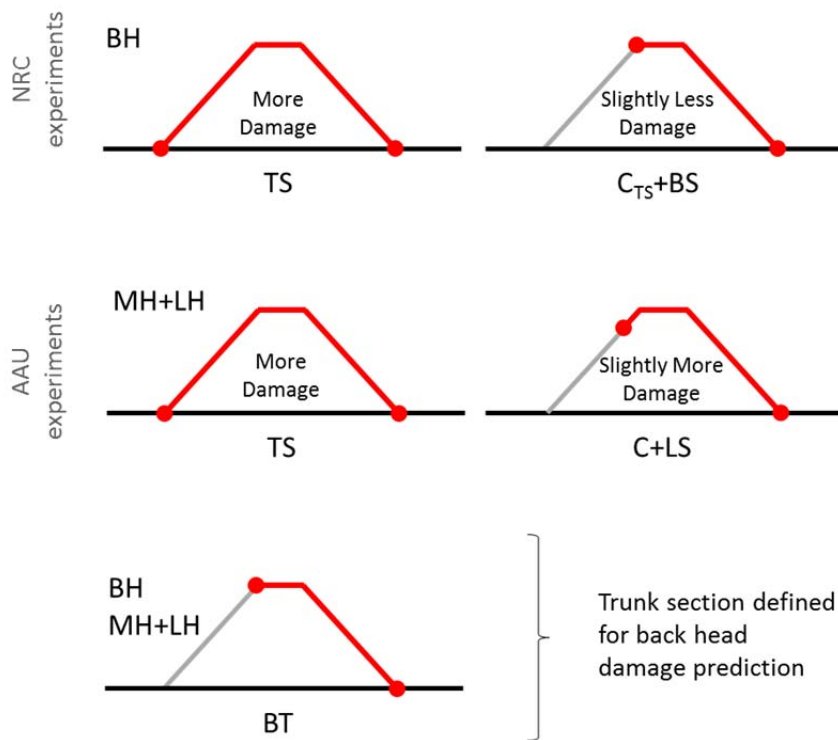


Figure 5-8: Definition of trunk section BT for back head damage prediction

5.2 Comparison with Data

Head damage prediction with CSHORE, based on damage similarity, is compared with NRC and AAU data.

5.2.1 NRC Data

Figure 5-9 shows the measured damage on front head (FH) and back head (BH) sections of NRC experiments in comparison with the computed damage on front trunk (FT) and back trunk (BT) sections, respectively.

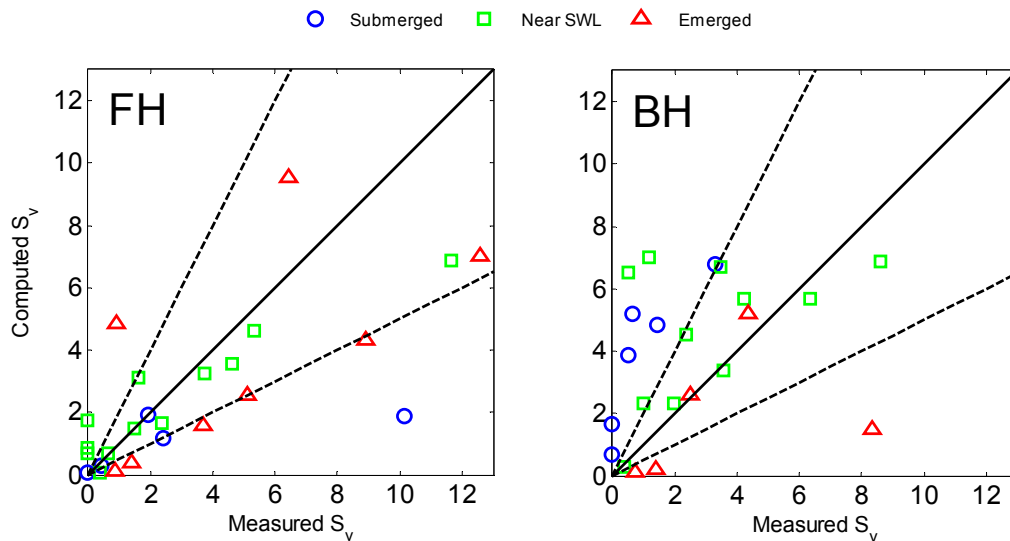


Figure 5-9: Measured and computed damage S_v for head sections FH and BH in NRC experiment

Damage on FH section is predicted mostly within a factor of two. Damage prediction on BH section shows similar agreement, except for submerged structures as expected from the damage data analysis in section 5.2.1.

5.2.2 AAU Data

Figure 5-10 shows the measured damage on the seaward head (SH) and the back head (MH+LH) sections of AAU experiments in comparison with the computed damage on front trunk (FT) and back trunk (BT) sections, respectively.

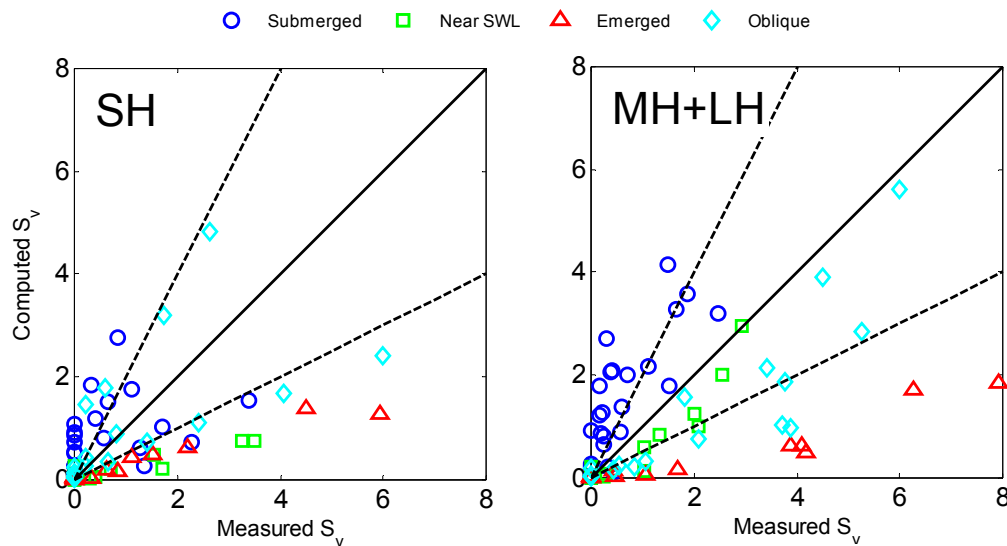


Figure 5-10: Measured and computed damage S_v for head sections SH and (MH+LH) in AAU experiment

Agreement for SH section is not as good as for FH section of NRC experiments. For (MH+LH) section, damage is overpredicted for submerged structures and underpredicted for emerged structures, which suggests that the back head section is more sensitive to freeboard effects than trunk sections, as also reported by Vidal, et al. (1995b).

Chapter 6

EXPERIMENTS

In NRC experiments the low-crested structure (LCS) was located outside the surf zone while in AAU experiments it was located outside the surf zone or in the outer surf zone. In both experiments, the structures were placed over fixed bottom. A low-crested breakwater constructed for shore protection is typically located on a sand beach and inside the surf zone during storms. Sumer, et al. (2005) investigated local scour around low-crested structures located outside the surf zone on sand bottoms. An experiment was conducted to examine damage on a low-crested stone structure and sand transport in the vicinity of the structure inside the surf zone in the presence of wave setup and undertow current.

Experimental setup and test conditions are described in the first section of this chapter. Experimental procedure is described in the second section. Data analysis is presented in the third section. Finally, the numerical model is compared with the data.

6.1 Experimental Setup

The experiment was conducted in the wave tank of the Center for Applied Coastal Research of the University of Delaware, which was 30 m long, 2.5 m wide and 1.5 m high. The bottom consisted of fine sand on a plywood bottom slope. A partition wall in the middle of the wave tank reduced the amount of sand used for the beach and seiching development in the wave tank. The instruments used in this experiment were installed by Figlus, et al. (2011).

6.1.1 Flume Layout

The experiment was carried out in a 23 m long and 1.15 m wide section of the wave tank. The experimental layout is shown in Figure 6-1.

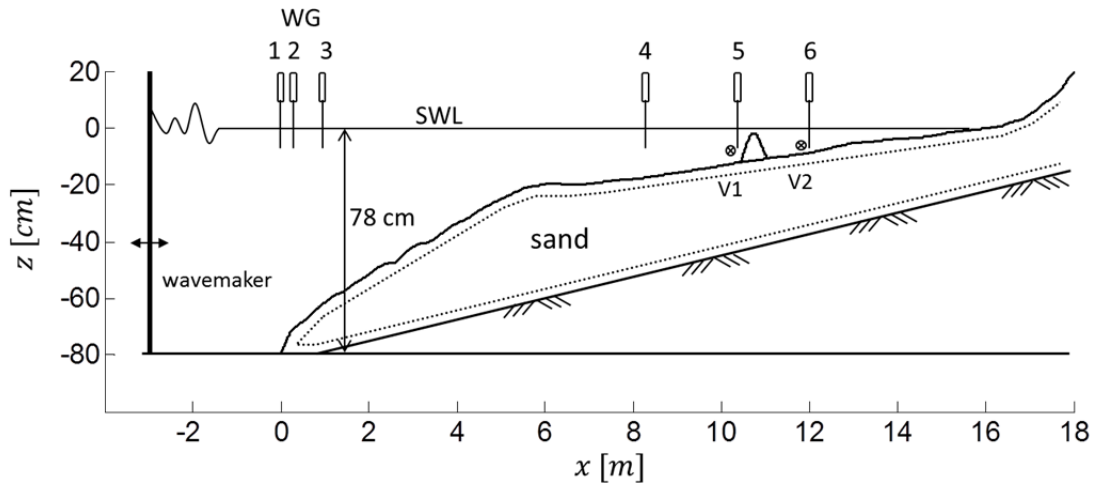


Figure 6-1: Experimental setup

Irregular waves were generated by a piston-type wave maker in water depth of 0.78 m. Six capacitance wave gauges were used to measure the cross-shore variation of the free surface elevation. Wave gauges WG1-WG3 were used to separate incident and reflected waves at approximately 3 m from the wave maker. Wave gauge WG4 was placed inside the surf zone to measure wave transformation. Wave gauges WG5 and WG6 were placed at the seaward toe and 1 m landward of the rear toe of the structure, respectively. Two Nortek Vectrino 3D acoustic Doppler velocimeters (V1 and V2) were used to measure fluid velocities at the same cross-shore locations of wave gauges WG5 and WG6. The horizontal location of each instrument is shown in Table 6-1, where the origin of the onshore coordinate x is located at WG1.

Table 6-1: Cross-shore location of instruments

Instrument	WG1	WG2	WG3	WG4	WG5	WG6	V1	V2
x [m]	0.00	0.24	0.95	8.25	10.40	12.05	10.40	12.05

A laser line scanner mounted on a motorized cart was used to measure three-dimensional bathymetry between $4.9 \text{ m} < x < 19.9 \text{ m}$. An array of three ultrasonic transducers was used to measure the beach profile between $0 \text{ m} < x < 5.9 \text{ m}$, where the 1 m overlapping zone ensured the smooth transition of the two measured profiles.

A fixed camera was installed on the top of the flume to detect stone displacements after each test. A fixed video camera was also installed on the side of the wave flume to record wave transformation and stone displacements.

6.1.2 Sand and Stones

Beach sand and stones used to build the low-crested stone structure are described in the following.

Well sorted sand was used in the wave flume, as summarized in Table 6-2.

Table 6-2: Characteristics of sand used in experiment

Parameter		value
median diameter	[mm]	0.18
density	[g/cm ³]	2.6
fall velocity	[cm/s]	2.0

Green (G), blue (B) and white (W) stones were used to build the breakwater. G and B stones were used as armor layers and W stones were used to build a small core.

A sample of 100 stones was taken to obtain the stone size distribution. For practically homogeneous B stones 50 stones were sampled. Each stone was weighted on a small scale in the range of 1 - 500 g. Stone density was estimated as the total weight of the sample divided by the stone volume measured using a graduated cylinder filled with water. The nominal diameter (D_n) of each stone was then calculated using the following relation:

$$D_n = \left(\frac{M}{\rho_s}\right)^{1/3} \quad (6-1)$$

Where

M : mass of each stone [kg]

ρ_s : stone density [kg/m³]

The stone size distribution is expressed as the percentage finer by mass as a function of the corresponding value of D_n .

Stone porosity was measured by placing stones in a large bucket. Water was poured until stones were covered. The total stone weight and water weight were measured after separating the stone and water. The corresponding volume was then calculated from the known density. Finally, the stone porosity was calculated with the following relation:

$$n_p = \frac{V_v}{V_s + V_v} \quad (6-2)$$

Where

V_v : measured volume of voids (equal to measured volume of water) [m³]

V_s : measured volume of stones [m³]

The measured stone characteristics are summarized in Table 6-3. Details of stone measurements are provided in Appendix C.

Table 6-3: Characteristics of three stones used in experiment

Parameter		G (green)	B (blue)	W (white)
ρ_s	[g/cm ³]	2.94	3.06	2.72
n_p		0.44	0.44	0.43
D_{n50} (50% finer)	[cm]	3.52	3.81	1.80
D_{n85} (85% finer)	[cm]	3.71	3.86	1.95
D_{n15} (15% finer)	[cm]	3.33	3.75	1.61
D_{n85}/D_{n15}		1.11	1.03	1.21

6.1.3 Test Conditions

Two test series were conducted: with no structure (N) and with structure (S). Each series consisted of 10 runs of a 400 s burst of irregular waves corresponding to a TMA spectrum. The same burst was used for all runs. Target significant wave height and spectral peak period were approximately 17 cm and 2 s, respectively. Water depth at the paddle was kept at 78 cm in the experiment.

6.2 Experimental Procedure

The following procedure was followed to conduct the tests.

6.2.1 Profile Construction

In a preliminary test, the beach was exposed to the same wave conditions used for both test series (N and S), and the profile was regarded to be quasi-equilibrium.

After performing the 10 runs for the N test series, small changes of 1 cm or less in sand profile were measured. The profile was not rebuilt at the beginning of the S test series because exact rebuilding was practically impossible.

A low-crested breakwater with two different armor stone layers over a small core was built on the local bottom whose slope was 1/50. The structure height was approximately 10 cm above the local bottom and the freeboard F of the structure was approximately -2 cm (submerged structure). The seaward and landward slopes of the structure were 1/2 and the crest width was approximately 15 cm, as depicted in Figure 6-2.

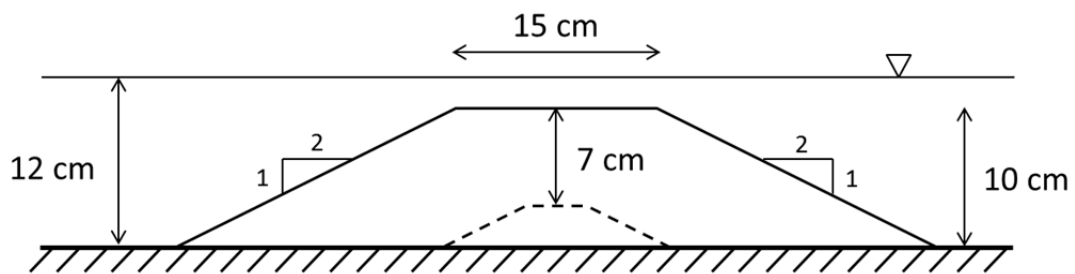


Figure 6-2: Structure dimensions

Stones were placed on a polyester fabric mesh with an opening of 0.074 mm that was laid over the well sorted sand of 0.18 mm. Stone W (white) was used to build the entire core. The breakwater was divided into two sections of 62 cm and 53 cm width. Stone G (green) and B (blue) were placed over the core stone and fabric mesh as shown in Figure 6-3. Toe protection is normally required against scour (Burcharth, et al., 2006) but it was not provided in S test to examine the interaction of the armor stone and sand.



Figure 6-3: Picture of the structure layout

6.2.2 Wave Generation

Waves were generated using a piston-type wave paddle, located at $x = -3$ m. Irregular waves corresponding to a TMA spectrum were generated by a 400 s time series of voltages read by the wave maker at a sampling rate of 20 Hz, as shown in Figure 6-4. Each voltage signal corresponds to a specific paddle displacement.

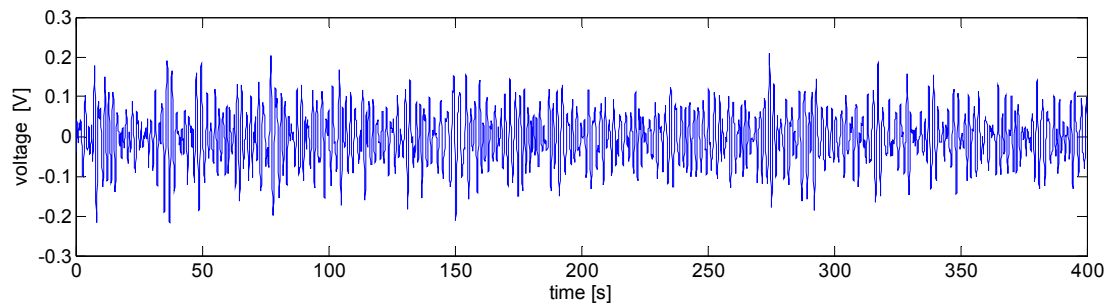


Figure 6-4: Time series of voltage input for the wavemaker

6.2.3 Measurements

Measurements were made of free surface elevations, velocities, bottom profile, structure damage and sand deposition.

6.2.3.1 Wave Gauges

Voltage signals from wave gauges WG1-WG6 were measured under quiet conditions to determine the still water level at each wave gauge after filling up the tank. Free surface elevations were measured at a sampling rate of 20 Hz by the six wave gauges installed along the flume. The first 20 s of the time series was removed to eliminate transitional waves. Bottom profile measurements required the drainage of the water in the flume every 5 runs. Wave gauges were calibrated before each profile measurement during the water draining. Figure 6-5 shows calibration relations for tests N01 to N05. A linear regression between voltage measurement and free surface level was accurate for all calibration relations.

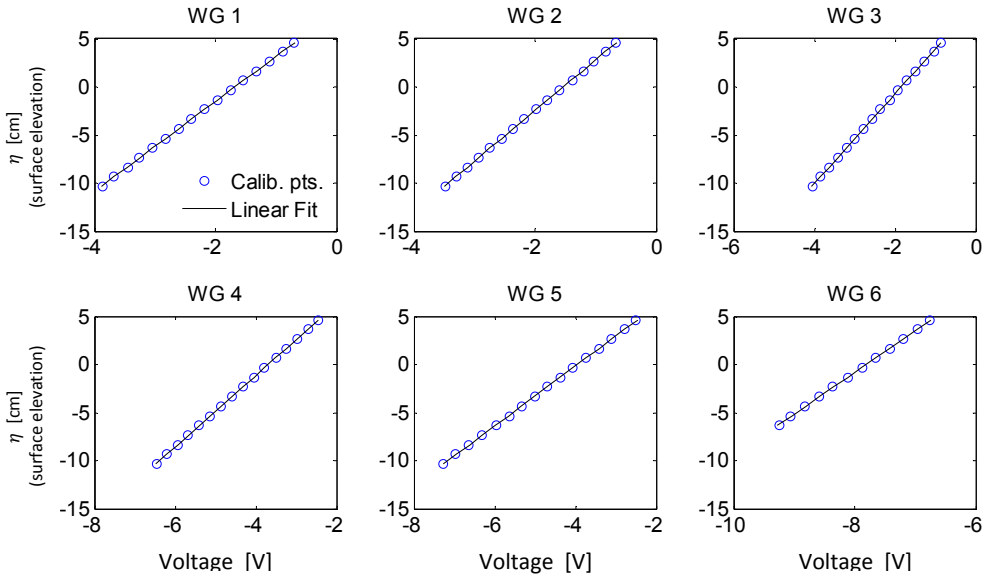


Figure 6-5: Calibration curves of wave gauges WG1-WG6

6.2.3.2 Acoustic Doppler Velocimeters

Two acoustic Doppler velocimeters, V1 and V2, were used to measure 3D velocity components at an elevation of 1/3 of the still water depth above the local bottom, at the same cross-shore locations of wave gauges WG5 and WG6, respectively. The free surface elevation and velocity data collection was synchronized at a rate of 20 Hz.

6.2.3.3 Bottom Profile

A laser line scanner mounted on a motorized cart was used to measure three-dimensional bathymetry after lowering the water level, at the beginning ($t = 0$ s) and after 5 ($t = 2,000$ s) and 10 runs ($t = 4,000$ s) of each test series. Measurements were taken at 2 cm intervals along the flume, between $4.9 \text{ m} < x < 19.9 \text{ m}$. An array of three ultrasonic transducers submerged in water was used to measure the beach profile between $0 \text{ m} < x < 5.9 \text{ m}$, at 10 cm intervals along the flume. These measurements were made at the beginning and end of each test series.

The three-dimensional laser data were averaged alongshore to get a two-dimensional profile. The average of the three transducer measurements was used for the remaining part of the profile. The overlapping region between $4.9 \text{ m} < x < 5.9 \text{ m}$ was used to merge both profiles smoothly.

6.2.3.4 Structure Damage

Structure profile measurements were also made at the beginning (initial profile) and after 5 and 10 runs (eroded profile). A fine resolution laser scan was used to measure the structure profile at 0.5 cm intervals, between $10.2 \text{ m} < x < 11.3 \text{ m}$. The measured profiles were used to compute the eroded area and damage S_p using Equation (4-2).

After each run, photos of the structure were taken from a stationary camera. These pictures in conjunction with the fine resolution laser scan measurements were used to count the number of dislodged stones during each run. The cumulative number of displaced stones was used to examine the temporal increase of damage S_v using Equation (4-1).

6.2.3.5 Sand Deposition

After S test series, sand deposition inside the structure was measured. Stones were removed carefully and wetted sand attached to some stones was removed at the same location. Once all stones were collected, the sand was slightly compacted for a fine resolution laser scan to measure deposited sand on the bottom at 0.5 cm intervals, between $10.2 \text{ m} < x < 11.3 \text{ m}$. Then, the sand was removed for a second fine resolution scan to obtain the deposited sand thickness. The collected sand was dried in an oven for 24 hr and then weighted to obtain the deposited sand porosity.

6.3 Analyzed Data

The measured free surface elevations, velocities, sand profiles and structure damage are analyzed in the following sections.

6.3.1 Free Surface Elevation

Offshore incident wave characteristics and reflection coefficient were obtained from wave gauges WG1-WG3, as summarized in Table 6-4 for each run, where: H_{m0} = spectral significant wave height; H_{rms} = root-mean-square wave height; H_s = average height of the highest 1/3 waves; T_p = spectral peak period; T_s = significant wave period; and R = average reflection coefficient.

Mean free surface elevation ($\bar{\eta}$) and standard deviation of the free surface (σ_{η}) calculated from the time series collected by each wave gauge are listed in Table 6-5 and Table 6-6, respectively.

Table 6-4: Incident wave conditions and reflection coefficient

Run	H_{m0} [cm]	H_{rms} [cm]	H_s [cm]	T_p [s]	T_s [s]	R
N_01	16.40	11.60	15.77	1.71	1.77	0.11
N_02	16.48	11.65	15.93	1.71	1.76	0.11
N_03	16.59	11.73	15.98	1.71	1.75	0.11
N_04	16.60	11.74	16.04	1.71	1.78	0.11
N_05	16.59	11.73	15.99	1.71	1.78	0.12
N_06	16.56	11.71	15.95	1.71	1.78	0.11
N_07	16.66	11.78	16.05	1.71	1.78	0.11
N_08	16.84	11.91	16.35	1.71	1.77	0.11
N_09	16.92	11.96	16.37	1.71	1.78	0.11
N_10	16.93	11.97	16.41	1.71	1.78	0.12
S_01	16.52	11.68	15.91	1.71	1.76	0.14
S_02	16.60	11.74	15.97	1.71	1.76	0.15
S_03	16.72	11.82	16.11	1.71	1.76	0.14
S_04	16.82	11.90	16.18	1.71	1.77	0.14
S_05	16.86	11.92	16.25	1.71	1.76	0.14
S_06	16.52	11.68	15.86	1.71	1.78	0.14
S_07	16.73	11.83	16.11	1.71	1.78	0.15
S_08	16.87	11.93	16.29	1.71	1.77	0.14
S_09	16.91	11.96	16.30	1.71	1.77	0.14
S_10	16.87	11.93	16.26	1.71	1.76	0.15

Table 6-5: Mean free surface elevation $\bar{\eta}$ at wave gauges WG1-WG6

Run	WG1	WG2	WG3	WG4	WG5	WG6
N_01	-0.22	-0.19	-0.18	0.15	0.37	0.66
N_02	-0.22	-0.20	-0.18	0.14	0.35	0.66
N_03	-0.21	-0.18	-0.19	0.14	0.37	0.66
N_04	-0.21	-0.17	-0.20	0.13	0.35	0.66
N_05	-0.19	-0.16	-0.21	0.13	0.34	0.66
N_06	-0.28	-0.20	-0.17	0.20	0.37	0.66
N_07	-0.30	-0.23	-0.19	0.18	0.37	0.65
N_08	-0.29	-0.23	-0.19	0.18	0.37	0.65
N_09	-0.29	-0.21	-0.20	0.20	0.37	0.65
N_10	-0.29	-0.19	-0.21	0.19	0.37	0.64
S_01	-0.32	-0.25	-0.25	0.13	0.27	1.48
S_02	-0.33	-0.24	-0.27	0.09	0.25	1.46
S_03	-0.32	-0.22	-0.28	0.10	0.25	1.46
S_04	-0.32	-0.21	-0.29	0.10	0.24	1.46
S_05	-0.31	-0.21	-0.30	0.10	0.24	1.46
S_06	-0.27	-0.24	-0.29	0.03	0.30	1.43
S_07	-0.27	-0.22	-0.32	0.02	0.30	1.43
S_08	-0.26	-0.21	-0.33	0.03	0.30	1.45
S_09	-0.26	-0.20	-0.35	0.03	0.30	1.44
S_10	-0.25	-0.17	-0.36	0.02	0.28	1.44

Table 6-6: Standard deviation of the free surface σ_η at wave gauges WG1-WG6

Run	WG1	WG2	WG3	WG4	WG5	WG6
N_01	4.05	4.03	4.09	2.85	2.18	1.78
N_02	4.08	4.05	4.11	2.86	2.17	1.78
N_03	4.10	4.08	4.13	2.84	2.18	1.79
N_04	4.11	4.07	4.13	2.86	2.19	1.78
N_05	4.11	4.07	4.13	2.83	2.18	1.79
N_06	4.09	4.11	4.10	2.90	2.27	1.84
N_07	4.11	4.13	4.14	2.91	2.29	1.85
N_08	4.16	4.17	4.17	2.91	2.29	1.85
N_09	4.18	4.20	4.19	2.90	2.30	1.87
N_10	4.19	4.20	4.20	2.90	2.30	1.88
S_01	4.08	4.08	4.12	2.87	2.36	1.36
S_02	4.10	4.10	4.13	2.86	2.37	1.38
S_03	4.13	4.12	4.16	2.85	2.36	1.39
S_04	4.16	4.16	4.18	2.88	2.38	1.42
S_05	4.16	4.17	4.21	2.87	2.38	1.40
S_06	4.07	4.07	4.13	2.88	2.40	1.42
S_07	4.13	4.12	4.17	2.88	2.41	1.43
S_08	4.17	4.16	4.20	2.87	2.43	1.43
S_09	4.17	4.18	4.21	2.89	2.43	1.44
S_10	4.17	4.16	4.20	2.89	2.44	1.44

6.3.2 Velocity

Mean cross-shore velocity (\bar{u}) and standard deviation of the cross-shore velocity (σ_u) calculated from the time series collected by each ADV are shown in Table 6-7.

Table 6-7: Cross-shore velocity statistics from velocimeters V1 and V2

Run	V1		V2	
	\bar{u} [cm/s]	σ_u [cm/s]	\bar{u} [cm/s]	σ_u [cm/s]
N_01	NR	NR	-5.87	13.66
N_02	-5.65	15.65	-5.18	13.68
N_03	-5.45	15.66	NR	NR
N_04	NR	NR	NR	NR
N_05	-5.48	15.26	-5.22	14.01
N_06	-5.00	15.29	-5.13	14.52
N_07	-5.44	15.59	-5.28	14.10
N_08	-5.16	15.56	-5.30	14.34
N_09	-4.34	15.83	NR	NR
N_10	-4.96	15.96	-5.12	14.39
S_01	-2.63	15.77	-2.31	9.86
S_02	-1.68	15.52	-2.42	10.10
S_03	-2.25	15.65	-2.74	10.22
S_04	-2.65	17.25	-2.87	10.32
S_05	-1.82	15.21	-2.16	10.30
S_06	-1.68	15.39	-3.01	10.35
S_07	-1.93	15.65	-3.03	10.38
S_08	-1.91	15.43	-3.00	10.23
S_09	-1.86	15.22	-2.89	10.17
S_10	-1.84	15.08	-2.76	9.98

NR: not reliable data

6.3.3 Bottom Profile

The bottom profile was measured at the beginning, middle and end of each test series. Figure 6-6 shows measured profiles and eroded depth (positive for erosion) relative to the initial profile for test series N. Figure 6-7 shows measured profiles and eroded depth relative to the initial profile for test series S.

In both test series, larger variations are seen in the zone measured by the ultrasonic transducers ($0 \leq x \leq 4.9$ m) at 10 cm intervals. These variations are possibly related to the sensitivity of sparse point measurements made with the transducers to bed forms.

Variations of the bottom profile for N test series are smaller than 1 cm, except for the vicinity of the shoreline location near $x = 16$ m. Differences between profiles measured at $t = 2000$ s and $t = 4000$ s are smaller than 0.5 cm, indicating the quasi-equilibrium condition of the sand profile.

Variations of the bottom profile for S test series are also smaller than 1 cm, apart from few spikes related to ripples. Differences between profiles measured at $t = 2000$ s and $t = 4000$ s are mainly due to increased size of ripples. A sequence of eroded and deposited zones seaward of the structure is also apparent, possibly related to a partially standing wave formed in front of the structure. The measured reflection coefficient at WG1 was approximately 0.14 for S test in comparison to 0.11 for N test.

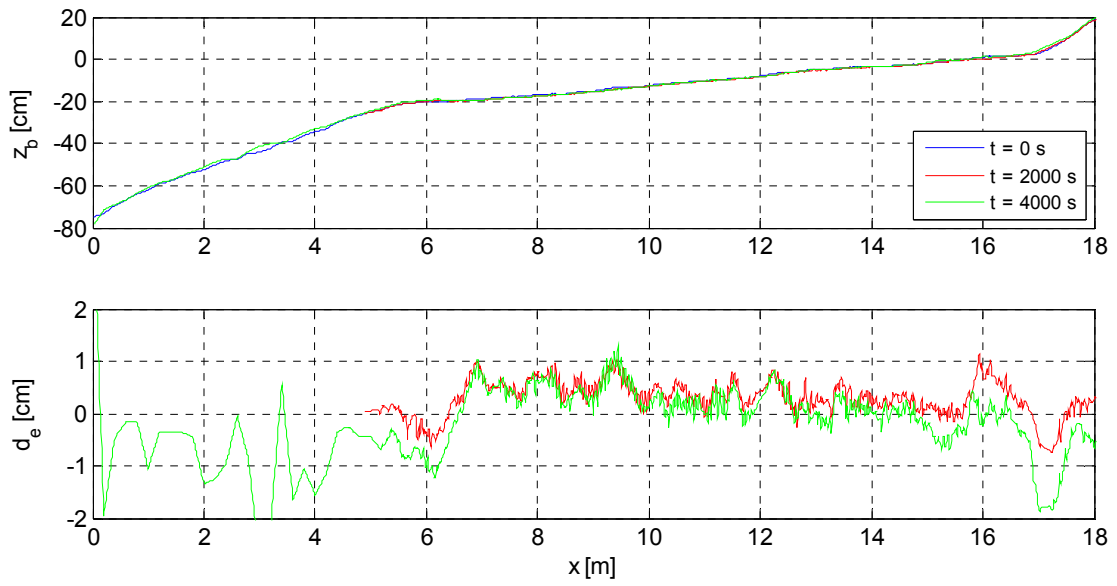


Figure 6-6: Measured bottom profile z_b and eroded depth d_e for N test series

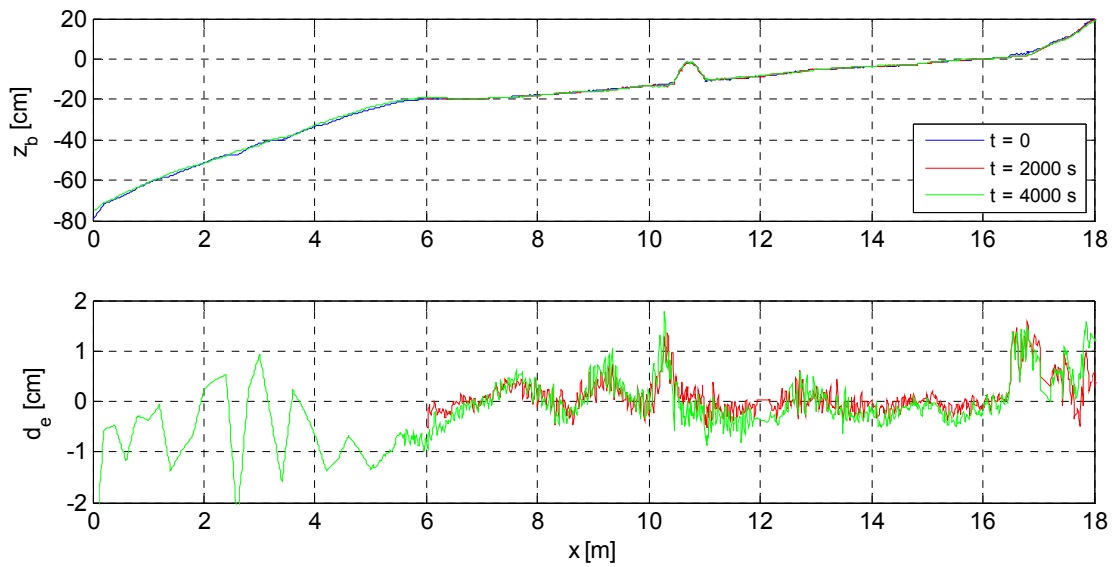


Figure 6-7: Measured bottom profile z_b and eroded depth d_e for S test series

6.3.4 Structure Damage

Structure damage was measured in two ways: by a fine resolution laser scan profile measurement and by counting the number of displaced stones.

The fine resolution laser scan profiles over the structure are shown in Figure 6-8, where the averaged profiles at the beginning and end of the test series are shown together with the eroded depth.

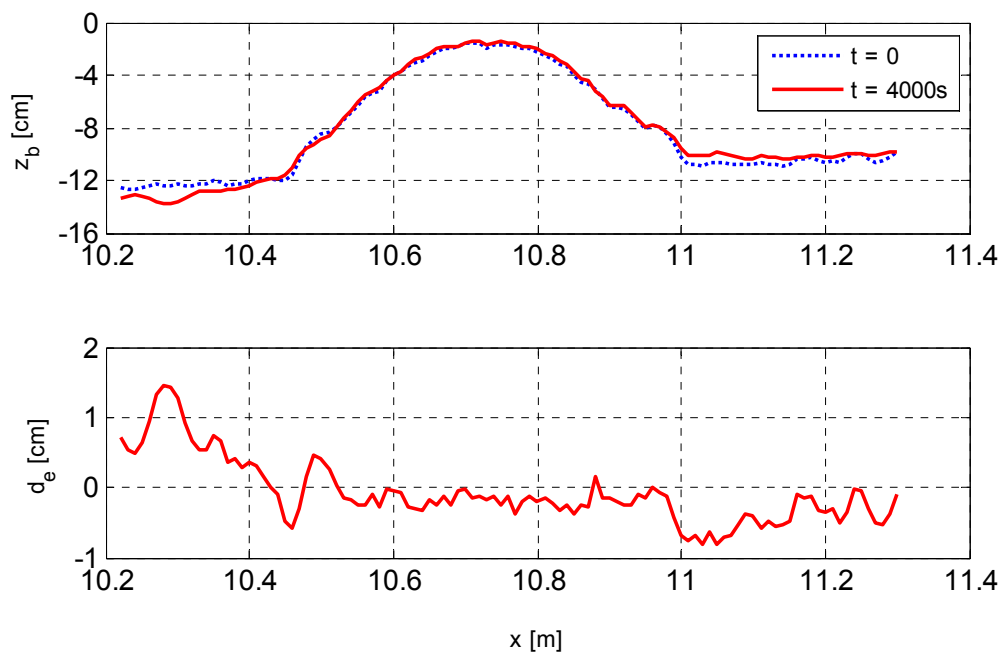


Figure 6-8: Measured structure profiles at the beginning and end of S test

Sand erosion and accretion occurred seaward and landward of the structure, respectively, probably because the structure interrupted the offshore sediment transport caused by the undertow current. Eroded depth of sand seaward of the structure is about 1 cm, while accretion landward of the structure is about 0.5cm.

Eroded depth along the structure is about 2 mm, similar to the magnitude of the measurement error obtained from consecutive profile measurements over the structure,

as detailed in Appendix D. Therefore, this measurement is considered to be unreliable for small damage.

The number of displaced green (G) and blue (B) stones was determined after each run using digital photographs taken from a fixed location in front of the structure and the fine resolution laser scan. The following figures show pictures and analyzed data from the fine resolution laser scan at the beginning (S 00), after five runs (S 05) and after ten runs (S 10) in the S test series. The dislodged stones are identified with numbers from 1 to 6.



Figure 6-9: Picture of the structure at the beginning of S test (S 00)



Figure 6-10: Picture of the structure after five runs in S test (S 05)



Figure 6-11: Picture of the structure after ten runs in S test (S 10)

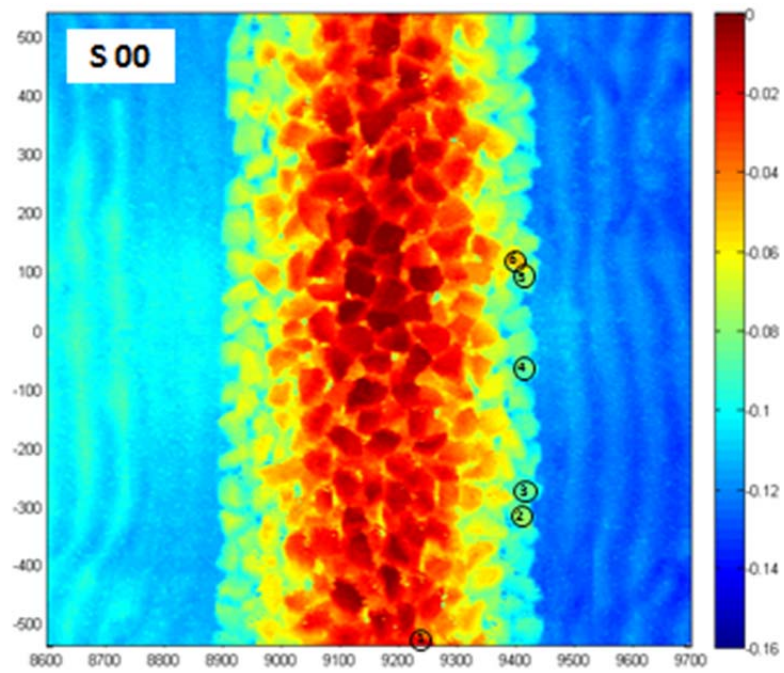


Figure 6-12: Fine resolution laser scan of the structure at the beginning of S test (S 00)

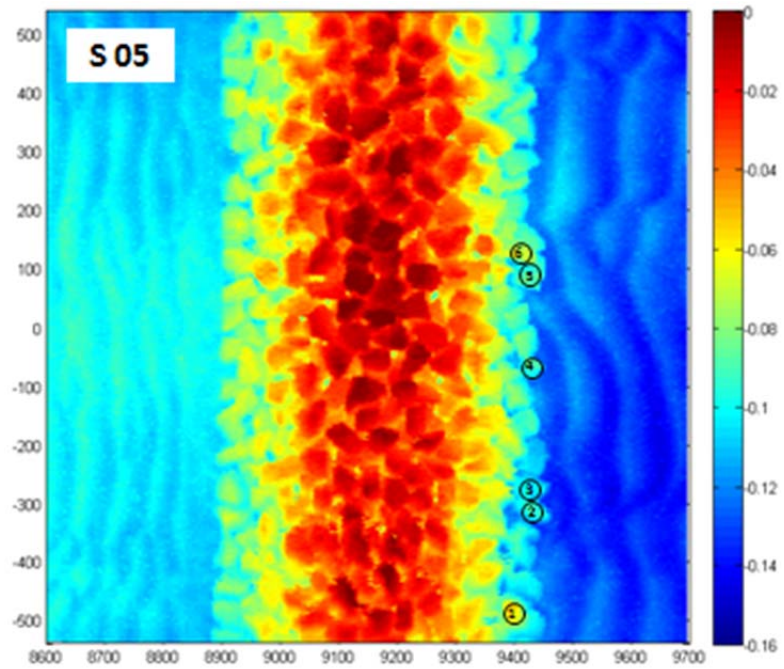


Figure 6-13: Fine resolution laser scan of the structure after five runs in S test (S 05)

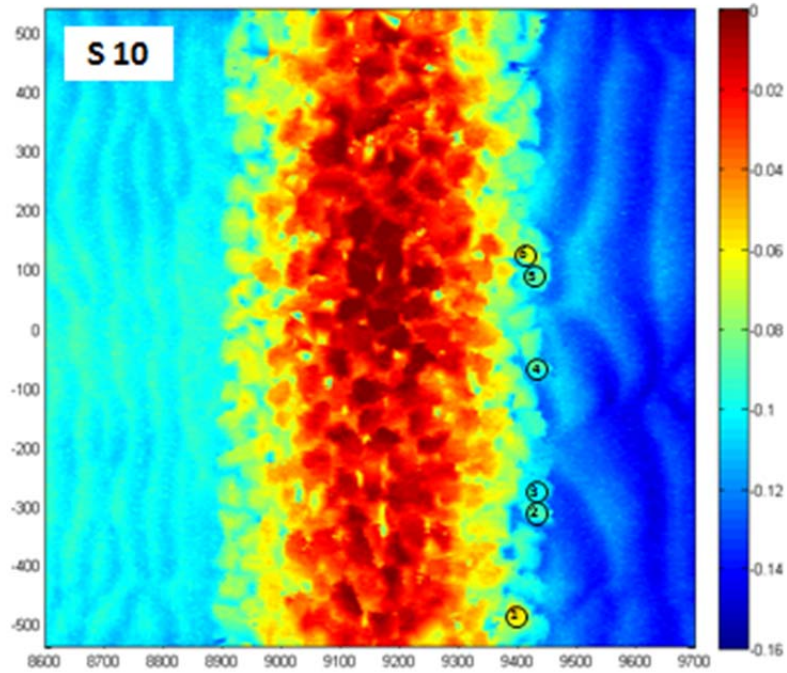


Figure 6-14: Fine resolution laser scan of the structure after ten runs in S test (S 10)

Pictures and analyzed laser scans show that stones located at the front toe of the structure were displaced. Only one stone moved more than the nominal stone diameter D_{n50} from its original position in Figure 6-15. Five stones moved more than $0.5 D_{n50}$ and are included in the calculated damage S_v using Equation (4-1) as summarized in Table 6-8, where N_y is the cumulative number of displaced stones up to the end of each run.

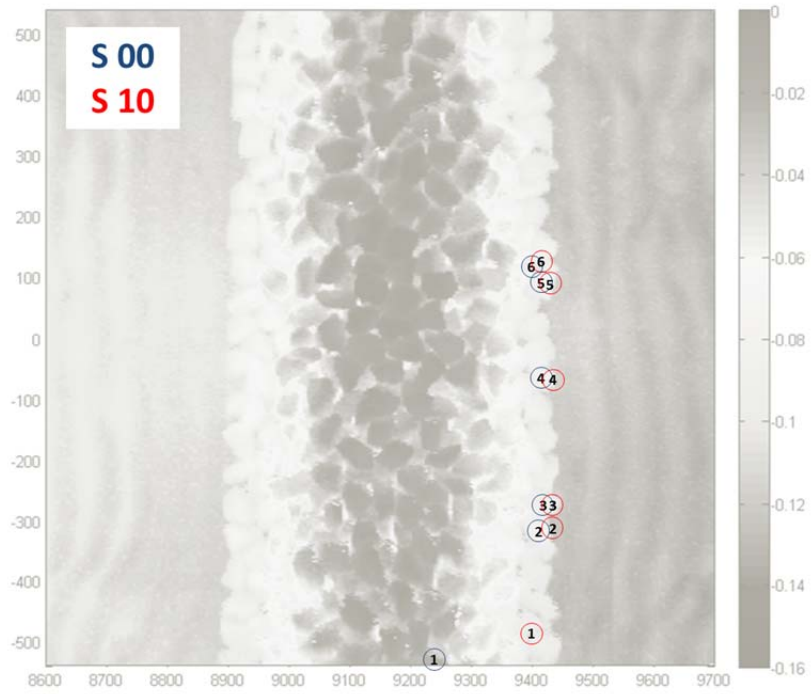


Figure 6-15: Identification of displaced stones during S test

Table 6-8: Measured damage for each stone type used in the experiment

Run	G stones		B stones	
	N_y	S_v	N_y	S_v
01	2	0.20	0	0.00
02	2	0.20	1	0.13
03	2	0.20	2	0.26
04	3	0.30	2	0.26
05	4	0.41	2	0.26
06	4	0.41	2	0.26
07	4	0.41	2	0.26
08	4	0.41	2	0.26
09	4	0.41	2	0.26
10	4	0.41	2	0.26

6.3.5 Sand Deposition

Deposited sand inside the structure was measured with the laser scan after S test. The deposited sand mass was also measured to estimate the porosity of the loose sand which was 0.53 in comparison to the porosity of 0.4 for the beach sand. The porosity difference was taken into account to convert the loose sand height to the beach sand height. Measured and adjusted values are summarized in Table 6-9. The converted sand height was about 0.3, 0.1 and 0.2 cm below the seaward slope, crest and landward slope of the structure, respectively, as shown in Figure 6-16.

Table 6-9: Deposited sand measurements

Parameter		value
sand weight	[g]	2,149
sand density	[g/cm ³]	2.6
sand volume	[cm ³]	827
deposited area A_d	[cm ²]	15.2
flume width	[cm]	115
deposited volume	[cm ³]	1,748
measured porosity		0.53
adjusted porosity		0.40
adjusted area A_a	[cm ²]	12.0

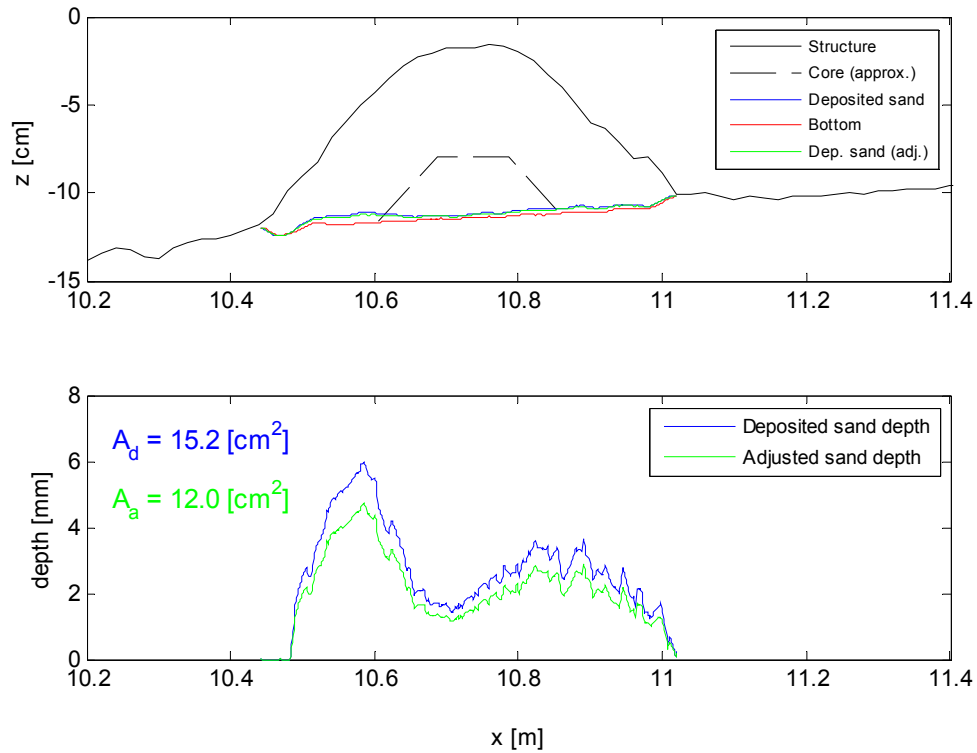


Figure 6-16: Measured profile and deposited sand depth inside the structure after S test

The present numerical model assumes a stone structure constructed on a fixed bottom to predict damage on the stone structure. This assumption may be acceptable for the hydrodynamic and damage computations because the erosion depth of 1 cm in front of the structure is much smaller than the structure height of 10 cm. Nevertheless, comparison of deposited sand height inside the structure with the 1 cm erosion depth in front and 0.5 cm accretion height in the lee of the structure indicates that sand deposition inside a porous structure needs to be included in the analysis of beach profile changes.

6.4 Comparison with Numerical Model

Measured values of $\bar{\eta}$, H_{m0} and T_p at $x = 0$ (WG1) for each run are specified as input for the numerical model. Empirical parameters in the model are kept the same as in the computations made for the NRC and AAU data.

For N tests, the plywood bottom slope of the flume was used to define the impermeable and fixed bottom $z_p(x)$ in the numerical model. The measured sand profile at the beginning of the test (N 00) was used to define the deformable bottom $z_b(x)$. In this computation, limited availability of sand above the fixed bottom is accounted for.

For S test, the measured sand profile at the beginning of the test (S 00) was used to define the impermeable and fixed bottom $z_p(x)$ in the numerical model, while the structure profile measured at the beginning of the test (S 00) was used to define the permeable bottom $z_b(x)$.

The computational domain extended from $x = 0$ to the sand dune located on the shoreward end of the flume. A local domain between WG 4-6 was used to compute damage on S test. Wave conditions at WG4 obtained from the entire domain computation were used as the offshore boundary conditions for the local domain computation.

The hydrodynamic variables and structure damage computed and stored at the end of each run are compared with the measured data.

6.4.1 Hydrodynamics

Figure 6-17 compares the measured and computed cross-shore variations of the mean water level $\bar{\eta}$, spectral significant wave height H_{m0} , and the mean \bar{U} and standard deviation σ_U of the horizontal velocity U for 10 runs in N test. The ten

measured values and computed variations are plotted together to indicate the variability of 10 runs in N test.

The mean water level $\bar{\eta}$ was negative (setdown) at WG 1-3 outside the surf zone and positive (setup) at WG 4-6 inside the surf zone. The wave height H_{m0} increased slightly due to wave shoaling and decreased almost linearly due to wave breaking. The numerical model overpredicts $\bar{\eta}$ and underpredicts H_{m0} slightly. The velocity comparison is uncertain because the computed depth-averaged velocity \bar{U} is not the same as the horizontal velocity measured at an elevation of 1/3 of the still water depth above the local bottom. The mean velocity \bar{U} is negative and represents an offshore return current (undertow). The standard deviation σ_U represents the magnitude of the oscillatory wave velocity. The degree of the agreement in Figure 6-17 is similar to that of the previous comparisons by Kobayashi, et al. (2009) and Figlus, et al. (2011).

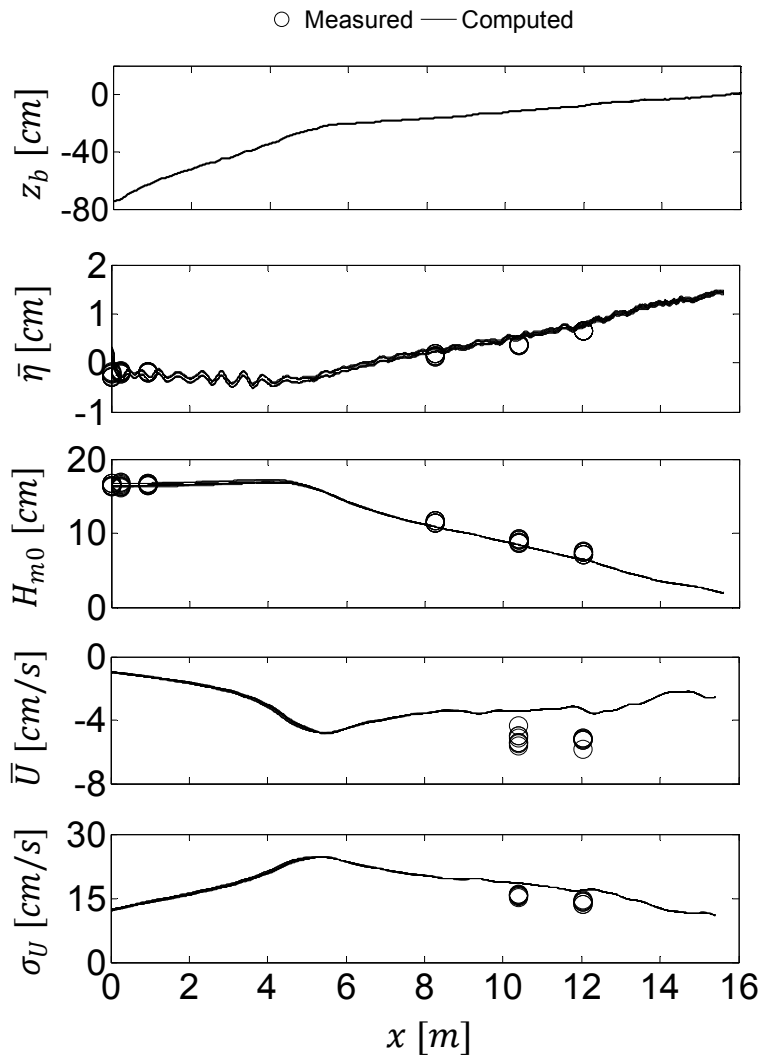


Figure 6-17: Initial bottom elevation z_b and measured and computed cross-shore variations of $\bar{\eta}$, H_{m0} , \bar{U} and σ_U for 10 runs in N test

Figure 6-18 compares the measured and computed cross-shore variations of the mean water level $\bar{\eta}$, spectral significant wave height H_{m0} , and the mean \bar{U} and standard deviation σ_U of the horizontal velocity U for 10 runs in S test. The local domain ($8.25 \text{ m} \leq x \leq 12.05 \text{ m}$) near the structure is depicted for clarity. The effects of the structure are essentially limited to the local domain. The ten measured values and computed variations are plotted together to indicate the variability of 10 runs in S test.

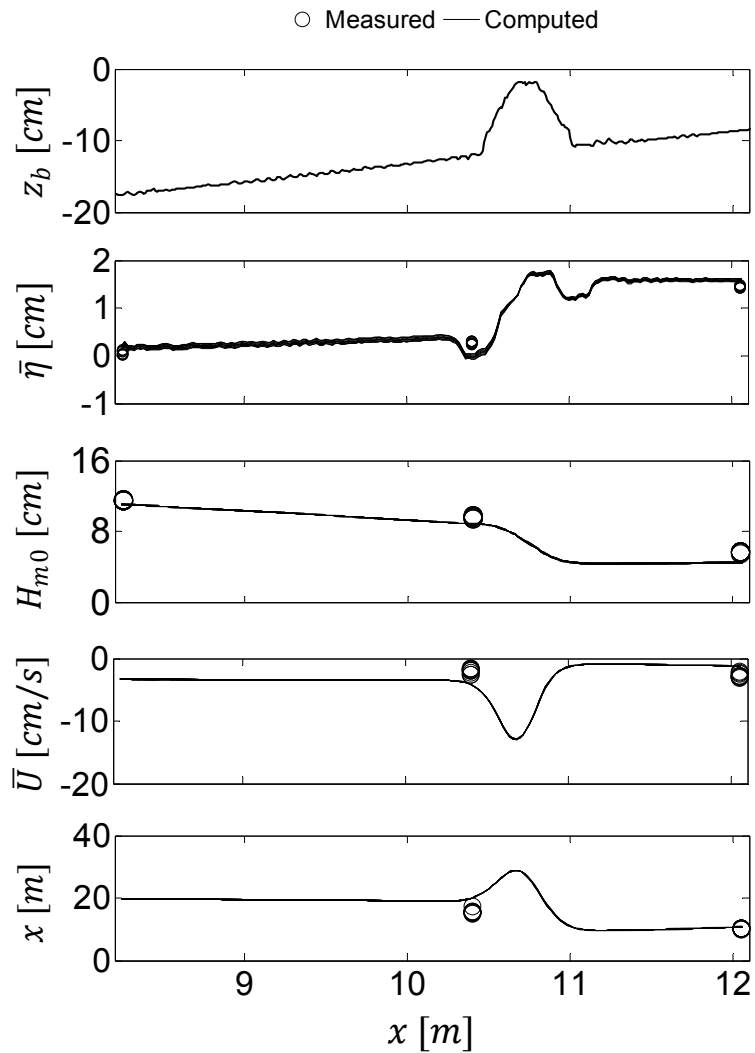


Figure 6-18: Initial bottom elevation z_b and measured and computed cross-shore variations of $\bar{\eta}$, H_{m0} , \bar{U} and σ_U for 10 runs in S test

The measured wave setup $\bar{\eta}$ was almost zero at WG4, increased slightly at WG5 at the seaward toe of the structure, and reached to the level of approximately 1.5 cm at WG6 located 1 m landward of the structure. The measured wave height H_{m0} decreased gradually from WG4 to WG5 and rapidly over the structure. The measured values of $(-\bar{U})$ and σ_U at WG6, landward of the structure, were smaller than the corresponding values in Figure 6-17 because of the reduction of H_{m0} over the

structure. The cause of the reduced offshore current at WG5 is not clear but may be related to the vertical variation of the undertow current and the elevation of the velocimeter V1 well below the structure crest as shown in Figure 6-1. The numerical model reproduces the measured cross-shore variations but the computed variations over the structure are uncertain due to lack of data.

6.4.2 Structure Damage

Measured and computed temporal variations of damage S_v for G and B stones is shown in Figure 6-19. The computed temporal variation is smooth because the numerical model does not predict the displacement of individual stones.

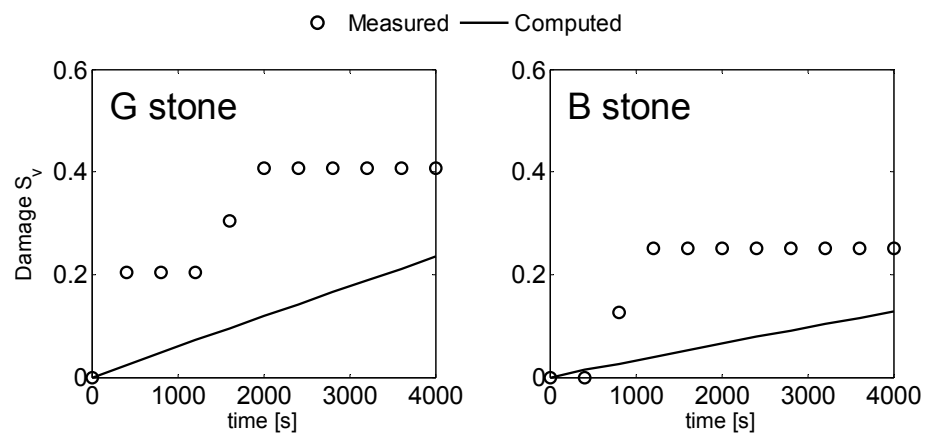


Figure 6-19: Measured and computed temporal variations of damage S_v in the experiment

The numerical model underpredicts the damage, partly because the measured damage includes three G stones and two B stones that were placed on the edge of the fabric mesh at the toe of the structure and displaced seaward over a distance of 2 to 3 cm (more than $0.5D_{n50}$ but less than D_{n50}) because of no toe protection. If these

displaced stones are excluded, the measured values of damage S_v would be 0.1 and 0.0 for G and B stones, respectively.

Chapter 7

CONCLUSIONS

Wave transmission, structure damage as well as other related topics on low-crested breakwaters (LCS) were analyzed in this study. Concluding remarks on each of these subjects are given in the following.

The cross-shore numerical model CSHORE extended to oblique waves, as described in the report of Kobayashi (2013), is used to compute wave transmission and structure damage.

The extended model is compared with available data on wave transmission consisting of 119 tests with normal and oblique wave incidence. When wave diffraction is excluded, the agreement between the measured and computed wave transmission coefficients is mostly within a factor of 2.

The model is used to predict the spatial variation of damage on the trunk of low-crested breakwaters. Comparison with two data sets consisting of 104 tests indicates that the model can predict damage on the front slope, back slope, and total section mostly within a factor of 2 except for small damage on the back slopes. Computed damage can be sensitive to the cross-shore extent of the specified section for some tests.

Similarity of trunk and head damage for low-crested structures is proposed to predict damage on the front head and back head sections using the cross-shore model developed for the trunk sections. The agreement for the head sections is not as good as

that for the trunk sections. The model overpredicts damage on the back head of a submerged structure, whose damage is sensitive to freeboard effects.

The proposed damage similarity for the back head of a low-crested breakwater may not be very accurate but allows to estimate the head damage in a wave-flume experiment and using a one-dimensional numerical model such as CSHORE.

The extended model may be used to predict damage progression during a severe storm with time-varying waves and water level conditions. Such a prediction is required for the design of a low-crested structure because of its sensitivity to both waves and water level.

An experiment was conducted in a wave flume for a LCS located inside the surf zone on a sand beach. The numerical model is shown to reproduce the measured cross-shore wave transformation on the beach without and with the structure as well as the measured small damage on the structure.

The measured beach profile change and deposited sand height inside the porous structure indicate that the interaction of sand and stone is important in predicting local scour and deposition in the vicinity of the porous structure. This interaction is not included in the present numerical model.

REFERENCES

- Burcharth, H., Kramer, M., Lamberti, A. and Zanuttigh, B., (2006). “Structural stability of detached low crested breakwaters”. *Coastal Engineering*, 53(4), pp. 381-394.
- Farhadzadeh, A., Kobayashi, N. and Gravens, M., (2012). “Effect of breaking waves and external current on longshore sediment transport”. *Journal of Waterway, Port, Coastal, and Ocean Engineering*, 138(3), pp. 256-260.
- Figlus, J., Kobayashi, N., Gralher, C. and Iranzo, V., (2011). “Wave overtopping and overwash of dunes”. *Journal of Waterway, Port, Coastal, and Ocean Engineering*, 137(1), pp. 26-33.
- Garcia, R. and Kobayashi, N., (2014). “Damage on trunk and head of low-crested breakwater”. *Journal of Waterway, Port, Coastal, and Ocean Engineering*, (in press).
- Goda, Y. and Ahrens, J., (2008). “New formulation of wave transmission over and through low-crested structures”. *Proceedings of 31st Int. Conf. on Coastal Engineering*, pp. 3530-3541.
- Kobayashi, N., (2013). “Cross-shore numerical model CSHORE 2013 for sand beaches and coastal structures”. Research Report. No CACR-13-01, Center for Applied Coastal Research, University of Delaware: s.n.
- Kobayashi, N., Buck, M., Payo, A. and Johnson, B., (2009). “Berm and dune erosion during a storm”. *Journal of Waterway, Port, Coastal, and Ocean Engineering*, 135(1), pp. 1-10.

- Kobayashi, N., Farhadzadeh, A. and Melby, J., (2010). "Wave overtopping and damage progression of stone armor layer". *Journal of Waterway, Port, Coastal, and Ocean Engineering*, 136(5), pp. 257-265.
- Kobayashi, N., Meigs, L., Ota, T. and Melby, J., (2007). "Irregular breaking wave transmission over submerged porous breakwater". *Journal of Waterway, Port, Coastal, and Ocean Engineering*, 133(2), pp. 104-116.
- Kobayashi, N., Pietropaolo, J. and Melby, J., (2013). "Deformation of reef breakwaters and wave transmission". *Journal of Waterway, Port, Coastal, and Ocean Engineering*, 139(4), pp. 336-340.
- Kramer, M. and Burcharth, H., (2003a). "Stability of low-crested breakwaters in shallow water short crested waves". *Proceedings of Coastal Structures, ASCE, Reston, Va.*, pp. 137-149.
- Kramer, M. and Burcharth, H., (2003b). "Wave basin experiment final form, 3-D stability tests at AAU". Report of DELOS EVK-CT-2000-0004 (www.delos.unibo.it).
- Sumer, B. et al., (2005). "Local scour at roundhead and along the trunk of low crested structures". *Coastal Engineering*, 52(10-11), pp. 995-1025.
- Tomasicchio, G., D'Alessandro, F. and Tundo, G., (2011). "Further developments in a new formulation of wave transmission". *Proceedings of 6th Int. Conf. on Coastal Structures, Volume 1*, pp. 634-645.
- Vidal, C., Losada, M. and Mansard, E., (1995b). "Stability of low-crested rubble-mound breakwater heads". *Journal of Waterway, Port, Coastal, and Ocean Engineering*, 121(2), pp. 114-122.
- Vidal, C., Losada, M., Medina, R. and Mansard, E., (1992). "A universal analysis for the stability of both low-crested and submerged breakwaters". *Proceedings of 23rd International Conference on Coastal Engineering, Issue 23*, pp. 1679-1692.

Vidal, C. and Mansard, E., (1995a). "On the stability of reef breakwaters". Technical Report. National Research Council of Canada, Ottawa, Canada.

Appendix A
AVAILABLE DATA ON LCS

Table A-1: Test conditions and measured data in NRC experiment

Test	ϕ [deg]	B_c [m]	h_c [m]	F [m]	H_s [m]	T_p [s]	s_0	K_t	Measured damage S_p				Measured damage S_v					
									TS	FS	C	BS	TS	FS	C	BS	FH	BH
1	0	0.15	0.40	0.00	0.048	1.39	0.016	0.54	0.78	0.23	0.54	0.14	0.45	0.45	0.72	0.00	0.39	0.39
4	0	0.15	0.40	0.00	0.075	1.40	0.025	0.45	1.85	0.63	1.07	0.51	1.27	0.81	1.00	0.09	0.00	1.97
5	0	0.15	0.40	0.00	0.075	1.40	0.025	0.45	1.07	0.18	0.19	0.12	2.08	0.36	1.09	0.18	0.66	0.98
2	0	0.15	0.40	0.00	0.094	1.41	0.030	0.45	5.06	2.12	4.29	0.52	4.53	2.90	4.98	0.45	2.38	2.38
3	0	0.15	0.40	0.00	0.111	1.41	0.036	0.41	5.15	2.64	1.71	0.47	5.16	3.44	3.08	0.18	3.73	3.47
13	0	0.15	0.60	0.00	0.127	1.40	0.042	0.47	17.61	9.19	9.83	0.99				0.82	13.73	12.12
9	0	0.15	0.40	-0.05	0.076	1.39	0.025	0.64	0.53	0.33	0.57	0.44	0.00	0.27	0.18	0.00	0.00	0.00
6	0	0.15	0.40	-0.05	0.092	1.41	0.030	0.60	2.31	0.12	1.15	0.42	1.63	0.63	1.36	0.09	0.40	0.00
7	0	0.15	0.40	-0.05	0.114	1.41	0.037	0.55	2.45	1.05	2.88	0.24	2.53	1.81	2.72	0.18	2.40	0.51
8	0	0.15	0.40	-0.05	0.126	1.41	0.041	0.54	4.06	3.50	1.92	0.35	5.07	5.89	2.44	0.27	1.93	0.64
14	0	0.15	0.60	-0.05	0.133	1.40	0.043	0.62	5.17	1.89	5.25	0.77	5.70	2.72	4.26	0.09	10.13	1.42
15	0	0.15	0.60	-0.05	0.151	1.41	0.049	0.60	10.72	4.70	10.22	0.57		5.61		0.54	14.33	3.30
16	0	0.15	0.60	0.02	0.052	1.40	0.017	0.46	2.02	0.70	0.44	1.15	1.36	0.27	0.09	0.18	0.00	1.16
12	0	0.15	0.40	0.02	0.075	1.41	0.024	0.39	2.53	0.98	0.67	0.02	3.89	2.44	1.09	0.27	1.48	3.55
10	0	0.15	0.40	0.02	0.094	1.41	0.030	0.38	6.43	3.26	0.46	0.31	6.70	6.07	1.27	0.27	1.63	6.35
11	0	0.15	0.40	0.02	0.105	1.41	0.034	0.36	8.80	5.10	2.84	0.32	11.04	6.61	3.80	0.63	5.34	8.62
17	0	0.15	0.60	0.02	0.146	1.40	0.048	0.43	43.76	11.83	8.63	2.18				1.54	23.18	15.38
18	0	0.15	0.60	0.04	0.046	1.41	0.015	0.48	1.24	0.60	0.17	0.35	0.45	0.27	0.09	0.00	0.85	0.71
19	0	0.15	0.60	0.04	0.079	1.40	0.026	0.43	3.45	1.42	0.79	0.36	4.62	2.81	1.27	0.36	3.68	4.36
20	0	0.15	0.60	0.04	0.096	1.40	0.031	0.43	6.68	4.39	1.38	1.22		5.07	1.99	0.54	13.78	12.18
21	0	0.15	0.60	0.04	0.117	1.40	0.038	0.41	22.31	11.22	1.19	0.78			2.62	1.27	19.14	18.24
22	0	0.15	0.60	0.04	0.136	1.41	0.044	0.41			4.62	0.31			4.89	0.91		
23	0	0.15	0.60	0.04	0.151	1.41	0.049	0.40			2.46	1.39			3.44	3.62		

Table A-1: Continued

Test						K_t	Measured damage S_p					Measured damage S_v					
	ϕ [deg]	B_c [m]	h_c [m]	F [m]	H_s [m]		T_p [s]	s_0	TS	FS	C	BS	TS	FS	C	BS	FH
24	0	0.15	0.60	0.06	0.054	1.41	0.017	0.33	0.73	0.11	0.44	1.09	0.91	0.00	0.00	1.41	1.41
25	0	0.15	0.60	0.06	0.079	1.42	0.025	3.17	2.87	0.29	0.20	5.34	2.99	0.18	0.00	5.10	8.32
26	0	0.15	0.60	0.06	0.092	1.41	0.030	5.12	5.62	0.90	0.53	7.15	7.61	0.36	1.00	8.92	16.43
27	0	0.15	0.60	0.06	0.110	1.41	0.035	19.56	11.09	1.42	1.79	25.54	16.02	1.18	2.26	12.58	
28	0	0.15	0.60	0.06	0.123	1.41	0.040		1.38	1.38	1.77			1.81	3.26		
29	0	0.15	0.60	0.06	0.132	1.41	0.043		1.46	1.46	2.01			2.35	3.62		
30	0	0.15	0.60	0.02	0.051	1.82	0.010	0.80		0.32	0.13	0.91	0.36	0.36	0.00	0.00	0.51
31	0	0.15	0.60	0.02	0.080	1.82	0.015	4.70	2.95	1.49	1.08	7.61	3.71	1.81	0.45	4.64	4.22
32	0	0.15	0.60	0.02	0.108	1.81	0.021	16.49	6.79	3.12	0.55	23.45	9.51	3.89	0.54	11.63	13.28
33	0	0.15	0.60	0.02	0.134	1.81	0.026		16.12	2.69	0.23		25.71	4.17	0.27	16.84	
34	0	0.15	0.60	0.06	0.072	1.82	0.014	3.87	1.38	0.15	0.68	5.98	3.17	0.27	0.00	0.91	2.48
35	0	0.15	0.60	0.06	0.099	1.82	0.019	26.55	8.87	0.49	0.76	11.23	0.36	0.72	6.44	15.59	

Table A-2: Test conditions and measured data in AAU wave transmission experiment

Test	ϑ [deg]	B_c [m]	h_c [m]	F [m]	H_s [m]	T_p [s]	s_0	K_t
1	-11	0.10	0.25	0.00	0.094	1.60	0.024	0.49
2	-11	0.10	0.25	0.00	0.120	1.83	0.023	0.45
3	-13	0.10	0.25	0.00	0.132	2.13	0.019	0.42
4	-6	0.10	0.25	0.00	0.063	1.22	0.027	0.51
5	-3	0.10	0.25	0.00	0.095	1.42	0.030	0.48
6	-9	0.10	0.25	0.00	0.112	1.51	0.032	0.46
7	-11	0.10	0.25	0.00	0.134	2.13	0.019	0.43
8	-9	0.10	0.25	0.00	0.127	1.60	0.032	0.45
9	-8	0.10	0.25	0.05	0.083	1.60	0.021	0.31
10	-9	0.10	0.25	0.05	0.096	1.60	0.024	0.32
11	-14	0.10	0.25	0.05	0.109	1.71	0.024	0.32
12	-7	0.10	0.25	0.05	0.060	1.07	0.034	0.23
13	-9	0.10	0.25	0.05	0.079	1.07	0.045	0.27
14	-8	0.10	0.25	0.05	0.095	1.35	0.034	0.29
15	-10	0.10	0.25	-0.05	0.094	1.60	0.024	0.65
16	-13	0.10	0.25	-0.05	0.131	1.97	0.022	0.57
17	-11	0.10	0.25	-0.05	0.157	2.13	0.022	0.52
18	-7	0.10	0.25	-0.05	0.076	1.42	0.024	0.68
19	-9	0.10	0.25	-0.05	0.106	1.42	0.034	0.61
20	-10	0.10	0.25	-0.05	0.144	1.51	0.041	0.53
21	38	0.10	0.25	0.00	0.095	1.60	0.024	0.44
22	38	0.10	0.25	0.00	0.127	1.71	0.028	0.42
23	45	0.10	0.25	0.00	0.129	1.83	0.025	0.39
24	32	0.10	0.25	0.00	0.120	1.71	0.028	0.45
25	36	0.10	0.25	0.00	0.144	1.97	0.024	0.42
26	32	0.10	0.25	0.00	0.072	1.11	0.037	0.47
27	35	0.10	0.25	0.00	0.103	1.22	0.044	0.47
28	41	0.10	0.25	0.00	0.110	1.22	0.047	0.41
29	31	0.10	0.25	0.00	0.103	1.28	0.040	0.49
30	35	0.10	0.25	0.00	0.130	1.42	0.041	0.44
31	36	0.10	0.25	0.00	0.144	2.13	0.020	0.44
32	35	0.10	0.25	0.00	0.131	1.51	0.037	0.45
33	36	0.10	0.25	0.00	0.123	1.51	0.035	0.48
34	34	0.10	0.25	0.00	0.133	1.51	0.038	0.47
35	38	0.10	0.25	0.05	0.080	1.60	0.020	0.24
36	41	0.10	0.25	0.05	0.096	1.71	0.021	0.24
37	40	0.10	0.25	0.05	0.120	1.97	0.020	0.25
38	47	0.10	0.25	0.05	0.114	1.97	0.019	0.23
39	35	0.10	0.25	0.05	0.116	1.83	0.022	0.28
40	28	0.10	0.25	0.05	0.060	1.11	0.031	0.20
41	30	0.10	0.25	0.05	0.084	1.22	0.036	0.21
42	37	0.10	0.25	0.05	0.099	1.28	0.039	0.24

Table A-2: Continued

Test	ϑ [deg]	B_c [m]	h_c [m]	F [m]	H_s [m]	T_p [s]	s_0	K_t
43	38	0.10	0.25	-0.05	0.102	1.60	0.026	0.64
44	34	0.10	0.25	-0.05	0.136	1.97	0.022	0.57
45	43	0.10	0.25	-0.05	0.135	1.97	0.022	0.54
46	26	0.10	0.25	-0.05	0.132	2.13	0.019	0.61
47	33	0.10	0.25	-0.05	0.165	2.13	0.023	0.51
48	30	0.10	0.25	-0.05	0.083	1.22	0.036	0.66
49	36	0.10	0.25	-0.05	0.123	1.42	0.039	0.55
50	44	0.10	0.25	-0.05	0.120	1.42	0.038	0.55
51	26	0.10	0.25	-0.05	0.124	1.28	0.048	0.60
52	34	0.10	0.25	-0.05	0.146	1.60	0.037	0.54
53	56	0.10	0.25	0.00	0.093	1.51	0.026	0.47
54	56	0.10	0.25	0.00	0.120	1.71	0.026	0.44
55	67	0.10	0.25	0.00	0.117	1.71	0.026	0.43
56	51	0.10	0.25	0.00	0.123	1.83	0.024	0.46
57	56	0.10	0.25	0.00	0.140	1.97	0.023	0.41
58	55	0.10	0.25	0.00	0.072	1.16	0.034	0.46
59	47	0.10	0.25	0.00	0.103	1.28	0.040	0.46
60	59	0.10	0.25	0.00	0.100	1.28	0.039	0.42
61	52	0.10	0.25	0.00	0.099	1.28	0.039	0.47
62	55	0.10	0.25	0.00	0.127	1.42	0.040	0.43
63	83	0.10	0.25	0.00	0.131	2.13	0.018	0.44
64	49	0.10	0.25	0.00	0.131	1.51	0.037	0.44
65	52	0.10	0.25	0.00	0.129	1.51	0.036	0.44
66	50	0.10	0.25	0.00	0.125	1.51	0.035	0.46
67	55	0.10	0.25	0.05	0.079	1.60	0.020	0.25
68	58	0.10	0.25	0.05	0.097	1.60	0.024	0.28
69	58	0.10	0.25	0.05	0.119	1.83	0.023	0.24
70	65	0.1	0.25	0.05	0.112	1.83	0.021	0.24
71	52	0.1	0.25	0.05	0.114	1.97	0.019	0.27
72	49	0.1	0.25	0.05	0.061	1.02	0.037	0.21
73	47	0.1	0.25	0.05	0.082	1.22	0.035	0.23
74	52	0.1	0.25	0.05	0.095	1.22	0.041	0.25
75	53	0.1	0.25	-0.05	0.104	1.60	0.026	0.65
76	54	0.1	0.25	-0.05	0.124	1.97	0.021	0.61
77	62	0.1	0.25	-0.05	0.133	1.83	0.026	0.56
78	47	0.1	0.25	-0.05	0.132	1.97	0.022	0.58
79	53	0.1	0.25	-0.05	0.157	2.33	0.019	0.49
80	50	0.1	0.25	-0.05	0.084	1.11	0.043	0.67
81	54	0.1	0.25	-0.05	0.123	1.35	0.043	0.58
82	64	0.1	0.25	-0.05	0.120	1.42	0.038	0.54
83	44	0.1	0.25	-0.05	0.124	1.35	0.044	0.58
84	53	0.1	0.25	-0.05	0.157	1.51	0.044	0.50

Table A-3: Test conditions and measured data in AAU structure stability experiment

Test	ϑ [deg]	B_c [m]	h_c [m]	F [m]	H_s [m]	T_p [s]	s_θ	Measured damage S_v							
								TS	SS	C	LS	SH	MH+LH		
1	0	0.10	0.30	0.05	0.049	1.27	0.020	0.11	0.11	0.00	0.00	0.00	0.00	0.00	0.00
2	0	0.10	0.30	0.05	0.065	1.55	0.020	1.94	0.91	0.46	0.57	0.00	0.00	1.04	0.00
3	0	0.10	0.30	0.05	0.092	1.79	0.020	4.33	1.25	1.14	1.94	1.11	1.11	4.17	0.00
4	0	0.10	0.30	0.05	0.120	2.00	0.020	8.78	3.65	2.28	2.85	5.94	5.94	7.92	0.00
5	0	0.10	0.30	0.05	0.037	0.90	0.035	0.00	0.00	0.00	0.00	0.00	0.00	0.00	0.00
6	0	0.10	0.30	0.05	0.062	1.10	0.035	0.00	0.00	0.00	0.00	0.30	0.30	0.45	0.00
7	0	0.10	0.30	0.05	0.091	1.27	0.035	1.48	0.34	0.91	0.23	0.84	0.84	1.67	0.00
8	0	0.10	0.30	0.05	0.117	1.42	0.035	3.08	0.80	1.14	1.14	1.51	1.51	3.89	0.00
9	0	0.10	0.30	0.00	0.051	1.27	0.020	0.00	0.00	0.00	0.00	0.00	0.00	0.00	0.00
10	0	0.10	0.30	0.00	0.076	1.55	0.020	1.03	0.11	0.91	0.00	0.00	0.00	0.00	0.00
11	0	0.10	0.30	0.00	0.095	1.79	0.020	1.25	0.23	1.03	0.00	0.00	0.00	1.31	0.00
12	0	0.10	0.30	0.00	0.121	2.00	0.020	4.33	1.71	2.62	0.00	3.50	3.50	2.55	0.00
13	0	0.10	0.30	0.00	0.038	0.90	0.035	0.00	0.00	0.00	0.00	0.00	0.00	0.00	0.00
14	0	0.10	0.30	0.00	0.062	1.10	0.035	0.34	0.11	0.23	0.00	0.00	0.00	0.24	0.00
15	0	0.10	0.30	0.00	0.085	1.27	0.035	0.57	0.23	0.34	0.00	0.40	0.40	1.01	0.00
16	0	0.10	0.30	0.00	0.109	1.42	0.035	1.71	0.46	1.14	0.11	0.68	0.68	1.03	0.00
17	0	0.10	0.30	0.00	0.126	1.55	0.035	2.28	0.80	1.37	0.11	1.55	1.55	2.01	0.00
18	0	0.10	0.30	-0.05	0.071	1.55	0.020	0.00	0.00	0.00	0.00	0.00	0.00	0.00	0.00
19	0	0.10	0.30	-0.05	0.095	1.79	0.020	0.34	0.00	0.34	0.00	0.00	0.00	0.00	0.00
20	0	0.10	0.30	-0.05	0.121	2.00	0.020	0.80	0.11	0.68	0.00	1.35	1.35	0.22	0.00
21	0	0.10	0.30	-0.05	0.143	2.19	0.020	2.62	0.23	2.39	0.00	2.28	2.28	1.52	0.00
22	0	0.10	0.30	-0.05	0.209	2.37	0.020	9.46	2.05	7.07	0.34	3.39	3.39	2.47	0.00
23	0	0.10	0.30	-0.05	0.063	1.27	0.035	0.00	0.00	0.00	0.00	0.00	0.00	0.00	0.00
24	0	0.10	0.30	-0.05	0.125	1.42	0.035	0.46	0.11	0.34	0.00	0.00	0.00	0.00	0.00
25	0	0.10	0.30	-0.05	0.149	1.55	0.035	1.25	0.11	1.03	0.11	0.00	0.00	0.18	0.00
26	0	0.10	0.30	-0.05	0.173	1.67	0.035	2.96	0.46	2.39	0.11	1.26	1.26	0.16	0.00
27	0	0.10	0.30	-0.05	0.191	1.79	0.035	4.22	0.91	3.19	0.11	1.71	1.71	0.29	0.00

Table A-3: Continued

Test	ϕ [deg]	B_c [m]	h_c [m]	F [m]	H_s [m]	T_p [s]	s_0	Measured damage S_v						
								TS	SS	C	LS	SH	MH+LH	
28	0	0.10	0.30	-0.10	0.147	2.00	0.020	0.80	0.11	0.68	0.00	0.56	0.56	
29	0	0.10	0.30	-0.10	0.189	2.19	0.020	1.37	0.34	1.03	0.00	0.39	0.59	
30	0	0.10	0.30	-0.10	0.222	2.37	0.020	2.05	0.57	1.37	0.11	0.32	1.11	
31	0	0.10	0.30	-0.10	0.247	2.53	0.020	5.47	0.57	4.45	0.46	0.83	1.66	
32	0	0.10	0.30	-0.10	0.116	1.42	0.035	0.34	0.00	0.23	0.11	0.00	0.41	
33	0	0.10	0.30	-0.10	0.139	1.55	0.035	0.68	0.11	0.34	0.23	0.00	0.31	
34	0	0.10	0.30	-0.10	0.171	1.67	0.035	1.14	0.11	0.68	0.34	0.00	0.22	
35	0	0.10	0.30	-0.10	0.189	1.79	0.035	1.82	0.11	1.25	0.46	0.00	0.20	
36	0	0.10	0.30	-0.10	0.204	1.90	0.035	2.05	0.11	1.48	0.46	0.00	0.71	
37	0	0.25	0.30	0.05	0.053	1.27	0.020	0.11	0.00	0.11	0.00	0.00	0.00	
38	0	0.25	0.30	0.05	0.075	1.55	0.020	1.48	0.80	0.68	0.00	0.62	0.41	
39	0	0.25	0.30	0.05	0.094	1.79	0.020	5.93	1.94	3.76	0.23	2.20	4.10	
40	0	0.25	0.30	0.05	0.116	2.00	0.020	8.89	2.28	5.82	0.80	4.49	6.27	
41	20	0.25	0.30	0.05	0.049	1.27	0.020	0.00	0.00	0.00	0.00	0.00	0.00	
42	20	0.25	0.30	0.05	0.071	1.55	0.020	1.37	0.34	0.80	0.23	0.63	0.52	
43	20	0.25	0.30	0.05	0.091	1.79	0.020	3.88	1.14	2.05	0.68	2.42	3.72	
44	20	0.25	0.30	0.05	0.115	2.00	0.020	7.98	2.39	3.65	1.94	6.01	5.26	
45	10	0.25	0.30	0.05	0.051	1.27	0.020	0.00	0.00	0.00	0.00	0.00	0.00	
46	10	0.25	0.30	0.05	0.073	1.55	0.020	1.03	0.34	0.57	0.11	0.00	0.00	
47	10	0.25	0.30	0.05	0.097	1.79	0.020	3.88	0.80	2.17	0.91	1.39	2.09	
48	10	0.25	0.30	0.05	0.119	2.00	0.020	5.47	1.48	2.51	1.48	4.07	3.43	
49	-10	0.25	0.30	0.05	0.054	1.27	0.020	0.00	0.00	0.00	0.00	0.00	0.00	
50	-10	0.25	0.30	0.05	0.079	1.55	0.020	0.23	0.00	0.23	0.00	0.21	0.82	
51	-10	0.25	0.30	0.05	0.099	1.79	0.020	2.28	0.46	1.25	0.57	0.79	3.87	

Table A-3: Continued

Test	ϑ [deg]	B_c [m]	h_c [m]	F [m]	H_s [m]	T_p [s]	s_θ	Measured damage S_v						
								TS	SS	C	LS	SH	MH+LH	
52	-20	0.25	0.30	0.05	0.055	1.27	0.020	0.00	0.00	0.00	0.00	0.00	0.00	0.00
53	-20	0.25	0.30	0.05	0.075	1.55	0.020	0.34	0.00	0.34	0.00	0.21	1.04	
54	-20	0.25	0.30	0.05	0.098	1.79	0.020	1.25	0.23	0.80	0.23	0.60	3.78	
55	-20	0.25	0.30	0.05	0.116	2.00	0.020	2.28	0.80	0.91	0.57	2.62	5.99	
56	30	0.25	0.30	0.05	0.050	1.27	0.020	0.00	0.00	0.00	0.00	0.00	0.00	0.00
57	30	0.25	0.30	0.05	0.069	1.55	0.020	0.23	0.00	0.23	0.00	0.00	0.42	
58	30	0.25	0.30	0.05	0.092	1.79	0.020	1.71	0.34	0.91	0.46	0.20	1.81	
59	30	0.25	0.30	0.05	0.110	2.00	0.020	5.82	0.91	2.96	1.94	1.72	4.49	
60	0	0.25	0.30	0.00	0.048	1.27	0.020	0.00	0.00	0.00	0.00	0.00	0.00	0.00
61	0	0.25	0.30	0.00	0.069	1.55	0.020	0.11	0.00	0.11	0.00	0.28	0.28	
62	0	0.25	0.30	0.00	0.098	1.79	0.020	2.28	0.23	2.05	0.00	1.71	2.08	
63	0	0.25	0.30	0.00	0.127	2.00	0.020	6.50	0.46	5.70	0.34	3.24	2.92	
64	0	0.25	0.30	-0.05	0.120	1.79	0.020	0.23	0.00	0.23	0.00	0.00	0.00	0.00
65	0	0.25	0.30	-0.05	0.153	2.00	0.020	2.51	0.00	2.39	0.11	0.00	0.36	
66	0	0.25	0.30	-0.05	0.184	2.19	0.020	6.73	0.23	6.27	0.23	0.63	1.47	
67	0	0.25	0.30	-0.10	0.147	2.00	0.020	1.03	0.00	0.91	0.11	0.00	0.16	
68	0	0.25	0.30	-0.10	0.183	2.19	0.020	3.65	0.00	3.19	0.46	0.00	0.39	
69	0	0.25	0.30	-0.10	0.222	2.37	0.020	7.18	0.23	6.39	0.57	1.10	1.87	

Appendix B
COMPUTED RESULTS

Table B-1: Computed wave transmission coefficient and damage S_p in NRC experiment

Test	K_t	Computed damage S_p (ISED _{AV} =1)					
		TS	FS	C	BS	FT	BT
1	0.09	0.27	0.05	0.27	0.01	0.05	0.23
4	0.20	2.39	0.55	2.39	0.17	0.55	1.85
5	0.20	2.39	0.55	2.39	0.17	0.55	1.85
2	0.26	4.88	1.30	4.88	0.55	1.30	3.58
3	0.30	7.90	2.57	7.90	0.87	2.57	5.33
13	0.24	8.62	3.19	8.59	1.04	3.19	5.43
9	0.55	0.62	0.06	0.62	0.06	0.06	0.56
6	0.54	1.53	0.23	1.53	0.23	0.23	1.30
7	0.53	4.02	0.94	4.02	0.52	0.94	3.08
8	0.53	5.63	1.52	5.63	0.76	1.52	4.11
14	0.46	5.35	1.50	5.35	0.77	1.50	3.85
15	0.46	7.91	2.51	7.87	1.32	2.51	5.40
16	0.03	6.24	0.68	6.24	1.29	0.68	5.56
12	0.66	3.89	1.19	3.89	0.10	1.19	2.70
10	0.15	6.99	2.46	6.99	0.31	2.46	4.52
11	0.17	9.10	3.66	9.09	0.36	3.66	5.44
17	0.19	14.60	6.82	13.70	1.26	6.82	7.74
18	0.00	0.17	0.08	0.17	0.00	0.08	0.09
19	0.48	5.38	1.24	5.38	0.55	1.24	4.13
20	0.46	7.75	2.48	7.75	0.60	2.48	5.27
21	0.57	12.30	5.55	11.90	0.43	5.55	6.70
22	0.11	18.30	8.67	17.00	0.89	8.67	9.60
23	0.13	19.50	9.50	17.70	1.45	9.50	10.00
24	0.11	0.46	0.30	0.46	0.00	0.30	0.16
25	0.20	3.20	2.02	3.04	0.03	2.02	1.17
26	0.06	5.78	3.41	5.44	0.14	3.41	2.37
27	0.23	10.00	5.57	9.30	0.51	5.57	4.48
28	0.22	13.50	6.77	12.50	1.04	6.77	6.75
29	0.42	16.10	8.67	14.40	0.93	8.67	7.41
30	0.33	6.57	1.40	6.57	0.55	1.40	5.17
31	0.12	7.31	2.81	7.31	0.08	2.81	4.50
32	0.20	12.20	5.44	12.00	0.71	5.44	6.80
33	0.25	19.00	9.78	17.50	1.14	9.78	9.21
34	0.13	5.89	3.83	5.69	0.04	3.83	2.05
35	0.27	13.30	7.57	12.40	0.61	7.57	5.72

Table B-2: Computed wave transmission coefficient in AAU wave transmission experiment

Test	K_t	Test	K_t	Test	K_t
1	0.40	35	0.13	69	0.06
2	0.41	36	0.18	70	0.45
3	0.43	37	0.33	71	0.22
4	0.36	38	0.16	72	0.03
5	0.40	39	0.30	73	0.12
6	0.39	40	0.20	74	0.10
7	0.43	41	0.14	75	0.65
8	0.40	42	0.12	76	0.63
9	0.25	43	0.64	77	0.62
10	0.25	44	0.61	78	0.61
11	0.42	45	0.61	79	0.60
12	0.24	46	0.63	80	0.66
13	0.16	47	0.58	81	0.57
14	0.20	48	0.67	82	0.62
15	0.68	49	0.57	83	0.56
16	0.63	50	0.57	84	0.51
17	0.62	51	0.56		
18	0.72	52	0.55		
19	0.63	53	0.32		
20	0.57	54	0.32		
21	0.35	55	0.33		
22	0.35	56	0.34		
23	0.35	57	0.34		
24	0.36	58	0.29		
25	0.38	59	0.28		
26	0.30	60	0.28		
27	0.29	61	0.28		
28	0.29	62	0.28		
29	0.31	63	0.52		
30	0.31	64	0.30		
31	0.39	65	0.30		
32	0.33	66	0.30		
33	0.33	67	0.12		
34	0.33	68	0.13		

Table B-3: Computed damage S_p in AAU structure stability experiment

Test	Computed damage S_p (permeable core)					
	TS	SS	C	LS	FT	BT
1	0.03	0.01	0.01	0.00	0.02	0.01
2	0.07	0.02	0.04	0.00	0.04	0.03
3	0.71	0.22	0.41	0.08	0.34	0.37
4	2.45	0.64	1.29	0.52	1.00	1.45
5	0.00	0.00	0.00	0.00	0.00	0.00
6	0.01	0.00	0.01	0.00	0.00	0.01
7	0.23	0.08	0.14	0.02	0.12	0.11
8	0.87	0.25	0.45	0.16	0.37	0.49
9	0.01	0.00	0.01	0.00	0.00	0.01
10	0.22	0.01	0.16	0.05	0.05	0.17
11	0.87	0.08	0.56	0.23	0.22	0.65
12	2.20	0.28	1.23	0.68	0.60	1.59
13	0.00	0.00	0.00	0.00	0.00	0.00
14	0.00	0.00	0.00	0.00	0.00	0.00
15	0.13	0.01	0.08	0.03	0.03	0.10
16	0.62	0.08	0.35	0.20	0.16	0.46
17	1.36	0.19	0.70	0.47	0.37	0.99
18	0.03	0.00	0.03	0.00	0.01	0.02
19	0.20	0.01	0.14	0.05	0.04	0.15
20	0.84	0.08	0.50	0.26	0.21	0.63
21	1.99	0.29	1.09	0.61	0.58	1.41
22	3.75	0.66	1.94	1.15	1.21	2.54
23	0.00	0.00	0.00	0.00	0.00	0.00
24	0.26	0.03	0.13	0.10	0.06	0.20
25	0.88	0.11	0.40	0.37	0.21	0.67
26	1.90	0.27	0.84	0.80	0.49	1.42
27	2.95	0.46	1.30	1.20	0.82	2.14
28	1.34	0.34	0.96	0.05	0.64	0.71
29	2.03	0.53	1.37	0.13	0.95	1.08
30	3.17	0.85	2.02	0.30	1.46	1.71
31	4.81	1.34	2.90	0.57	2.19	2.61
32	0.11	0.01	0.09	0.00	0.04	0.07
33	0.24	0.03	0.17	0.03	0.08	0.16
34	0.72	0.10	0.39	0.23	0.21	0.51
35	1.41	0.21	0.71	0.50	0.40	1.01
36	2.26	0.37	1.10	0.79	0.67	1.59

Table B-3: Continued

Test	Computed damage S_p (permeable core)					
	TS	SS	C	LS	FT	BT
37	0.03	0.01	0.02	0.00	0.02	0.01
38	0.26	0.10	0.16	0.00	0.15	0.11
39	0.96	0.32	0.64	0.00	0.49	0.48
40	2.45	0.73	1.68	0.04	1.10	1.35
41	0.04	0.02	0.02	0.00	0.03	0.01
42	0.45	0.17	0.28	0.00	0.26	0.18
43	1.67	0.57	1.11	0.00	0.87	0.81
44	4.17	1.27	2.85	0.05	1.92	2.25
45	0.03	0.01	0.02	0.00	0.02	0.01
46	0.32	0.12	0.20	0.00	0.19	0.13
47	1.18	0.38	0.80	0.00	0.58	0.60
48	3.01	0.88	2.07	0.06	1.32	1.69
49	0.05	0.02	0.03	0.00	0.03	0.01
50	0.38	0.13	0.25	0.00	0.21	0.17
51	1.48	0.47	1.01	0.01	0.71	0.77
52	0.08	0.04	0.05	0.00	0.06	0.02
53	0.58	0.21	0.37	0.00	0.34	0.25
54	2.88	0.94	1.94	0.00	1.41	1.47
55	8.31	2.62	5.63	0.06	3.84	4.47
56	0.07	0.02	0.04	0.00	0.04	0.02
57	0.21	0.06	0.16	0.00	0.10	0.11
58	2.40	0.77	1.63	0.00	1.16	1.24
59	5.63	1.68	3.89	0.05	2.53	3.10
60	0.01	0.00	0.01	0.00	0.00	0.01
61	0.08	0.00	0.07	0.00	0.01	0.06
62	0.96	0.06	0.83	0.07	0.17	0.78
63	2.94	0.25	2.31	0.38	0.59	2.35
64	1.14	0.16	0.98	0.00	0.42	0.73
65	2.36	0.30	1.95	0.11	0.72	1.64
66	4.50	0.53	3.45	0.52	1.20	3.30
67	1.54	0.27	1.27	0.00	0.58	0.97
68	2.52	0.41	2.11	0.00	0.86	1.66
69	4.22	0.72	3.42	0.07	1.39	2.83

Appendix C

CHARACTERISTICS OF STONES USED IN THE EXPERIMENT

Table C-1: G stone measurements

Stone density 2.94 g/cm³

D_{n50} 3.52 cm

Total mass 12,787 g

Stone #	Mass [g]	Dn [cm]	f	F
61	100.0	3.24	0.8%	0.8%
24	100.7	3.25	0.8%	1.6%
62	101.1	3.25	0.8%	2.4%
23	101.3	3.25	0.8%	3.2%
95	101.6	3.26	0.8%	3.9%
55	102.2	3.26	0.8%	4.7%
57	102.4	3.27	0.8%	5.5%
33	102.8	3.27	0.8%	6.4%
67	102.9	3.27	0.8%	7.2%
85	103.3	3.28	0.8%	8.0%
39	104.7	3.29	0.8%	8.8%
88	106.3	3.31	0.8%	9.6%
31	107.4	3.32	0.8%	10.5%
92	107.7	3.32	0.8%	11.3%
77	108.3	3.33	0.8%	12.1%
16	108.8	3.33	0.9%	13.0%
6	109.1	3.34	0.9%	13.8%
60	109.3	3.34	0.9%	14.7%
68	109.8	3.34	0.9%	15.6%
9	110.0	3.34	0.9%	16.4%
86	111.4	3.36	0.9%	17.3%
75	112.0	3.36	0.9%	18.2%
38	112.7	3.37	0.9%	19.0%
14	113.6	3.38	0.9%	19.9%
5	113.8	3.38	0.9%	20.8%

Stone #	Mass [g]	Dn [cm]	f	F
99	114.6	3.39	0.9%	21.7%
53	114.8	3.39	0.9%	22.6%
93	115.9	3.40	0.9%	23.5%
26	116.2	3.41	0.9%	24.4%
89	116.4	3.41	0.9%	25.3%
83	117.5	3.42	0.9%	26.3%
100	117.7	3.42	0.9%	27.2%
36	118.1	3.42	0.9%	28.1%
11	118.3	3.43	0.9%	29.0%
78	118.9	3.43	0.9%	30.0%
81	119.1	3.43	0.9%	30.9%
49	119.8	3.44	0.9%	31.8%
29	120.9	3.45	0.9%	32.8%
69	121.3	3.46	0.9%	33.7%
56	121.4	3.46	0.9%	34.7%
96	121.7	3.46	1.0%	35.6%
46	122.3	3.46	1.0%	36.6%
25	122.6	3.47	1.0%	37.5%
42	122.7	3.47	1.0%	38.5%
91	122.8	3.47	1.0%	39.5%
71	123.0	3.47	1.0%	40.4%
54	123.5	3.48	1.0%	41.4%
51	124.0	3.48	1.0%	42.4%
1	125.1	3.49	1.0%	43.3%
40	125.9	3.50	1.0%	44.3%

Table C-1: Continued

Stone #	Mass [g]	Dn [cm]	f	F
27	126.0	3.50	1.0%	45.3%
15	126.5	3.50	1.0%	46.3%
35	126.8	3.51	1.0%	47.3%
18	127.2	3.51	1.0%	48.3%
70	127.3	3.51	1.0%	49.3%
41	128.2	3.52	1.0%	50.3%
7	128.7	3.52	1.0%	51.3%
76	130.8	3.54	1.0%	52.3%
3	131.0	3.55	1.0%	53.3%
90	131.2	3.55	1.0%	54.4%
32	132.5	3.56	1.0%	55.4%
37	133.0	3.56	1.0%	56.4%
47	133.5	3.57	1.0%	57.5%
79	133.7	3.57	1.0%	58.5%
44	134.5	3.58	1.1%	59.6%
87	134.7	3.58	1.1%	60.6%
94	135.1	3.58	1.1%	61.7%
58	135.6	3.59	1.1%	62.8%
73	136.1	3.59	1.1%	63.8%
50	139.8	3.62	1.1%	64.9%
20	140.0	3.62	1.1%	66.0%
97	140.0	3.62	1.1%	67.1%
59	140.4	3.63	1.1%	68.2%
52	143.0	3.65	1.1%	69.3%
22	143.2	3.65	1.1%	70.4%

Stone #	Mass [g]	Dn [cm]	f	F
2	143.7	3.66	1.1%	71.6%
21	144.0	3.66	1.1%	72.7%
45	144.8	3.67	1.1%	73.8%
12	145.1	3.67	1.1%	75.0%
80	145.3	3.67	1.1%	76.1%
84	146.1	3.68	1.1%	77.2%
64	146.4	3.68	1.1%	78.4%
65	146.8	3.68	1.1%	79.5%
98	147.5	3.69	1.2%	80.7%
19	148.0	3.69	1.2%	81.8%
63	149.3	3.70	1.2%	83.0%
30	149.7	3.71	1.2%	84.2%
74	149.7	3.71	1.2%	85.3%
17	150.2	3.71	1.2%	86.5%
10	152.7	3.73	1.2%	87.7%
13	153.5	3.74	1.2%	88.9%
34	154.2	3.74	1.2%	90.1%
28	154.2	3.74	1.2%	91.3%
4	155.2	3.75	1.2%	92.5%
66	156.8	3.76	1.2%	93.8%
8	157.6	3.77	1.2%	95.0%
82	158.4	3.78	1.2%	96.2%
72	159.3	3.78	1.2%	97.5%
48	159.9	3.79	1.3%	98.7%
43	161.9	3.80	1.3%	100.0%

Table C-2: B stone measurements

Stone density 3.06 g/cm³

D_{n50} 3.81 cm

Total mass 8,413 g

Stone #	Mass [g]	Dn [cm]	f	F
3	151.8	3.67	1.8%	1.8%
18	157.1	3.72	1.9%	3.7%
10	158.8	3.73	1.9%	5.6%
24	159.9	3.74	1.9%	7.5%
22	160.4	3.74	1.9%	9.4%
35	160.5	3.74	1.9%	11.3%
17	160.6	3.74	1.9%	13.2%
28	160.7	3.74	1.9%	15.1%
26	160.8	3.75	1.9%	17.0%
50	160.8	3.75	1.9%	18.9%
46	162.0	3.75	1.9%	20.8%
12	162.4	3.76	1.9%	22.8%
19	162.5	3.76	1.9%	24.7%
42	162.6	3.76	1.9%	26.6%
23	162.8	3.76	1.9%	28.6%
34	163.7	3.77	1.9%	30.5%
39	164.1	3.77	2.0%	32.5%
13	164.6	3.77	2.0%	34.4%
45	165.1	3.78	2.0%	36.4%
5	165.2	3.78	2.0%	38.4%
14	165.3	3.78	2.0%	40.3%
41	165.7	3.78	2.0%	42.3%
48	166.8	3.79	2.0%	44.3%
1	167.2	3.79	2.0%	46.3%
27	168.1	3.80	2.0%	48.3%

Stone #	Mass [g]	Dn [cm]	f	F
11	168.6	3.81	2.0%	50.3%
2	168.8	3.81	2.0%	52.3%
38	169.5	3.81	2.0%	54.3%
43	169.6	3.81	2.0%	56.3%
25	169.9	3.81	2.0%	58.3%
36	170.3	3.82	2.0%	60.3%
30	171.8	3.83	2.0%	62.4%
33	171.9	3.83	2.0%	64.4%
49	172.9	3.84	2.1%	66.5%
4	173.2	3.84	2.1%	68.5%
31	173.2	3.84	2.1%	70.6%
20	173.9	3.84	2.1%	72.7%
37	173.9	3.84	2.1%	74.7%
40	173.9	3.84	2.1%	76.8%
7	174.3	3.85	2.1%	78.9%
47	175.0	3.85	2.1%	81.0%
21	176.4	3.86	2.1%	83.0%
32	176.4	3.86	2.1%	85.1%
15	176.6	3.86	2.1%	87.2%
8	177.0	3.87	2.1%	89.3%
29	178.2	3.88	2.1%	91.5%
6	178.5	3.88	2.1%	93.6%
9	178.5	3.88	2.1%	95.7%
44	180.1	3.89	2.1%	97.9%
16	180.8	3.89	2.1%	100.0%

Table C-3: W stone measurements

Stone density 2.72 g/cm³

D_{n50} 1.8 cm

Total mass 1,512 g

Stone #	Mass [g]	Dn [cm]	f	F
63	2.9	1.02	0.2%	0.2%
70	8.5	1.46	0.6%	0.8%
98	8.7	1.47	0.6%	1.3%
27	9.3	1.51	0.6%	1.9%
65	9.3	1.51	0.6%	2.6%
92	9.6	1.52	0.6%	3.2%
64	10.1	1.55	0.7%	3.9%
6	10.2	1.55	0.7%	4.5%
94	10.4	1.56	0.7%	5.2%
1	10.5	1.57	0.7%	5.9%
88	10.7	1.58	0.7%	6.6%
100	10.7	1.58	0.7%	7.3%
96	10.9	1.59	0.7%	8.1%
74	11.0	1.59	0.7%	8.8%
46	11.1	1.60	0.7%	9.5%
71	11.1	1.60	0.7%	10.2%
18	11.2	1.60	0.7%	11.0%
67	11.3	1.61	0.7%	11.7%
89	11.3	1.61	0.7%	12.5%
51	11.4	1.61	0.8%	13.2%
80	11.4	1.61	0.8%	14.0%
82	11.4	1.61	0.8%	14.7%
37	11.5	1.62	0.8%	15.5%
38	11.7	1.63	0.8%	16.3%
77	11.8	1.63	0.8%	17.1%

Stone #	Mass [g]	Dn [cm]	f	F
40	11.9	1.64	0.8%	17.8%
73	12.0	1.64	0.8%	18.6%
62	12.1	1.64	0.8%	19.4%
3	12.2	1.65	0.8%	20.2%
15	12.3	1.65	0.8%	21.1%
97	12.3	1.65	0.8%	21.9%
55	12.5	1.66	0.8%	22.7%
58	12.5	1.66	0.8%	23.5%
41	12.6	1.67	0.8%	24.4%
60	12.8	1.68	0.8%	25.2%
61	12.8	1.68	0.8%	26.1%
99	12.8	1.68	0.8%	26.9%
8	13.0	1.68	0.9%	27.8%
59	13.0	1.68	0.9%	28.6%
13	13.1	1.69	0.9%	29.5%
42	13.1	1.69	0.9%	30.4%
72	13.3	1.70	0.9%	31.2%
93	13.5	1.71	0.9%	32.1%
84	13.6	1.71	0.9%	33.0%
90	13.8	1.72	0.9%	33.9%
75	13.9	1.72	0.9%	34.9%
22	14.0	1.73	0.9%	35.8%
45	14.0	1.73	0.9%	36.7%
91	14.1	1.73	0.9%	37.6%
76	14.2	1.73	0.9%	38.6%

Table C-3: Continued

Stone #	Mass [g]	Dn [cm]	f	F
20	14.9	1.76	1.0%	39.6%
32	14.9	1.76	1.0%	40.5%
53	14.9	1.76	1.0%	41.5%
66	14.9	1.76	1.0%	42.5%
11	15.0	1.77	1.0%	43.5%
83	15.7	1.79	1.0%	44.6%
10	15.8	1.80	1.0%	45.6%
30	15.8	1.80	1.0%	46.6%
56	15.8	1.80	1.0%	47.7%
29	15.9	1.80	1.1%	48.7%
33	15.9	1.80	1.1%	49.8%
36	15.9	1.80	1.1%	50.8%
5	16.1	1.81	1.1%	51.9%
81	16.2	1.81	1.1%	53.0%
9	16.3	1.82	1.1%	54.1%
21	16.4	1.82	1.1%	55.1%
78	16.5	1.82	1.1%	56.2%
26	16.6	1.83	1.1%	57.3%
19	17.0	1.84	1.1%	58.5%
4	17.1	1.85	1.1%	59.6%
39	17.1	1.85	1.1%	60.7%
28	17.4	1.86	1.2%	61.9%
68	17.5	1.86	1.2%	63.0%
17	17.7	1.87	1.2%	64.2%
48	17.9	1.87	1.2%	65.4%

Stone #	Mass [g]	Dn [cm]	f	F
85	17.9	1.87	1.2%	66.6%
14	18.0	1.88	1.2%	67.7%
2	18.1	1.88	1.2%	68.9%
47	18.1	1.88	1.2%	70.1%
52	18.7	1.90	1.2%	71.4%
23	18.9	1.91	1.2%	72.6%
24	18.9	1.91	1.2%	73.9%
86	18.9	1.91	1.2%	75.1%
54	19.2	1.92	1.3%	76.4%
7	19.3	1.92	1.3%	77.7%
50	19.3	1.92	1.3%	79.0%
16	19.4	1.92	1.3%	80.2%
35	19.5	1.93	1.3%	81.5%
79	19.9	1.94	1.3%	82.8%
95	20.1	1.95	1.3%	84.2%
49	20.5	1.96	1.4%	85.5%
25	20.6	1.96	1.4%	86.9%
31	21.6	2.00	1.4%	88.3%
87	22.8	2.03	1.5%	89.8%
43	23.9	2.06	1.6%	91.4%
44	25.1	2.10	1.7%	93.1%
12	25.7	2.11	1.7%	94.8%
34	25.9	2.12	1.7%	96.5%
69	26.6	2.14	1.8%	98.2%
57	26.7	2.14	1.8%	100.0%

Appendix D

LASER LINE SCANNER ERROR OVER THE STONE STRUCTURE

MEASUREMENT ERROR

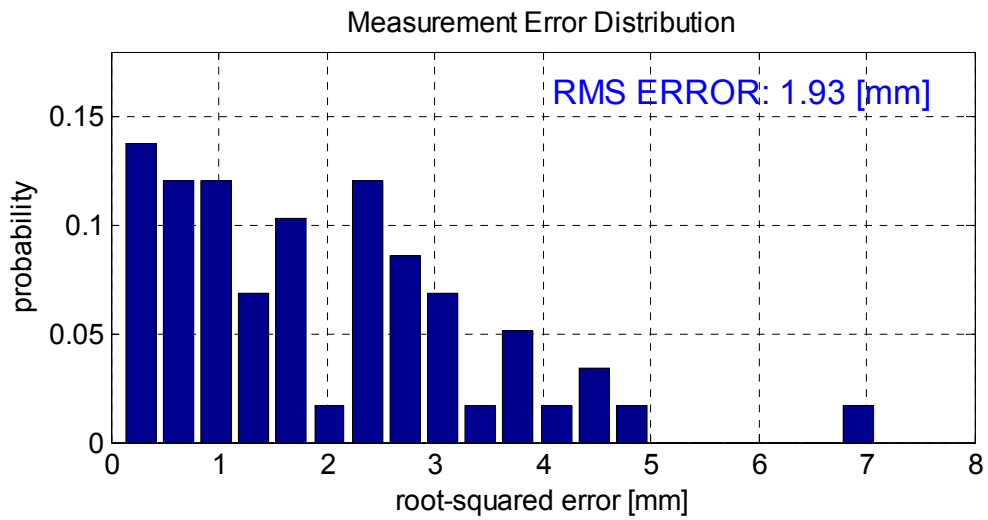
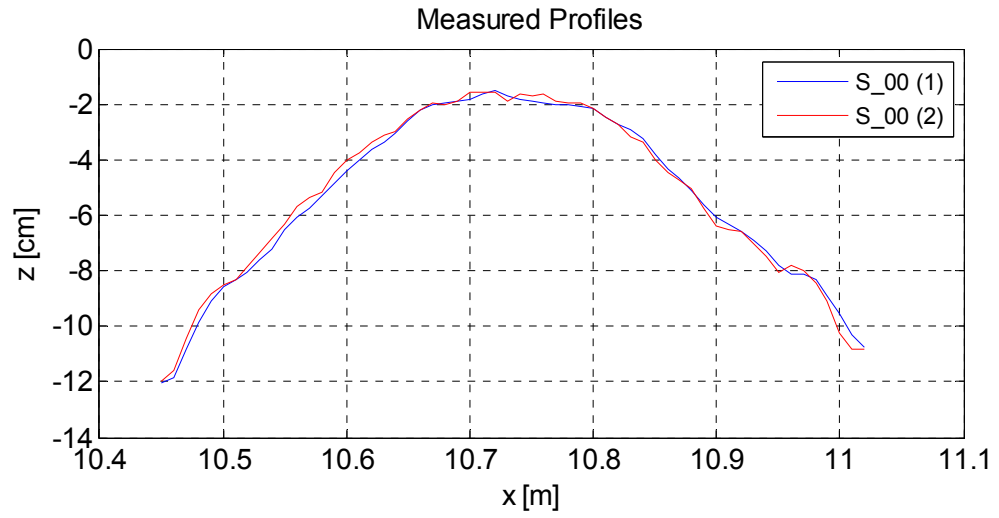


Figure D-1: Laser scan error over the structure in S 00 test

MEASUREMENT ERROR

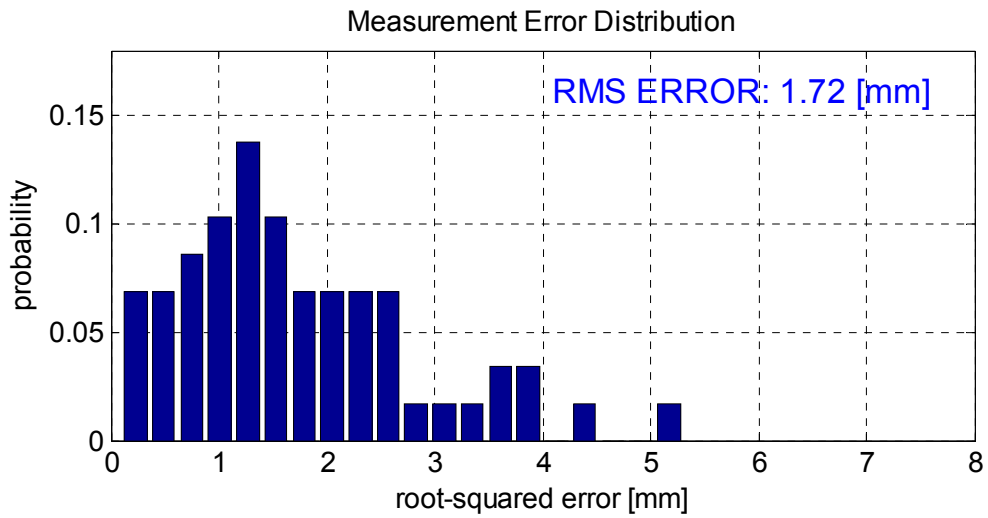
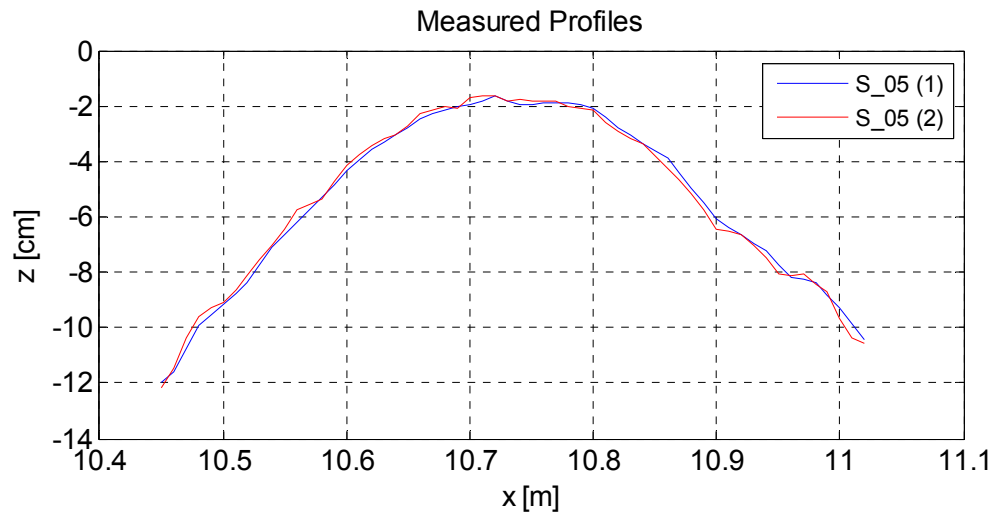


Figure D-2: Laser scan error over the structure in S 05 test

MEASUREMENT ERROR

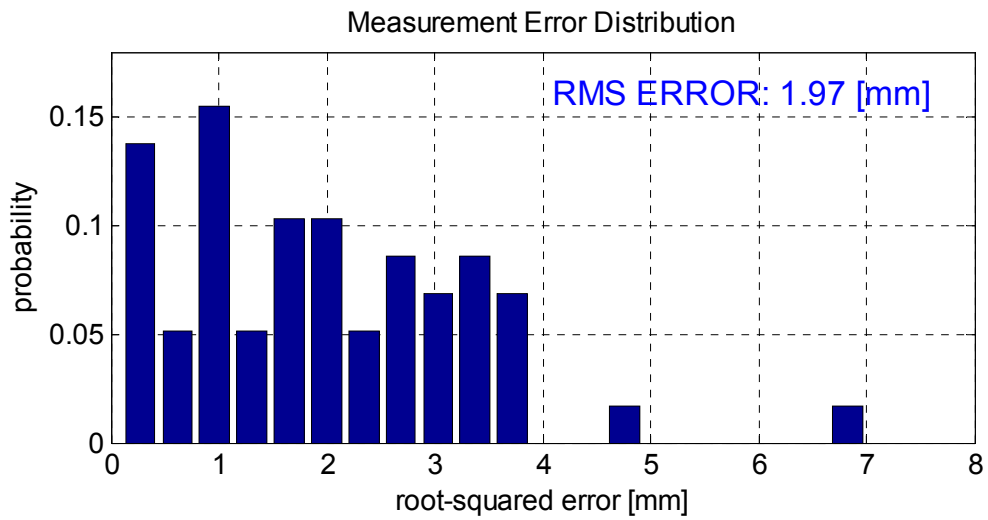


Figure D-3: Laser scan error over the structure in S 10 test